Sensorimotor Adaptation to Perturbations of Vowel Acoustics and its Relation to Perception

By

Virgilio Mangubat Villacorta

B.S., Physics with Specialization in Biophysics
University of California, San Diego, 1995

SUBMITTED TO THE
HARVARD-MIT DIVISION OF HEALTH SCIENCES AND TECHNOLOGY
IN PARTIAL FULFILLMENT OF THE
REQUIREMENTS FOR THE DEGREE OF

DOCTOR OF PHILOSOPHY IN
SPEECH AND HEARING BIOSCIENCE AND TECHNOLOGY
AT THE
MASSACHUSETTS INSTITUTE OF TECHNOLOGY

FEBRUARY 2006

Signature of Author ____
Harvard-MIT Division of Health Sciences and
Technology
September 19, 2005

Certified by____
Joseph S. Perkell, D.M.D., Ph.D.
Senior Research Scientist, Research Laboratory of Electronics
Harvard-MIT Division of Health Sciences and Technology
Thesis Supervisor

Accepted by____
Martha L. Gray, Ph.D.
Edwin Hood Taplin Professor of Medical and Electrical Engineering
Co-Director, Harvard-MIT Division of Health Sciences and Technology

This page intentionally left blank.

Acknowledgements

I would like to start by thanking the members of my committee for their sage advice. My deepest gratitude goes to my advisor and friend, Joe Perkell, without whose constant support and guidance I would not have been able to start—let alone finish—this work. Along with Joe, I am also greatly indebted to Frank Guenther, who has also spent innumerable hours guiding me on this project from its inception. I am also grateful for the valuable feedback I received from Tom Quatieri and Steve Massaquoi, and for the time they have spent reading and discussing with me the various drafts of this work.

Over these past six years, I feel like I've asked for advice or help from every member of the speech communications group at one point or another. I especially want to thank Ken Stevens for his insight as chair of my oral qualifying exam committee; Majid Zandipour, for helping me get the SA project off the ground; Mark Tiede, for developing a comprehensive set of Matlab tools that made my life so much easier; and Satra Ghosh, for always having an answer ready to my random queries. I also want to thank Arlene Wint; I think the lab would fall apart without you. To the people I've shared an office with—Laura Dilley, Xuemin Chi, Tony Okobi, and Xiaomin Mou: thanks for listening to my rantings, and letting me throw things at/with you. And to the remaining friends I've made in the speech group—Harlan Lane, Stephanie Shattuck-Hufnagel, Janet Slifka, Nicole Marrone, Ellen Stockmann, Steven Lulich, Kushan Surana, Annika Imbrie, Lan Chen, Neira Hajro, Seth Hall, Sharon Manuel, Melanie Matthies, Helen Hanson, Nancy Chen, Margaret Denny and others: thanks for sharing good times, intriguing conversation and the occasional libation.

My life at MIT was also shaped substantially by things I did outside the lab. I would like to recognize the following friends I've made along the way: my former roommates (Martin McKinney, Leonardo Cedolin, Mia Kiistala, Milena Virrankoski, Petra Aminoff, Sandrine Arnaud, Edward Ha, and Nigela Xhamo);

fellow members of the Graduate Student Council (especially Emmi Snyder, Barun Singh, Hector Hernadez, Lucy Wong, and Jess Vey); fellow soldiers (especially Colonel Michael Brennan); and fellow grad students (especially Tim Wagner, Zach Smith, and Dan Shub). Thank you all for making the time I spent at MIT an adventure. Thanks as well to lifelong friends who have made my entire life an adventure: Don Gurskis, Arlene Yang, Clinton Yee, Chuck Nguyen, Josh Burrell, Monika Garcia, and Julie Ting.

Above all, I would like to thank my family. I could not have completed this work without the lifetime of support and dedication from Mom and Dad; the encouragement from my sisters, Estella and Genie; and the love and companionship of my partner in life, Jenny.

* * * * * * * * * * *

This work has been supported by the National Institute of Deafness and Communication Disorders Grant R01-DC01925, and by the Harvard-MIT Division of Health Science and Technology.

* * * * * * * * * * *

I dedicate this work to the memory of my father.

Sensorimotor Adaptation to Perturbations of Vowel Acoustics and its Relation to Perception

By

Virgilio Mangubat Villacorta

Submitted to the Division of Health Sciences and Technology
on September 19, 2005 in Partial Fulfillment of the
Requirements of the Degree of Doctor of Philosophy in
Speech and Hearing Bioscience and Technology

Abstract

The overall goal of this dissertation was to study the auditory component of feedback control in speech production. The first study investigated auditory sensorimotor adaptation (SA) as it relates to speech production: the process by which speakers alter their speech production in order to compensate for perturbations of normal auditory feedback. Specifically, the first formant frequency (F1) was shifted in the auditory feedback heard by naive adult subjects as they produced vowels in single syllable words. These results indicated that subjects demonstrate compensatory formant shifts in their speech. This compensation was maintained when auditory feedback was masked by noise. The second study investigated perceptual discrimination of vowel stimuli differing in F1 frequency, using the same subjects as in the SA studies. This study showed that the extent of adaptation was positively correlated with subject auditory acuity. The last study consisted of a series of simulations of SA experiments using a model which describes the motor planning and control of human speech by the brain; these simulations showed that the model can account for several properties of adaptation as measured from the human subjects.

The findings in this dissertation support the idea that phonemic speech movements are planned as goal regions in an auditory space, and that mappings between this auditory space and the speech motor plan are adaptable. Moreover, the size of these goal regions—as reflected in speaker auditory acuity—influences the degree to which speakers adapt to errors in auditory feedback.

Thesis Supervisor: Joseph S. Perkell
Title: Senior Research Scientist, Research Laboratory of Electronics

This page intentionally left blank.

TABLE OF CONTENTS

TABLE OF FIGURES

LIST OF TABLES

This page intentionally left blank.

Chapter 1. Introduction.

This dissertation investigates the role of sensory feedback in the motor planning of speech, and specifically focuses on speech *sensorimotor adaptation*. Sensorimotor adaptation is an alteration of a motor task that results from the alteration of sensory feedback; psychophysical experiments that present human subjects with altered sensory environments have revealed the relationship of sensory feedback to motor control in both non-speech and speech contexts. Experiments on limb movements have demonstrated the influence of proprioceptive feedback—i.e. feedback pertaining to limb orientation and position—(Bhushan and Shadmehr, 1999; Blakemore et al., 1998)—and visual feedback (Bedford, 1989; Welch, 1978). Feedback-modification studies have also been conducted on speech production, including a number of studies that have induced compensation by altering the configuration of the vocal tract in some way (Abbs and Gracco, 1984; Lindblom et al., 1979; Savariaux et al., 1995). Other experiments have investigated speech adaptation to novel acoustic feedback, such as delayed auditory feedback (Yates, 1963) or changes in loudness (Lane and Tranel, 1971). Several studies of sensorimotor adaptation have investigated responses based on real-time alterations of the perceived pitch of vowel sounds (Kawahara, 1993; Xu et al., 2004) and a limited number have shown compensatory responses to real-time modifications of vowel formant structure (Houde and Jordan, 1998; Max et al., 2003).

The series of studies reported here investigate acoustic speech sensorimotor adaptation resulting from perturbations of specific vowel formant frequencies, and how this adaptation relates to vowel perception in cross-subject correlation studies. The data obtained from these experiments are compared to results from simulations from a well developed neural network model of speech motor planning, the DIVA (*Directions Into Velocities* of *Articulators*) model (Guenther and Ghosh, 2003).

1.1. Organization of this thesis.

Following this introduction, chapter 2 summarizes relevant research in the field of sensorimotor adaptation and sensorimotor control, with a focus on relevance to speech motor control and the DIVA model. Chapter 3 presents the results of study 1, an experiment that measured sensorimotor adaptation in response to acoustic perturbations in the first formant of vowels. Chapter 4 describes study 2, in which subjects' perceptual acuity to the acoustic perturbation was measured and related to the extent of their adaptive response in study 1. Chapter 5 describes study 3, which compared the results from studies 1 and 2 with simulations using the DIVA model. Finally, chapter 6 suggests future directions for studies of speech motor control using acoustic sensorimotor adaptation.

Chapter 2. Sensorimotor adaptation and the motor control of speech.

The motor control of speech—the manner in which the brain commands the vocal tract to produce speech—has been one of the longest studied aspects of the speech communication process. Issues related to speech motor control include speech acquisition, adaptation to changes during normal human growth and development, and adjustment to novel conditions (both pathological and experimentally induced). Work in this field has benefited immensely from the parallel progress made in non-speech sensorimotor control—the study of how the brain incorporates sensory information to guide movements in order to achieve some desired goal or outcome. Additional understanding of speech motor control has been derived from the use of neural network models such as the DIVA model (Guenther et al., 2005). Such models incorporate and expand upon many theories that have resulted from the general study of sensorimotor control to develop a cohesive and neuro-anatomically valid model that account for how the brain accomplishes the extremely complicated task of controlling the articulatory movements of speech production.

2.1. Sensorimotor adaptation and sensorimotor control

One way of investigating the relationship between sensory information and the control of motor movements is to modify the sensory feedback available to a subject, then measure the manner and degree to which that subject alters motor movements in response. Such a change in movements in response to distorted sensory feedback is termed *sensorimotor adaptation (SA)*. Before investigating the relationship of acoustic feedback to the motor control of speech, it is useful to understand SA findings in a somewhat analogous task: that of visual feedback to the motor control of reaching. This visual-reaching relation has been well characterized by wedge prism adaptation experiments (von Helmholtz, 1962). In these experiments, subjects wore prism glasses that altered their visual field. In compensatory responses, the subjects changed movement behavior in a way that was consistent with a temporary modification of neural mappings relating their visual perception to motor commands. Moreover, when the prism glasses were removed, these subjects demonstrated *aftereffect* adaptation: temporary retention of compensatory movements once the visual input was returned to normal.

Such SA experiments have been useful in demonstrating the dependence of reaching movements on visual feedback. For example, the aforementioned experiments utilizing visual-field shifting prism glasses have demonstrated that the visuomotor system is plastic, and can adapt to a number of perturbations (Welch, 1978). A modern equivalent version of the prism paradigm—using a computer to visually altered the perceived location of the finger during a pointing task—has also demonstrated visuomotor remapping that compensates for an alteration azimuth position (Bedford, 1989). Variant experiments of this perturbed pointing task—designed to cause two-dimensional visuomotor adaptation—have also shown visuomotor remappings that generalized greatest at the site of perturbation and decayed away from it (Ghahramani et al., 1996). The results of these experiments—and other related visuomotor SA experiments—led to the inference that reaching movements rely on neural mappings that relate sensory (visual) feedback to motor commands. Moreover, the latter experiments (Bedford, 1989; Ghahramani et al., 1996)—which visually altered the finger location via a computer—provided the inspiration to the design of a speech SA experiment, discussed below (Houde and Jordan, 1998).

Some adaptation-inducing experiments performed in the domain of speech include experiments that alter the vocal tract in some persistent way, such as compensation in vowel productions found when the position of the mandible is fixed with a bite-block (Lindblom et al., 1979), compensatory tongue movements in production of the vowel /u/ when the lip opening is fixed with a lip tube (Savariaux et al., 1995; Savariaux et al., 1999), and adaptations found in /s/ productions in response to the introduction of an artificial palate (Baum and

McFarland, 1997). There are also a number of speech experiments in which some aspect of somatosensory sensation[1] is blocked or altered by the unexpected perturbations of some aspect of movement. These include the compensatory orofacial muscle responses that were induced by unanticipated load perturbations on the lips during speech (Abbs and Gracco, 1984), compensatory responses due to unexpected perturbations of the palate shape (Honda et al., 2002), or in jaw movement (Tourville et al., 2004). Such compensation experiments have demonstrated the reliance of speech on somatosensory feedback from the articulators involved in speech. In particular, the palatal shape perturbation study (Honda et al., 2002) highlights adaptation to specific somatosensory feedback perturbations and is the only work referenced above which combines articulator perturbation with masking noise, thereby separating the effects of somatosensory feedback from auditory feedback.

Feedback-modification experiments using acoustic perturbations have also been used to understand how speech production is influenced by auditory feedback. Early research in this field was limited to modifying the amplitude of speech auditory feedback—showing that normal subjects spoke louder when their perceived loudness was decreased (Lane and Tranel, 1971; Yates, 1963)—or to delays in acoustic feedback—showing that fluent speech production is seriously impaired by small time delays in hearing one's own voice (Yates, 1963). With the advent of digital signal processing (DSP), researchers have been able to make near real-time (i.e. short time delay) adjustments to the spectral content of speech. DSP has been used in pitch-shift experiments, in which the fundamental frequency (F0) of sustained vowels was raised or lowered in subjects' auditory feedback (Burnett et al., 1998; Jones and Munhall, 2000; Kawahara, 1993). When F0 shifts were introduced during production of tonal sequences in Mandarin (a tone language), subjects responded with compensatory F0 shifts in the opposite direction, with delays as short as 150 msec (Xu et al., 2004).

[1] Somatosensory sensation generally refers to the perception of sensory stimuli from the skin and internal organs. In the context of speech motor control, somatosensory sensation refers to the perception of stimuli—tactile and positional information—from the vocal tract organs.

Some researchers have specifically investigated the sensorimotor adaptation when the feedback of the spectral content of a subject's speech is perturbed in nearly real-time (Houde and Jordan, 1998; Max et al., 2003). All these feedback modification experiments have found compensatory responses which show the strong influence of acoustic feedback on speech motor control. These latter two experiments are discussed in further detail in Section 3.1.

2.2. Feedback and feedforward motor control mechanisms.

The aforementioned evidence showing specific compensatory adjustments of speech parameters in response to sensory feedback perturbations indicates that movements make use of feedback control mechanisms. In feedback control systems, the output of the plant (that is, the controlled object) is fed back to the controller, so that this feedback signal can be incorporated into the command produced by the controller. Typically, the signal output by the controller is the error (that is, the difference between the input and feedback signal), weighted by a gain factor. (Refer to Figure 2.1) the amount of gain used in the controller plays a principal role in determining how quickly a system adapts to change, as well as how stable that system is. While potentially simple in design, high-performance feedback control systems may require large loop gains (Sinha, 1994). Given the signal transmission and processing delays in biological neural systems, one potential risk of feedback control loops is instability (Ito, 1974).

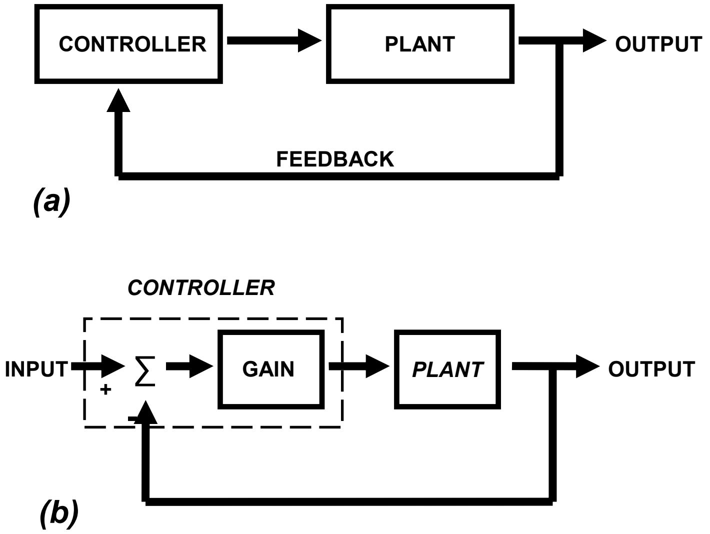

Figure 2.1: The feedback control system. (a) The controller governs the plant (i.e. the controlled object), utilizing feedback information from the output of the plant. (b) A simple implementation of a feedback control system, in which the controller generates an error signal from the feedback and input, and weighs (with gain) the resulting signal appropriately.

Instabilities that may result in feedback control can be avoided by *feedforward* control. Since feedforward control does not rely directly on feedback input, it can operate without the delays of feedback loops and thus at higher gains. To operate in a feedforward mode, motor control systems make use of *internal models*—neural representations that mimic the behavior of the motor system (Miall and Wolpert, 1996). Specifically, internal models allow feedforward control by predicting the sensory feedback that is used in a feedback controller—the forward model (see Figure 2.2a)—or by directly predicting the desired motor command that results in the desired state—the inverse model (see Figure 2.2b). One major problem with a feedforward controller is that internal models must somehow learn to make accurate predictions; moreover, the predictions of internal models are not accurate in the presence of unexpected perturbations.

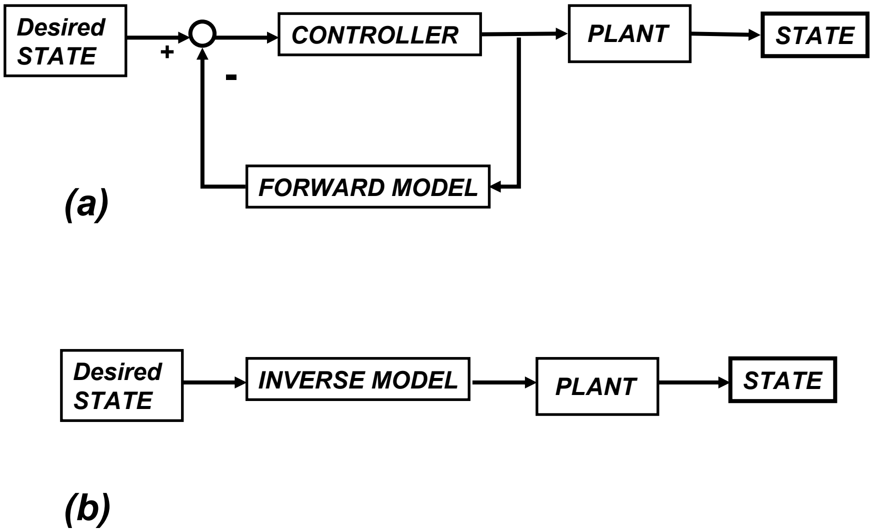

Figure 2.2: Two simple control schemes that involve internal models. a) A forward model predicts the expected feedback from the output *state*, and can replace the actual feedback without its inherent delays. b) An inverse model can directly predict the control commands that act on the plant to achieve the desired state. (Miall and Wolpert, 1996).

The feedback error learning control scheme (Kawato and Gomi, 1992) takes advantage of the beneficial properties of feedback and feedforward control by using both types of controllers into to determine the overall motor command (see Figure 2.3). In particular, the overall command in this control scheme is the summation of the computed feedforward component and the feedback component; the feedback command is also used to train the inverse model, which is used to calculate the feedforward command. The DIVA model utilizes a similar control scheme to explain the motor planning of speech.

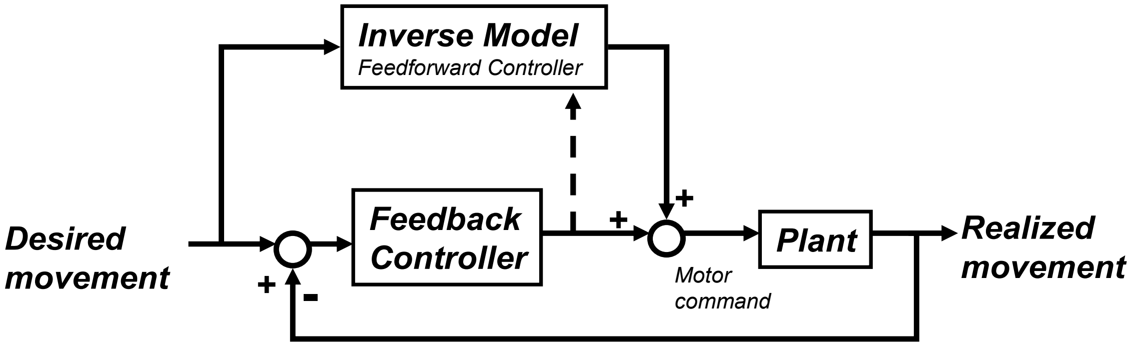

Figure 2.3: Feedback error learning motor control scheme. This control scheme sums both the feedback controller component and the feedforward controller component (the inverse model), yielding the *motor command* and eventually the realized movement. The output of the feedback controller is used to train the feedforward controller (dashed line). (Kawato and Gomi, 1992).

Before discussing a model of speech motor planning in detail, it is helpful to clarify some of the terminology, especially as it relates to the larger body of motor control research. Theories of motor control often distinguish between kinematic control—which refers to the control of the position and velocities of the controlled object—and dynamic control—which refers to the control of the forces needed to move the controlled object—(Atkeson, 1989). While kinematic and dynamic theories of motor control can be used within the same control scheme—including speech motor planning (Perkell et al., 2000)—the DIVA model discussed below is largely a kinematic one. Such approaches assume that the dynamic control factors are relatively unimportant. This assumption is based on observations that the masses of most vocal tract structures (articulators) are small, and the maximum forces generated by articulator muscles are generally much greater than needed in speech movements[2]. Internal models involving dynamic motor control have also been studied extensively (Kawato, 1999), but are beyond the scope of the current investigation.

2.3. An overview of a model for the motor planning of speech (*DIVA*).

One promising line of modeling research is exemplified by a neural network model (the *DIVA* model) which postulates that speech movements are planned by incorporating feedforward control with sensory feedback control in somatosensory and auditory dimensions (Guenther et al., 1998). Feedback control allows the model to train the feedforward controller, as well as deal with unexpected changes. Evidence for the role of somatosensory feedback has been discussed in Section 2.1, under articulatory speech SA experiments. Evidence for the planning of auditory feedback comes from many sources, and includes the aforementioned SA experiments in speech acoustics, as well as findings in the speech of cochlear implant users that they produce speech with greater contrast in their acoustic cues when their implant is turned on (Perkell et al., 2000). Feedforward control is incorporated into the model as well, since

[2] The DIVA model is pseudo-dynamic, in that it does account for neural and sensory delays.

feedback control may potentially be too slow to allow for the control of relatively brief speech movements (Perkell, 1997).

Figures 2.3 - 2.5 summarize the major features of the DIVA neural network model of speech motor control (Guenther et al., 2005). The DIVA model identifies projections from primary motor and pre-motor speech cortical areas to auditory and somatosensory cortical areas that instantiate the auditory and somatosensory expectations (goals) for the speech motor command (Figure 2.4). Projections from auditory and somatosensory cortical areas back to the primary speech motor areas transform errors between the aforementioned sensory expectations and actual sensory signals from the auditory and somatosensory areas, providing the *feedback* component of the speech motor commands. (Figure 2.5). The DIVA model is an acronym for *Directions into Velocities* of *Articulators;* it is so named because of its reliance on these mappings. The *feedforward* component of its speech motor commands are instantiated in projections from premotor areas to primary motor areas of speech directly and via the cerebellum (Figure 2.6); feedforward control is independent of feedback and instead predicts the expected movement needed to produce a phonemic correctly. These projections are learned over time from the previous motor commands consisting of attempts to produce target sounds.

Ultimately, speech motor commands are produced by combining both feedback control (Figure 2.5) and feedforward control (Figure 2.6). During initial periods of speech learning, feedforward control is not yet developed, so that the feedback controller dominates motor control. Through training, the feedforward controller gradually improves in its ability to predict the correct movements that correspond to a given speech sound (phoneme); eventually, it is the dominant controller in normal adult speech. For mature speakers, the role of the feedback controller becomes apparent when sensory feedback differs from the sensory expectations—e.g., in the presence of perturbations.

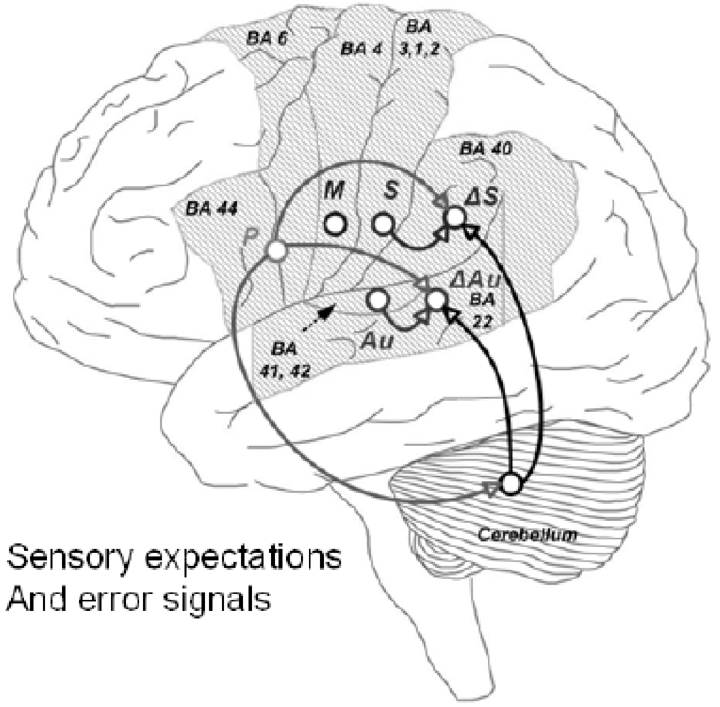

Figure 2.4: Sensory expectations or goals are encoded by the projections from premotor cortex (*P*) to auditory and somatosensory error cells (*ΔAu* and *ΔS*), and contain cortico-cortical and cerebellar components. Also shown here are the projections from the sensory cortices (*Au* and *S*) to the sensory error cells. (Ghosh, 2004)

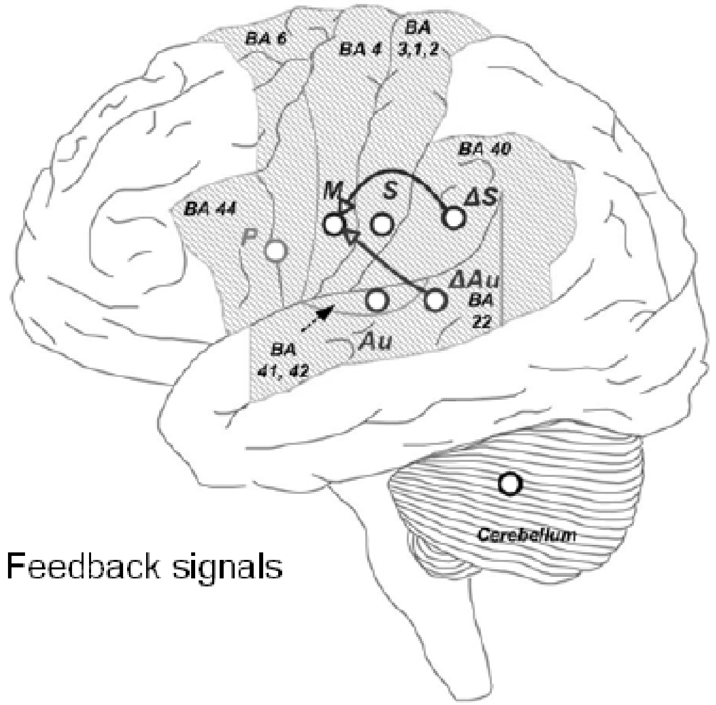

Figure 2.5: Projections from the auditory and somatosensory error cells (*ΔAu and ΔS*) to motor cortex (*M*) form the feedback controller. (Ghosh, 2004)

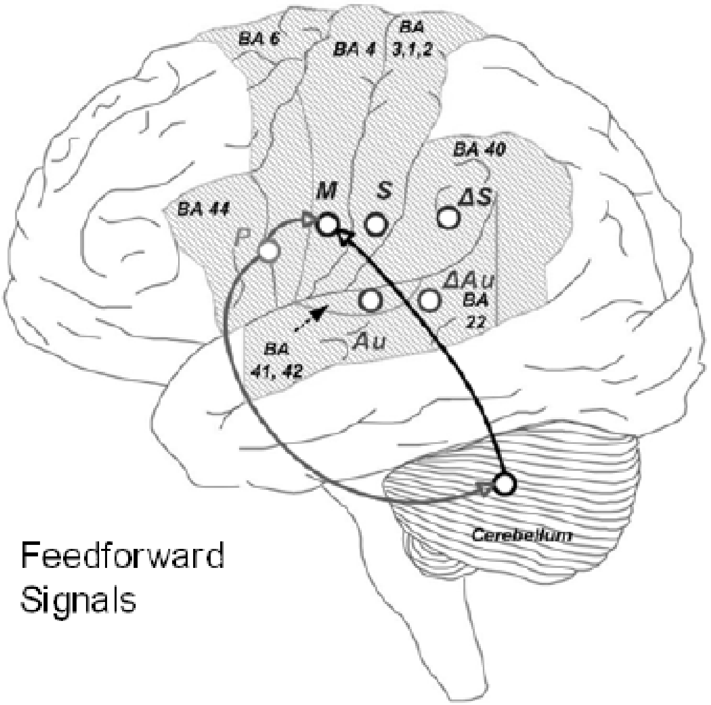

Figure 2.6: Projections (directly and via the cerebellum) from premotor cortex (*P*) to primary motor cortex *(M*) form the feedforward controller. (Ghosh, 2004).

The DIVA model has been able to account for several properties of speech production, including aspects of speech acquisition, speaking rate effects and coarticulation (Guenther, 1995); adaptation to developmental changes in the articulatory system (Callan et al., 2000); and the inverse relation between articulatory variability and acoustic stability measured in American English /r/ production (Nieto-Castanon et al., 2005). Recent work has also tested a prediction of the DIVA model on the relation between speech perception and production—that speakers with more acute perception of speech acoustics will learn smaller auditory goal regions[3] and thus produce phonemes with greater contrast than subjects with less acute perception (see Figure 2.7). This predicted relation—that a subject with greater discrimination will produce phonemes with greater contrast—has been observed in cross-subject correlations in phoneme contrasts. Specifically, subject discrimination between the contrasting vowel pairs was found to be correlated with contrast distance between the vowel pairs, measured both in articulatory movement and in acoustic separation (Perkell et

[3] Goal regions are discussed in greater detail in Sections 4.1.1 and 5.1.2.

al., 2004a). Similar correlation was also found between the discrimination of the contrasting silibants /s/ and /ʃ/ and acoustic contrast distance (Perkell et al., 2004b).

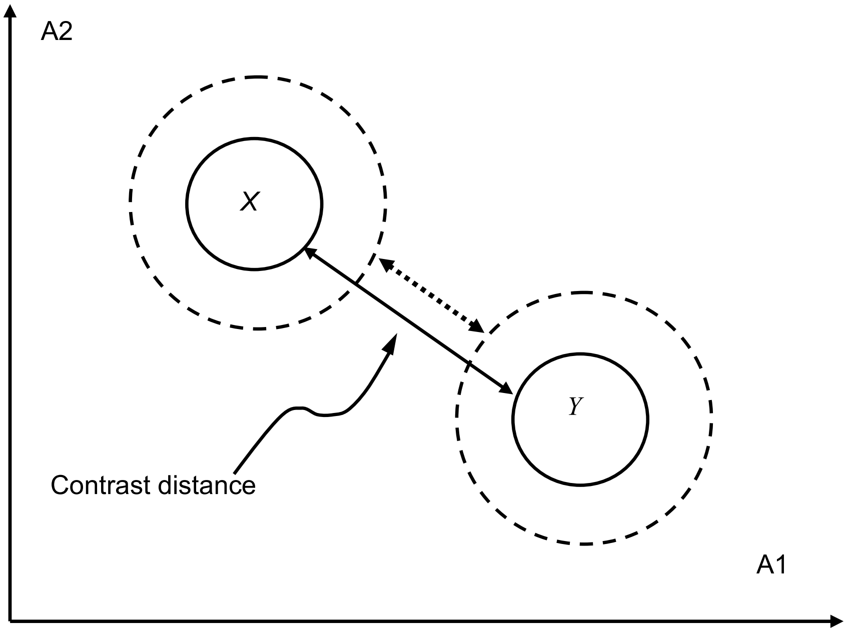

Figure 2.7: Relation between perceptual acuity and contrast distance for two hypothetical phonemes *X* and *Y*. The axes shown in this diagram are abstract auditory dimensions A1 and A2. Shown for both phonemes are the auditory goal regions for a more acute subject (solid, smaller circles) and a less acute subject (dashed, large circles). For subjects with greater auditory acuity, the contrast distance between these phonemes is larger, and vice versa. *Adapted with permission from Perkell, et al (unpublished).*

Chapter 3. Sensorimotor adaptation (SA) to acoustic perturbations in the first formant of vowels and relation to vowel spacing (Study 1).

As reflected in the function of the DIVA model, human speech production is expected to rely on auditory feedback. It follows then that speakers should adapt their speech production to acoustic perturbations in their speech. The experiment described here tests this prediction for vowels in voiced speech; additionally, it characterizes a number of properties of speech sensorimotor adaptation.

3.1. Review of past formant perturbation SA experiments

The initial speech-acoustic SA experiments (Houde and Jordan, 1998; Houde and Jordan, 2002) revealed several properties of the relationship between auditory feedback and speech production. The authors were able to demonstrate that subjects shifted the formant structure of the vowels they produced in response to altered formant structure of their speech that they heard over earphones (defined as *compensation*). This compensatory behavior persisted even when auditory feedback was blocked by masking noise (defined by them as *adaptation*)[4]. While only words containing vowel /ɛ/ were trained with perturbation, the resulting adaptive behavior (under masked noise) generalized to other vowels—such as /æ/ and /i/—which were not trained with altered feedback. Also, the adaptation generalized from the trained vowel presented in a particular phonetic context ("pep') with perturbed feedback to the same vowel presented in different phonetic contexts—e.g. "peg", "gep", and "teg—again presented with feedback again blocked with masking noise.

[4] Note that if the perturbation were removed without the substitution of masking noise, the subject could hear his unperturbed speech via bone conduction, in which case he might not continue to compensate for the previously-introduced perturbation. Thus, masking noise was necessary to test for the persistence of the compensation.

While the Houde and Jordan study revealed much about acoustic SA in speech, their paradigm had certain limitations. One major limitation was that the experiment was performed with whispered speech, as opposed to the normal voiced mode of speech. (Whispered speech was used for two reasons: (1) the authors wanted to minimize the perception of the unaltered speech heard through bone-conduction; and (2) the speech perturbation algorithm used in these experiments only worked with whispered speech.) Also, the researchers did not incorporate epochs (blocks of stimuli) that would measure aftereffect adaptation (i.e. persistence of the adapted behavior following return to normal feedback). Furthermore, while the perturbations were made of acoustic parameters (i.e. shifting the first and second formants), these perturbations and the resulting responses were measured in a phonetic dimension defined here as the “path projection”. Because adaptation and compensation measures incorporate this value, it is not obvious from the results how individual formants adapted; that is, one formant could have accounted for more of the response than the other. Note that in his doctoral thesis (Houde, 1997) examined individual formants for each of the participating subject; nevertheless, cross-subject trends in individual formants were not examined or summarized.

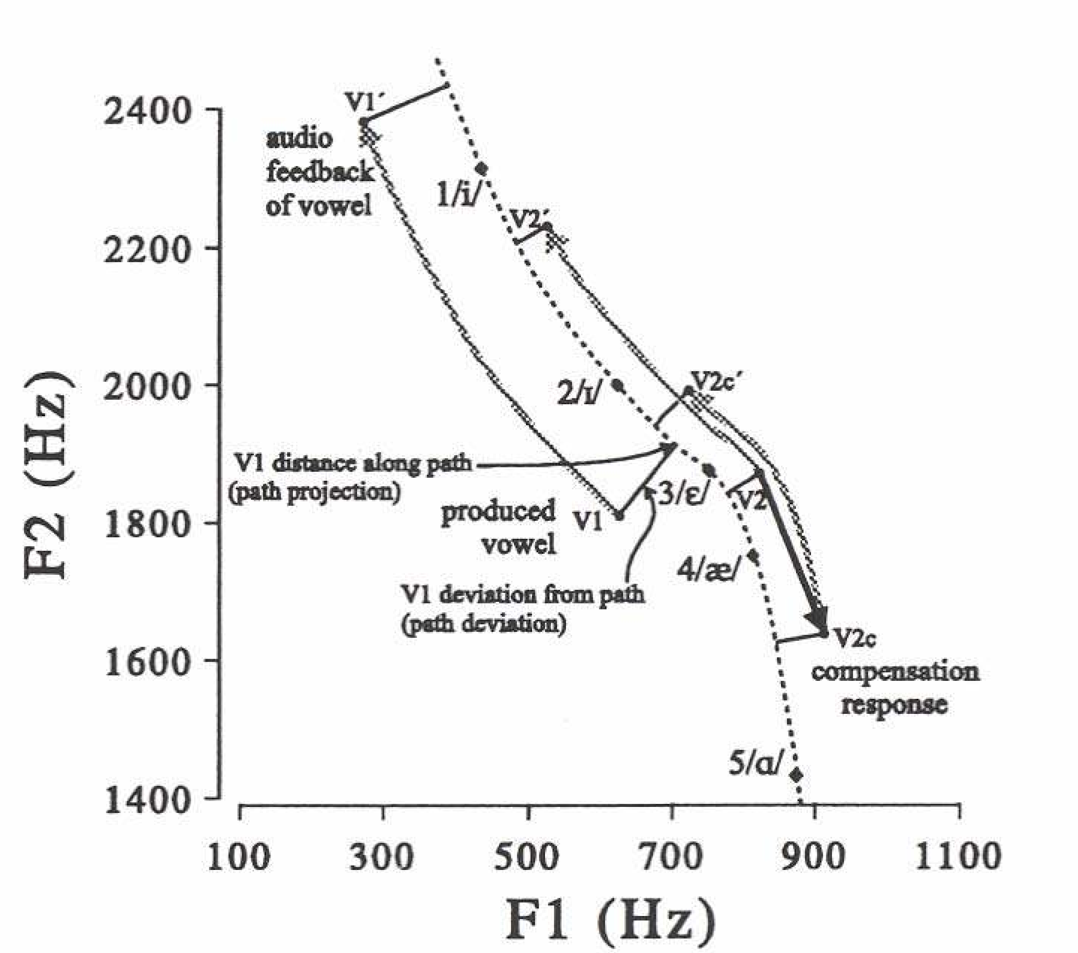

Figure 3.1: Feedback transformation used in the Houde and Jordan SA speech experiment. The dashed line shows specific subject's /i/ - /ɑ/ path in (F1, F2) space. This path is not straight, and the distance between vowels on the path is variable. The path projection is determined from the point on the /i/ - /ɑ/ path that is closest to the produced vowel, and this distance is normalized so that adjacent vowels have a path projection equal to 1.0. In this figure, the gray arrows show the action of the -2.0 transformation—one of the two formant-shifting audio transformations used in the experiments. The points V1, V2 and V2c refer to vowels as they are produced by the speaker during the SA experiment, while the prime-labeled points (V1', V2', and V2c') refer to vowels as perceived by the speaker (post-perturbation). The gray arrow pointing from V1 to V1' represents the audio feedback of the vowel at the onset of the perturbation, shifting the vowel from /ɛ/ towards /i/. The dark black arrow shows the compensatory response in the opposite direction, toward the vowel /ɑ/. The gray arrow from V2 to V2' represents the feedback with intermediate compensation; the gray arrow from V2c to V2' represents the feedback after the compensatory response. (Houde and Jordan, 2002).

Another speech SA experiment (Max et al., 2003; Wallace and Max, 2004) was performed with voiced speech; subjects in this experiment also demonstrated adaptation, with aftereffects persisting once the perturbation was removed. Additionally, the authors designed the experiment to allow simultaneous measure of articulatory movements: lip, jaw and tongue movements during the SA experiment were measured using an electromagnetic midsagittal articulograph. These measures demonstrated showed high amounts of inter-subject variability; that is, a variety of motor-equivalent vocal tract configurations were used to adapt to the acoustic perturbation (Wallace and Max, 2004).

It should be noted that this latter experiment (Max et al., 2003) utilized an acoustic perturbation that either shifted the fundamental frequency (F0), or shifted all of the formants in the same direction. This is an important distinction from the former SA experiment (Houde and Jordan, 1998)—as well as the acoustic perturbation discussed in this thesis (see Section 3.3.1). Changing the formants in the same direction essentially amounts to changing the perceived length of the vocal tract (e.g. shifting the formants up can be accounted for by shortening the vocal tract), while the formant perturbations used by Houde and Jordan presumably caused more complex perceived changes in vowel articulation (i.e. causing the perceived vowel to sound like another vowel).

3.2. Specific hypotheses of the sensorimotor adaptation experiment.

Previous findings (Houde and Jordan, 1998; Houde and Jordan, 2002; Max et al., 2003) confirm the DIVA model prediction of compensation and adaptation to acoustic perturbations of vowel formants. However, the experiment (study 1) described here differs significantly from previous studies, in order to test several specific properties of acoustic-speech SA simultaneously.

3.2.1. Adaptation properties measured in voiced speech.

The Houde and Jordan (2002) experiment measured a number of properties of adaptation using whispered speech, including *compensation* (referred to in study 1 as **+feedback adaptation**), “true” *adaptation* (referred to in study 1 as **-feedback adaptation**), and *generalization*, both to other vowels not perturbed and other phonetic contexts (referred to in study 1 as **generalized adaptation** to other vowels and phonetics contexts, respectively). These terms and their definitions are summarized in Appendix A. The study 1 protocol repeated these measurements, but for voiced speech. This is an important difference, since the normal mode of speaking is the voiced, not whispered, mode.

3.2.2. Aftereffect adaptation.

As a consequence of including a control experiment containing no perturbation one month after the real experiment, (Houde, 1997) reported in his doctoral dissertation that subjects' "compensating production changes … were retained over a period of more than one month" (pg 161). Because whispered speech is not the normal speaking mode, Houde surmised that the adaptation was maintained because the subjects did not unlearn the adapted changes for their whispered vowels. The study 1 protocol includes an immediate *post-perturbation phase*, in which subjects are given normal feedback after given *full perturbation* feedback. This allows for the measurement of **aftereffect adaptation**—that is, how long adaptive changes are maintained until they return to normal levels. (Max et al., 2003) do measure this property in their experiment, but again in an experiment using a different kind of perturbation (shifting all formant frequencies rather than individual formants).

3.2.3. Adaptation specificity.

Study 1 introduced an acoustic perturbation specific to the first formant (F1) of vowels. This differs from the study of Houde and Jordan (1998)**,** which induced a perturbation which shifted both F1 and F2 along a continuum that was specific to the subjects' vowel spacing. This also differs from the Max, Wallace & Vincent (2003) study, which shifted all formants spoken by a subject in the same direction.. By constraining the perturbation to F1, the specificity of adaptation is investigated in study 1.

The adaptation is hypothesized to be restricted to F1, since alterations in other formants will lead to error in the auditory representation of those formants. However, the physiological constraints of the vocal tract may limit the ability of speakers to manipulate formants independently. In the simple acoustic tube model of the vocal tract, the total length of the vocal tract is conserved; thus, altering the length of one cavity (for instance, shortening the longer cavity to increase F1) will also affect the length of the other vocal tract cavity, and consequently the formants that result from it (Stevens, 1998).

Moreover, it is possible that vowel formants are not perceived as their frequency values in isolation. Formant-ratio theory (Miller, 1989) proposes that vowels are perceived by metrics that are scaled by log-ratios of the formant frequencies and the fundamental frequency:

Equation 3.1:

$$\begin{aligned} y &= \log(F1/SR) \\ z &= \log(F2/F1) \\ x &= \log(F3/F2) \\ (SR &= 168(F0/168)^{1/3}) \end{aligned}$$

The formant-ratio theory presented in Equation 3.1 has been incorporated into the certain configurations of the DIVA model, and has been used to account for speech production training during developmental changes in vocal tract size (Callan et al., 2000). Relating Equation 3.1 to the current SA experiment, it is hypothesized here that adaptation will be evident in the second formant and the fundamental frequency, since the metrics (*y* and *z*) that incorporate perception of the first formant also involve these quantities. Further, Equation 3.1 implies that F0 and F2 should change in an inverse manner with regard to F1 adaptive changes.

3.2.4. Contribution of F0 to adaptation.

As mentioned above in 3.2.1, the acoustic perturbation of the current study is designed to work in voiced speech, as opposed to whispered speech used in Houde and Jordan (1998; Houde and Jordan, 2002) This approach allows the measurement of the fundamental frequency (F0), and allows the investigation of whether or not changes in F0 contribute to adaptation, as would occur if the adapted parameter were the difference or ratio between F1 and F0 (as discussed above in 3.2.3). Previous work involving lip-tube perturbations suggest that (at least for articulatory perturbations) acoustic compensatory strategies have incorporated the use of F0 (Menard et al., 2004; Menard et al., 2002).

3.2.5. Within token adaptation.

The data collection process of study 1 is designed to allow for the investigation of adaptation that occurs while a vowel is spoken. The hypothesis presented here is that subjects cannot react instantly to novel perturbations, so a lag in the compensatory action—within-token adaptation—should be evident and measurable. Thus, it is hypothesized that when the perturbation is introduced initially, subjects will produce unshifted formants in the initial portion of the vowel, but will shift F1 in the tail end of the vowel. As the exposure to the perturbation continues, subjects will begin to shift F1 earlier within the vowel until the subject eventually anticipates the perturbation, and produces a vowel with shifted formants throughout the word. (Figure 3.2 graphically depicts within-vowel adaptation described here.)

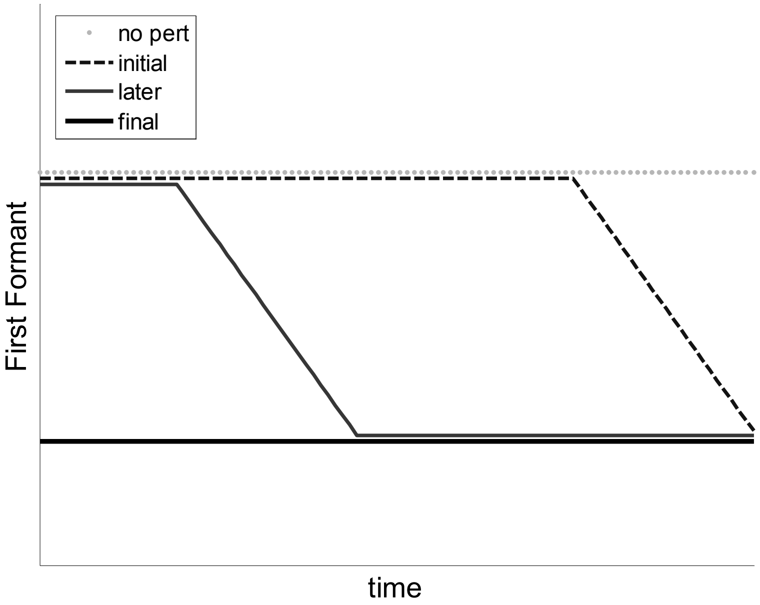

Figure 3.2: Idealized example of within token adaptation. Hypothesized data from a subject exposed to an auditory perturbation that shifts the first formant up. The first formant is plotted as a function of time throughout the produced vowel. The dotted line represents the baseline level of F1 (without exposure to acoustic perturbation). When subject initially experiences the acoustic perturbation, there is a lag in his reaction time to the perturbation, so that he can only shift F1 in the tail end of the vowel (dashed line). As subject continues to experience the acoustic perturbation, he is able to shift F1 earlier in the vowel (thinner, solid line), until the subject is able to anticipate the perturbation and shift F1 throughout the vowel (thicker, solid line).

3.3. Methodology of study 1: the sensorimotor adaptation (SA) experiment.

This experiment is composed of two essential components: 1) a method of shifting vowel formants (specifically F1) with minimal delay and 2) an easily repeated protocol designed to elicit adaptive responses in subjects.

3.3.1. Minimal delay formant shift in voiced speech.

The acoustic speech perturbation used in this experiment is designed to fulfill several design requirements. One requirement is that the perturbation must work on voiced speech; for this purpose, a method of shifting formants using linear prediction coding (LPC) analysis (Markel and Gray, 1976) was developed. Another constraint is that subject awareness of the perturbation should be minimized. Part of this constraint is fulfilled by the incremental changes in amount of perturbation made during the experiment (see Section 3.3.2). It is also fulfilled by minimizing the delay between when speaking and hearing the altered feedback, and by limiting the perturbation to vowels, as opposed to consonants within the carrier token.

A digital signal processing (DSP) algorithm was developed for realizing the formant shifts using a Texas Instruments C6701 Evaluation Module DSP board. (The signal processing theory used to design the formant shifting algorithm is addressed in further detail in Appendix A.) Figure 3.3 illustrates how the perturbation algorithm functioned. (The parenthetical numbers in the following three paragraphs refer to this figure.) The DSP board received an analog speech signal from the microphone and converted this signal to a digital signal (1), which is sent to the receiving (Rx) buffer. One of the first functions was to calculate the sum of all values within the Rx buffer to determine its amplitude (2), and then determine if this value was above or below a threshold value (3). The assumption made here is that buffers of the signal occurring within a vowel have large amplitude values. The threshold value was set so that values below it were not sent through the formant shifting algorithm (4), while values above it—presumably within a vowel—were sent to the formant shifting portion of the algorithm (5).

Assuming the Rx buffer is within a vowel, the signal is then pre-emphasized (6) to increase the amplitude of higher formants (thus improving the likelihood of the LPC analysis detecting them). The current Rx buffer was coupled with the previous buffer to create an analysis buffer of double the size (7), improving the frequency resolution. This buffer was then sent to the heart of the formant analysis—the autocorrelation linear prediction coding (LPC) block (8). The resulting output of this block is an 8th order polynomial, which can resolve up to the first four formants. However, to pick out individual formants from this polynomial, it was necessary to determine its complex roots. Here, a root-finding algorithm based on the Hessenberg QR method (Press et al., 2002) was used (9).

Once the complex roots were determined, it was fairly straightforward to determine and shift the first formant (F1). The roots were sorted based on angle of the complex root, which was directly related to the formant value it represents (10). Since complex conjugate pairs of roots determine each formant, the F1 is then determined from these sorted array of roots as the lowest non-negative, non-zero root (11). The root related to the shifted F1 was calculated by simply rotating the angle of the complex root representing the original F1 (12). A simple recursion formula was used to convert the roots of the original and shifted F1 values to polynomial coefficients (13). With new filter coefficients, the perturbation algorithm generated speech with the shifted F1 value. A direct-form II transposed filter (Oppenheim and Schafer, 1999) was used to filter data within the Rx (i.e. most current) buffer (14); it simultaneously zeroed out the original F1 (numerator coefficients), while also introducing the new perturbed F1 value (denominator coefficients).

Regardless of whether the current buffer was shifted (output of 14) or not (output of 4), the resulting speech was put into the transfer (Tx) buffer, which was converted back to an analog signal and sent to the output of the DSP board (15).

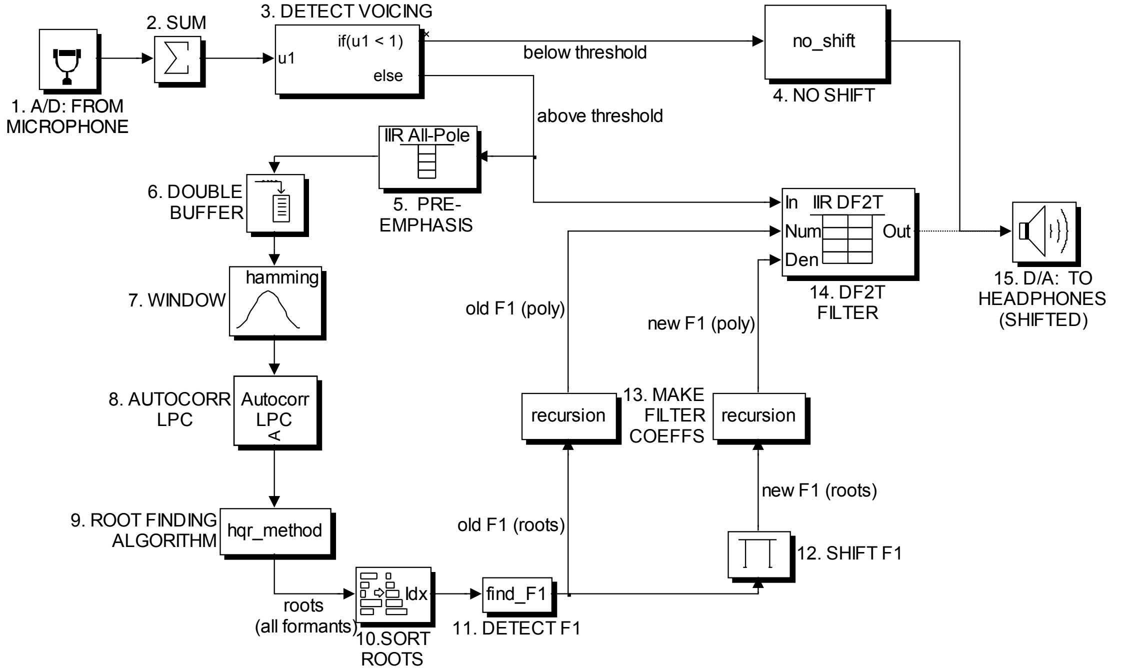

Figure 3.3: Formant shifting algorithm used to introduce acoustic perturbation in SA experiment. This algorithm programmed onto a DSP board takes in speech audio input at (1), and has either non-perturbed speech audio output (4) or shifted speech audio output (14). The shifted output (14) is perturbed if the pert value set at shift F1 (12) is not equal to unity. In either case, the output is converted to an audio signal (15) for playback via headphones. See the text (Section 3.3.1) for detailed explanation.

The Rx and Tx buffer lengths were set at 64 samples, but an error-checking double buffering scheme implemented in this board made the actual sample delay 128 samples. A few more samples of delay were introduced by the anti-aliasing filter implemented before the A/D conversion. At a sampling rate of 8000 Hz, this processing yielded a time delay between the subject's original speech and the processed speech (used for feedback) of 18 msec, which has been measured and verified.

The first formant was only shifted when the original formant fell within a certain window of frequencies:

Equation 3.2:

$$\begin{array}{ll} 250Hz < F1 < 950Hz & (male \quad subjects) \\ 400Hz < F1 < 950Hz & (female \quad subjects) \end{array}$$

F1 values below the lower limit of the window tended to be near the value of the fundamental frequency, while F1 values above the window's upper limit tended to be very close to the value of the second formant. That is, a formant value detected outside the window is likely to not be the actual F1, which is the reason for excluding these detected F1 values. However, it is possible that subjects can have F1 that naturally occurs outside of this window; this is a basis for rejecting data sets from certain subjects for further analysis (see 3.3.5). Note that, for a given buffer, when the board fails to detect F1 within the criterion values, or if that energy within that buffer falls below the threshold value, then that buffer is unaltered by the perturbation algorithm.

To simplify discussion of the formant shift made by the DSP board, a unit of formant shift—*perts*—is introduced here. *Perts* simply represent a multiplier of the original formant. A formant shift of 1.3 perts increased the formant by 130 percent (shift-up), while a 0.7 perts shift decreased the formant to 70 percent of its original value (shift-down). A formant shift of 1.0 perts indicates that the formant was not shifted.

3.3.2. Experimental design and protocol for SA training.

The SA experiment was set up so that the following cycle of events occurs during one presentation of a token (refer to Figure 3.4). A monitor in front of the subject displayed the token (a CVC word, such as "bet") for two seconds (1). The subject spoke into a Sony ECM-672 directional microphone six inches from the lips (2), utilizing visual cues that displayed the target loudness and duration of the vowel. This signal was digitized by an A/D board, and recorded for post-experiment analysis (3); the same speech signal was concurrently sent to the TI DSP board to synthesize formant shifted speech (4). This signal was sent to a feedback selector switch which determined, depending on which token was presented to the subject, whether the subject heard masking noise or the perturbed speech signal (5). The appropriate signal was then presented to the subject over Shure insert earphones (6). The perturbed speech signal from the TI DSP board, and the output signal from the selector switch were also digitized by an A/D board and saved for post-experiment analysis (not shown).

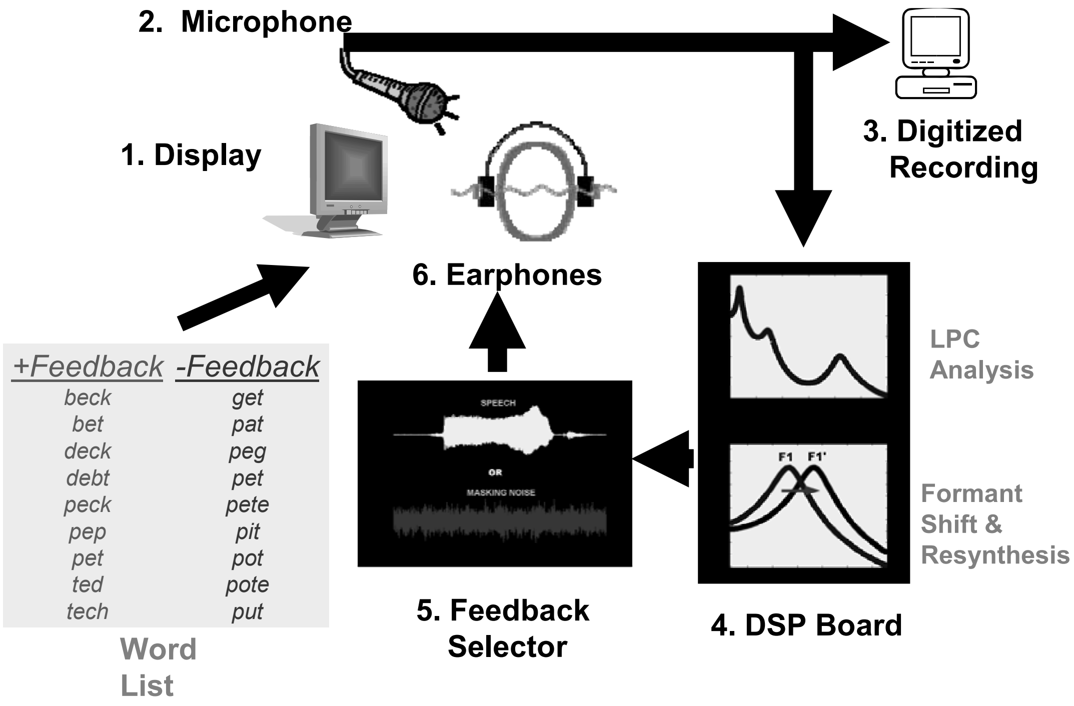

+Feedback	-Feedback
beck	get
bet	pat
deck	peg
debt	pet
peck	pete
pep	pit
pet	pot
ted	pote
tech	put

Figure 3.4: Outline of the cycle that occurred during the presentation of one token during the SA experiment. 1. A token from the word list was displayed on monitor. 2. The subject spoke this word into the microphone. 3. This signal was digitized for off-line analysis. 4. The signal was also processed by the DSP board, which used LPC analysis to shift F1. 5. The feedback selector determined whether subject heard the feedback speech signal (+feedback tokens) or masking noise without the feedback signal (-feedback tokens). 6. The desired signal was played to subject through insert earphones. See the text (Section 3.3.2) for a detailed explanation.

A total of 18 different tokens were selected for each subject for repeated presentation and speech recording (see Table 3.1 for a list of these 18 tokens). Nine of these words (*+feedback*) were presented with the subjects able to hear (perturbed or unperturbed) speech feedback over the earphones; all of these words contained the vowel /ɛ/ (the only trained vowel). The other nine words (*–feedback*) were presented with masking noise (87 dB SPL); this masking noise was loud enough to sufficiently mask the subject’s vowel quality. Three of the

–feedback words contained the vowel /ɛ/: one in the same phonetic context as the word presented in the *+feedback* list ("pet") and two in different phonetic contexts ("get" and "peg"). The other six *–feedback* words contained different vowels than the training vowel. The order of the +feedback tokens and –feedback tokens was randomized from epoch to epoch; however, all of the +feedback tokens were always presented before the –feedback tokens within an epoch.

+Feedback Tokens	- Feedback Tokens	(notes)
beck	***pat***	(these –feedback tokens contain a vowel that is different than /ɛ/, which is the only vowel present in the +feedback tokens)
bet	***pete***	
deck	***pit***	
debt	***pot***	
peck	***pote***	
pep	***put***	
pet	***pet***	(same /ɛ/ token)
ted	***get***	(contain /ɛ/ in a context different than "pet")
tech	***peg***	

Table 3.1: Tokens presented to the subject during the SA experiment. The left column shows all nine +feedback tokens; all of these tokens contained the vowel /ɛ/. The center column shows all nine –feedback tokens. As the comments in the right column explain, six tokens contained vowels different from /ɛ/. Three –feedback tokens contained the vowel /ɛ/; one token ("pet") was identical to the token presented in the +feedback case, while two others contained /ɛ/ in a different phonetic context.

For each subject, the SA experiment was divided into four phases: baseline, ramp, full perturbation and post-perturbation. This protocol is summarized in Figure 3.5. Each phase consisted of a fixed number of epochs, and each epoch was comprised of a single presentation of each of the eighteen tokens used in this study. The baseline phase consisted of the first 15 epochs, and was performed with the speech feedback set at 1.0 pert (no formant shift). The following ramp phase (epochs 16-20) was used to incrementally introduce the formant shift by increasing or decreasing the pert level by 0.05 pert per epoch. During the full perturbation phase (epochs 21-45), the speech feedback had either the 1.3 pert shift for shift-up subjects, or the 0.7 pert shift for shift-down subjects. During post-perturbation phase (epochs 46-65), the speech feedback was returned to 1.0 pert shift; this phase allowed for the measurement of the persistence of any adaptation learned during the full-perturbation phase. An entire experiment for one subject consisted of 65 epochs, comprising a total of 1170 tokens; the experiment lasted approximately 90 to 120 minutes.

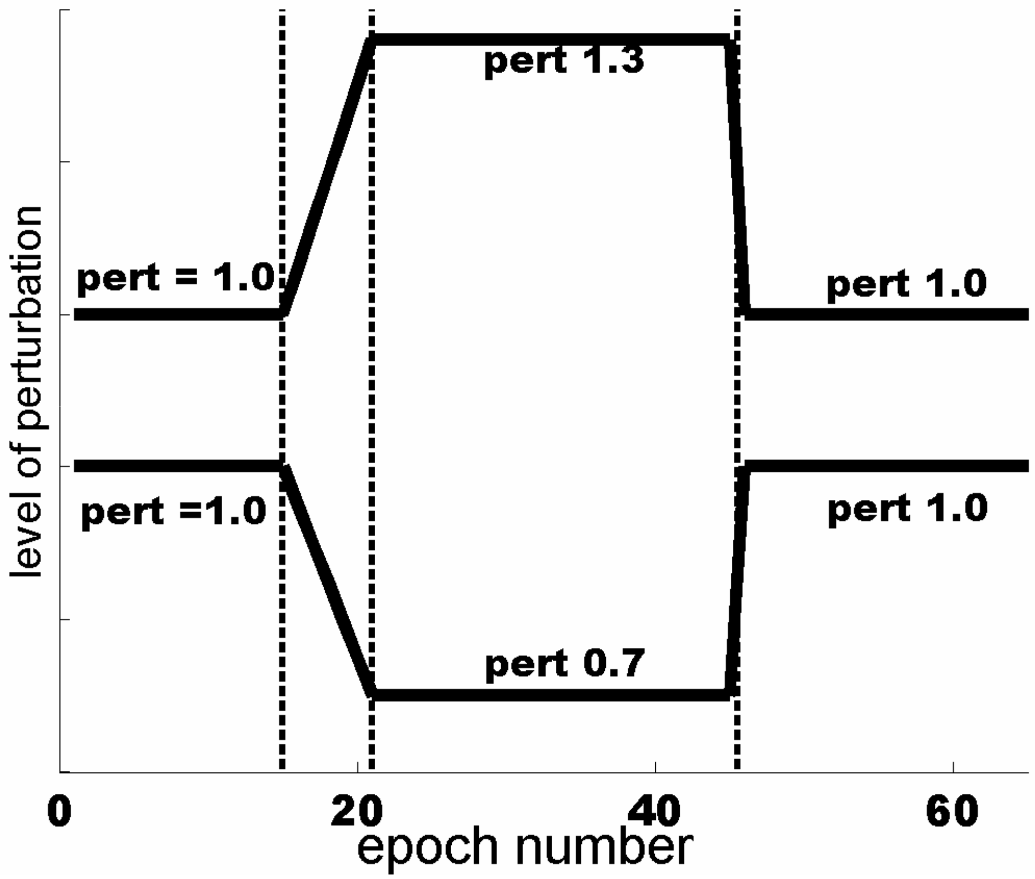

Figure 3.5: Diagram of the level of first formant perturbation presented during one experimental session, as a function of epoch number. The 65 epochs of an experimental session are divided into four phases (demarcated by dashed vertical lines). From left to right, these phases are baseline (epochs 1-15), ramp (epochs 16-20), full perturbation (epochs 21-45), and post-perturbation (epochs 46-65). Shown here are two possible types of experiments, the upper line indicating F1 shifted up, and the lower line indicating F1 shifted down. Refer to Section 3.3.2 for further explanation.

A separate pre-experiment phase (typically two to three epochs in duration) was conducted prior to the SA experiment. The beginning epochs of this phase were used to allow the subject to become accustomed to utilizing the on-screen cues to determine the ideal loudness and duration at which each word should be spoken. The target loudness was set at 69 dB SPL (+/- 2 dB), significantly less than the feedback loudness of 87 dB SPL. The target vowel duration was set at 300 msec, though the actual duration can be longer due to reaction delay.[5] The last preliminary epoch was used to determine if the loudness of the masking noise (87 dB SPL) was a tolerable for the subject, while still preventing the subject from discerning his or her own vowel quality[6].

3.3.3. Subject selection criteria and description.

Subjects who participated in the sensorimotor adaptation conformed to the following criteria: adult native speakers of North American English with normal hearing and speech abilities. Twenty-one subjects were run on this experiment: ten adult males and eleven adult females. One female subject was excluded from further analysis because initial analysis indicated that the DSP algorithm failed to detect her first formant (see Section 3.3.5). The remaining subjects had an age range from 18 to 44 with a median age of 21.

3.3.4. Vowel formant and F0 extraction.

While speech from both the microphone and from the output of the DSP board are digitized for recording, only the microphone (i.e. pre-perturbation) speech recordings are analyzed in the current work. Each recorded token—sampled at 16kHz—was labeled manually for the beginning and ending of the vowel on the sound-pressure waveform. Each labeled token was then analyzed for the first two formants utilizing an automated algorithm designed to minimize the occurrence of missing or spurious values. Formants were derived from an LPC spectrum taken over a sliding 30 msec window. This spectrum was repeatedly measured between 10% and 90% of the delimited vowel interval, in 5% increments, and the mean formant values over these repeated measures were recorded. The majority of the analysis uses an “optimal” LPC order determined by a heuristic method which utilizes a reflection coefficient cutoff (Vallabha and

[5] Target loudness and word duration were achieved via visual cues displayed on the monitor. The displayed loudness cue displayed the SPL as a bar with the ideal range marked off. The duration cue consisted of a change in display background color from white to gray after 300msec from the onset of voicing.

[6] This was determined by asking the subject if they could hear themselves speaking.

Tuller, 2002). For subjects with a large number of missing or spurious formants, the analysis was repeated using LPC orders of 14 to 17 inclusive.

The fundamental frequency (F0) was calculated from each token using a pitch estimator that is based on a modified autocorrelation analysis method (Markel and Gray, 1976). For certain tokens, F0 appeared to be under-estimated, so F0 values that were below 50 Hz were excluded from analysis. For all but one subject, this exclusion criterion removed less than 3 percent of the tokens. One subject had 44 percent of tokens excluded by this criterion, so this subject was removed from the F0 analysis.

3.3.5. Rejection of an SA subject from analysis based on produced F1.

The algorithm coded on the DSP board requires that F1 is shifted only when it falls within a certain range of frequencies. However, if a number of the subject's tokens have F1 falling outside of this range, especially during the ramp and full-pert phases, then it is unlikely that the subject will hear the perturbation in his or her speech, which is necessary to cause adaptation. To determine the extent of this possible occurrence, +feedback tokens within epochs 16-45 (the ramp and full-pert phase) were analyzed for their mean F1 value. The number of tokens that had F1 values falling outside the following range of frequencies were then counted:

Equation 3.3:

$$\begin{aligned} &250Hz < F1_{mean} < 950Hz \qquad &(male \quad subjects) \\ &400Hz < F1_{mean} < 950Hz \qquad &(female \quad subjects) \end{aligned}$$

For the count of missed tokens, the acceptable range is narrower than the acceptable range programmed into the board (Equation 3.2) because the F1 used in this analysis represents the mean F1 within a token; it is possible that a significant part of the token had F1 fall outside the range set by (Equation 3.2) while its mean may fall within it.

Figure 3.6 demonstrates the percentage of tokens (out of nine + feedback tokens times 30 epochs or 270 total tokens) that, during any pert phase, had F1 outside the range set in Equation 3.3. Twenty of the subjects had less than five percent of their tokens rejected, while subject 21 had more than 35 percent of her tokens rejected. Data from this subject were not used for further analysis, because a significant portion of her tokens would not have been perturbed acoustically.

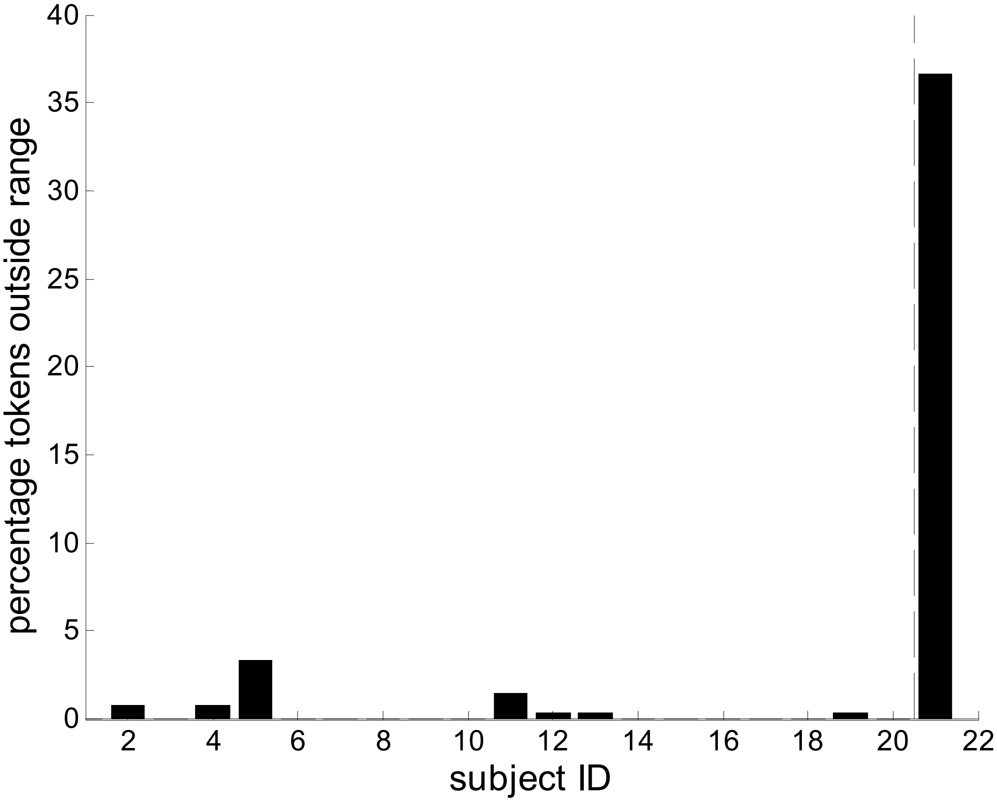

Figure 3.6: Percentage of tokens with F1 outside the window of frequencies which is shifted by the DSP algorithm. The ordinate is the percentage of tokens (out of 270) with F1 outside of the window of frequencies indicated by Equation 3.3. This is a narrower acceptable range than was actually programmed into the DSP algorithm (Equation 3.2). The abscissa indicates subject identification number. Only the +feedback tokens during the ramp and full pert phases were analyzed to calculate this percentage. The bars to the left of the dashed line indicate that less than 5 percent of the tokens had F1 outside the acceptable range, while subject 21 (bar to the right of the dashed line) had over 35 percent of tokens outside the acceptable range.

3.4. Results and analysis of the sensorimotor adaptation experiment.

Results for study 1 are summarized in this section, and address the specific aims and hypotheses proposed in Section 3.2. To allow comparison among subjects with differing baseline formants—especially differences related to gender, F1 values were initially normalized to each subject's mean value of F1 during the entire baseline phase (epochs 1-15). As shown in Figure 3.7, both the 1.3 pert and 0.7 pert subjects showed a gradually increasing F1 value *during* the baseline (in spite of the calibration phase in which all subjects were run before the experiment). This increased F1 during the baseline may be a concern when the rest of the data are normalized to these values; note that the 0.7 pert subjects (upper curve) appear to not return to baseline, while the 1.3 pert subjects (lower curve) seem to overshoot the baseline.

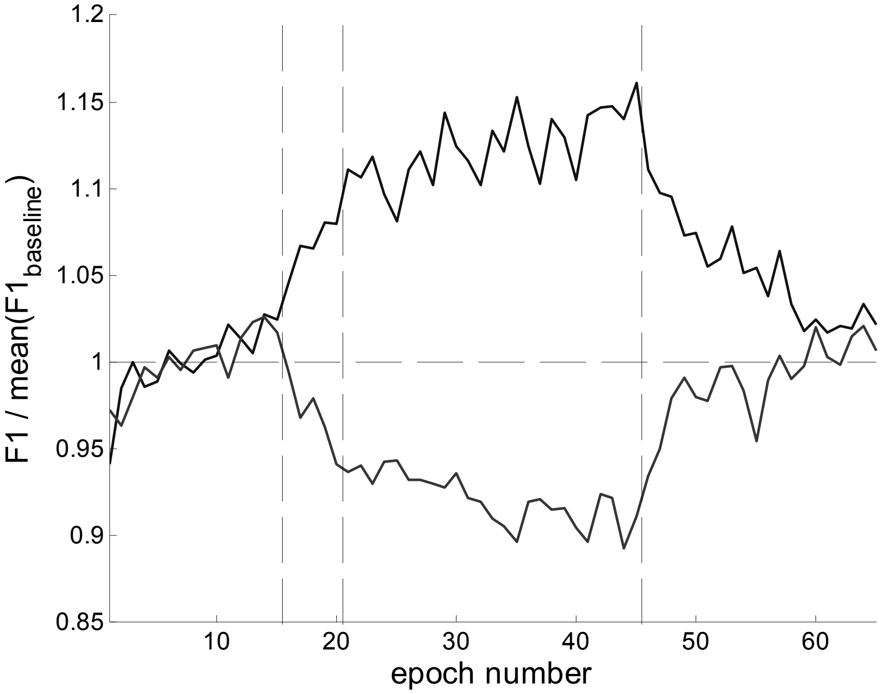

Figure 3.7: Produced first formants, normalized to the mean baseline value, in +feedback words for all subjects. The ordinate corresponds to the formant normalized by the baseline. The abscissa shows the epoch number during the SA experiment. The upper curve corresponds to normalized F1 for the ten subjects run on the 0.7 pert protocol; the lower curve corresponds to the 1.3 pert protocol. Each data point is the mean value of the nine +feedback words for all ten subjects (five male, five female). The dashed vertical lines show the phase transitions of the protocol; the dashed horizontal line corresponds to the baseline F1 values.

To account for the low F1 values in the early part of the baseline phase, the normalization (shown in Equation 3.4) instead used epochs 6-15 (an adjusted baseline phase).

Equation 3.4:
$$norm\_F1 = F1_{full\ \ pert\ \ epoch} / mean(F1)_{adjusted\ \ baseline\ \ phase}$$

Figure 3.8 shows F1 and F2—normalized to the mean formant values during the adjusted baseline phase—for the +feedback tokens of all subjects. This figure shows that subjects adapted their first formant in a manner that compensated partially for the acoustic perturbation to which they were exposed. Subjects ran on the 0.7 pert protocol increased F1 during the experiment (black line), while subjects ran on the 1.3 pert protocol decreased F1 during the experiment (dark gray line).

It is important to note that the standard error here (and in further analyses) represents inter-subject variation. In other words, the mean of all +feedback for a given subject was first calculated at every epoch (thus averaging out phonetic context-dependent variation). The mean and the variation shown in Figure 3.8 was then calculated over all 10 subjects.

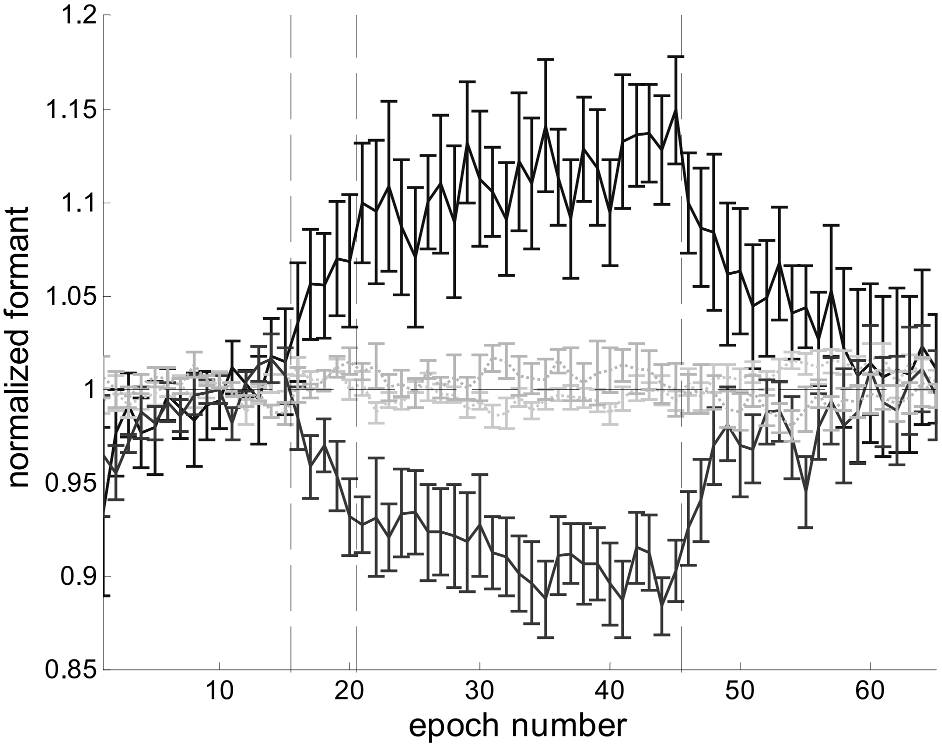

Figure 3.8: Produced first and second formant frequencies, normalized to the adjusted baseline, in +feedback words for all subjects. This is similar to **Figure 3.7**, except that all formants are normalized to the adjusted baseline (epochs 6-15). The normalized F2 values are shown as the lighter curves. The error bars depict the standard error of the mean among ten subjects.

To allow the combination of 0.7 pert subject data with 1.3 pert subject data, the measures *adaptive response* and *adaptive response index* are defined here and used in further analysis.

3.4.1. Adaptive Response Index.

The normalized formant obtained from each subject's SA experiment represents the mean F1 value of all +feedback words spoken during the full pert epochs, normalized by the mean F1 value of all +feedback words spoken during the baseline epochs (Equation 3.4). To highlight that change from baseline (normalized F1 = 1.0), and to allow the combination of scores from 0.7 pert subjects with 1.3 pert subjects, the following transformation was also made according to Equation 3.5:

Equation 3.5:

$$ARI = \begin{cases} mean(norm\_F1-1)_{full\ \ pert\ \ phase}, & if\ pert = 0.7 \\ mean(1-norm\_F1)_{full\ \ pert\ \ phase}, & if\ pert = 1.3 \end{cases}$$

For individual subjects, a value of the ARI > 0 indicated that the subject shifted F1 in a manner that compensated for (i.e. was in the opposite direction of) the perturbation, while values of the ARI<0 indicated that F1 shifted in a manner that followed (i.e. was in the same direction of) the perturbation. Similar transformations were made to measure the adaptive response index in normalized F2 (ARI_{F2}), and in the normalized F1 of –feedback /ɛ/ tokens ($ARI_{-feedback}$). (For convenience, Table 3.2—at the end of Section 3.4.3—contains a summary of all *ARI* values reported for study 1.) Unless otherwise noted, the statistics also reported with *ARI* values are determined from a two-tail t-test which tests the hypothesis that the value is significantly different from baseline (*ARI* = 0); the p-value corresponds to the probability that the null-hypothesis is supported (i.e. the value is not significantly different from zero).

The adaptive response (*AR*) is defined similarly to Equation 3.5, but using the normalized formant of a given token (rather than the mean over the entire full pert phase):

Equation 3.6:
$$AR = \begin{cases} norm\_F1 - 1, & if\ pert = 0.7 \\ 1 - norm\_F1, & if\ pert = 1.3 \end{cases}$$

For comparison, the adaptive response for the 0.7 pert and 1.3 pert subjects are shown in Figure 3.9. The adaptive response in the 0.7 pert subjects appear to be slightly larger than in 1.3 pert subjects, but the two groups have scores within the standard error of each other. To determine whether the two subject groups, represented in this way, came from distributions of the same mean, two-tailed t-test ($p < 0.05$) analysis between the two groups was performed on an epoch-by-epoch basis. This analysis determined that the two groups were statistically distinct only in epoch 2.

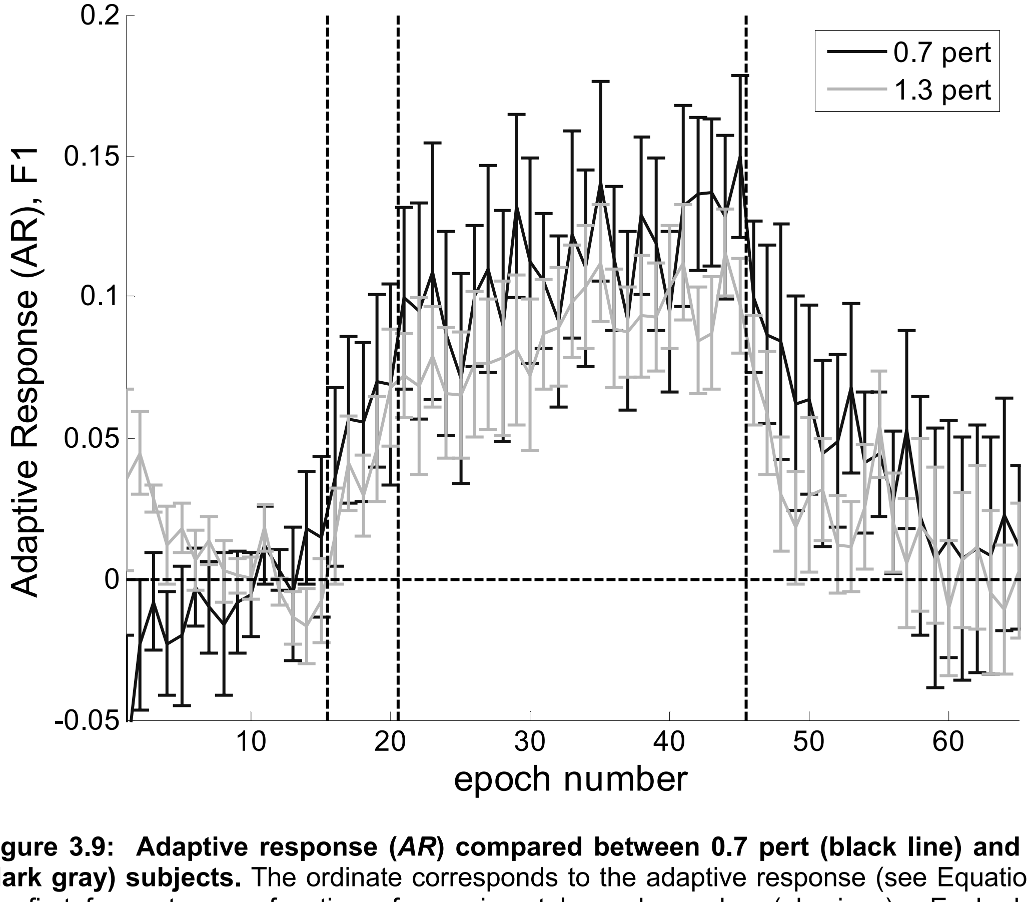

Figure 3.9: Adaptive response (*AR*) compared between 0.7 pert (black line) and 1.3 pert (dark gray) subjects. The ordinate corresponds to the adaptive response (see Equation 3.6) of the first formant, as a function of experimental epoch number (abscissa). Each data point represents the context-average mean of ten subjects (five male, five female); the error bars depict the standard error about the mean. The baseline and the transition epochs in the experimental protocol are represented by the dashed horizontal and vertical lines, respectively

Since the two subject groups did not statistically differ, they were subsequently combined into one group of twenty subjects for the remaining analysis in this chapter. Note that analysis in this chapter investigates trends of the average performance on the SA protocol; performance on the SA protocol by individual subject can be found in Appendix C**.**

3.4.2. Analysis of +feedback adaptation.

Figure 3.10 depicts the *AR* changes for F1 +feedback tokens, demonstrating that subjects do adapt their speech to the acoustic perturbation, and that this adaptation occurs significantly for F1. Data points marked by the black circle indicate that the *AR* for that epoch was significantly increased from baseline, as determined from a right-tailed t-test ($p < 0.05$).

The *ARI* for F1 *(ARI_{F1})* for all subjects increased from baseline to 0.998 in the full-pert phase (refer Table 3.2), and all epochs during the full-pert phase were significantly increased from baseline. As a whole, subjects are sensitive to the acoustic perturbation, with the first significant increase ARI_{F1} occurring during the second epoch in the ramp phase (epoch 17). Aftereffect adaptation is also evident in the +feedback adaptation results, and is also highlighted in Figure 3.10: AR_{F1} remains significantly increased during the post-pert phase (epochs 46-65) until after epoch 55 (roughly 15 to 20 minutes into the post-pert phase). Note that even after epoch 55, AR_{F1} is still above the baseline (though this increase is not significant).

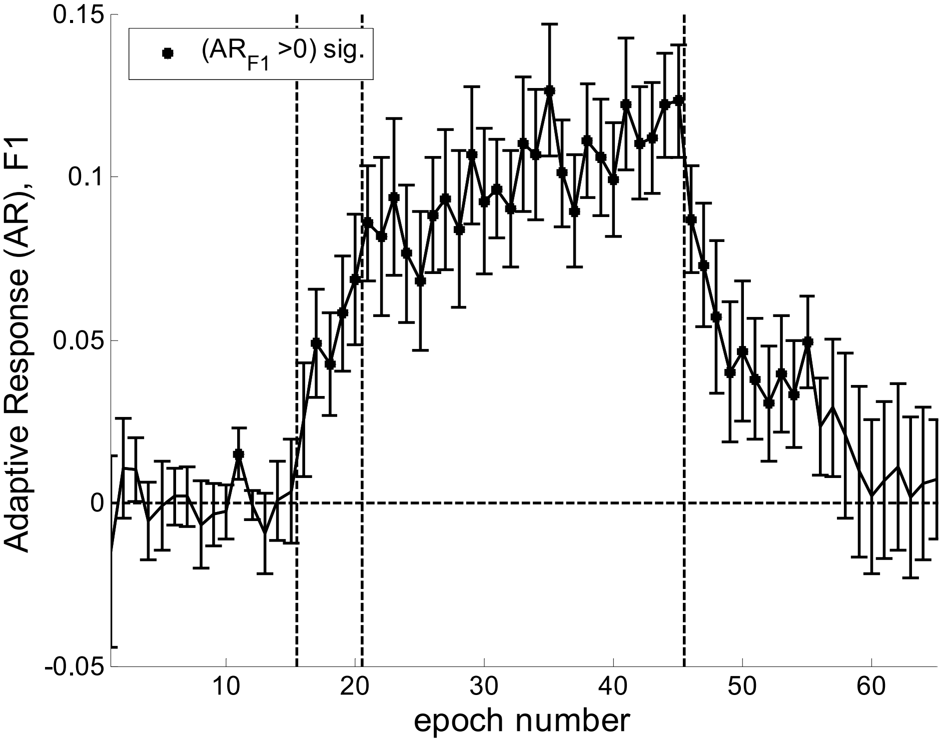

Figure 3.10: Adaptive response (*AR*) for the first formant in +feedback words for all subjects. Each data point representing the context-averaged mean for all twenty subjects (ten male, ten female); the error bars depict the standard error about the mean. The filled in circles indicate that AR_{F1} for that epoch represents a significant increase from baseline ($p < 0.05$). Refer to Figure 3.9 for axes details.

The data presented in Figure 3.11 were used to investigate the issue of specificity of the adaptation to just F1. The increase in adaptive response in F1 (Figure 3.10) during the full pert phase (ARI_{F1}) is sixteen times greater than the comparable measure in F2: $ARI_{F2} = -6.3\text{x}10^{-3}$ (refer to Table 3.2). This can be seen graphically by comparing the scale of in Figure 3.11 (for F2) with that of Figure 3.10. Moreover, AR_{F2} is significantly[7] different from zero in only three of the twenty-five full-pert epochs, as represented by the open circled points in Figure 3.11.

[7] Two-tailed, t-test (testing only if the change in F2 was *different* from the baseline value) was used to determine statistical significance for the adaptive response in F2.

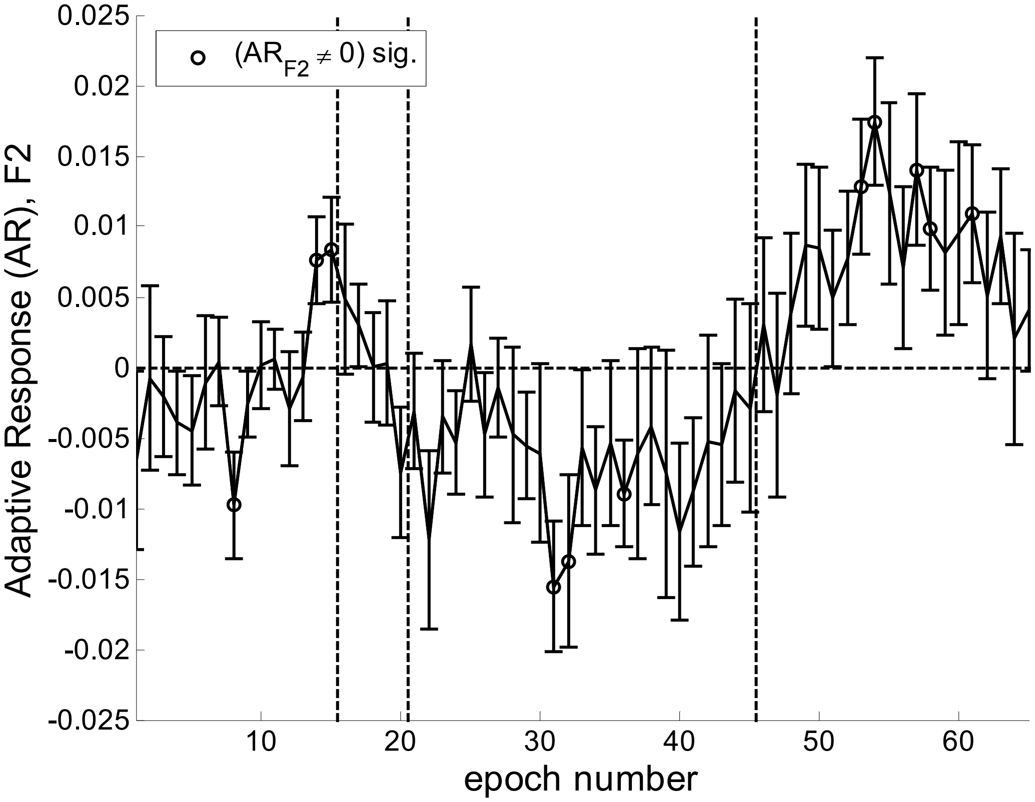

Figure 3.11: Adaptive response (*AR*) for the second formant in +feedback words for all subjects. The ordinate corresponds to the adaptive response (see Equation 3.6) of the second formant, as a function of experimental epoch number (abscissa). Each data point representing the mean value of the nine +feedback words for all twenty subjects (ten male, ten female); the error bars depict the standard error about the mean. The filled in circles indicate that AR_{F2} for that epoch represents the point is significantly different from baseline ($p < 0.05$). The baseline and the transition epochs in the experimental protocol are represented by the dashed horizontal and vertical lines, respectively.

Interestingly, nearly all of the changes in AR_{F2} during the post-pert phase are significant, and the direction that AR_{F2} changed to appears to be in the opposite direction that AR_{F1} changed. Figure 3.12 further investigates this relation, showing how the mean AR_{F1} (averaged over all subjects in an epoch) co-varies with mean AR_{F2} from the ramp phase through the post-pert phase parts of the experiment. For this subset of epochs, the adaptive responses for F1 and F2 are inversely related with significant correlation ($r = -0.65$, $p < 0.001$). For comparison, the relation between mean AR_{F1} and mean AR_{F2} in the baseline phase is shown in Figure 3.13; the lack of significant correlation between F1 and

F2 in the baseline suggests that the significant relation between changes in the two formants results in response to the SA protocol. It should be noted that more points were used in the correlation in Figure 3.12 than in Figure 3.13 (50 points versus 15 points); the fewer points used in the correlation in Figure 3.13 could partly account for the lack of significance.

As discussed in Section 3.2.3, this inverse relation may be the result of the physiological constraints of the vocal tract. On the other hand, it may also result from constraints on how auditory dimensions for vowels are represented (such as in Miller ratio dimensions). It is important to note that the variability within the second formant is small (+/-0.015 pert, which would correspond to roughly +/- 15-30 Hz for F2); thus, even if the F2 alterations were significant, they were still minor contributing factors in the overall adaptation. (Appendix D addresses the issue of whether or not the changes in F2 production result from the perturbation algorithm introducing an unintended shift in F2).

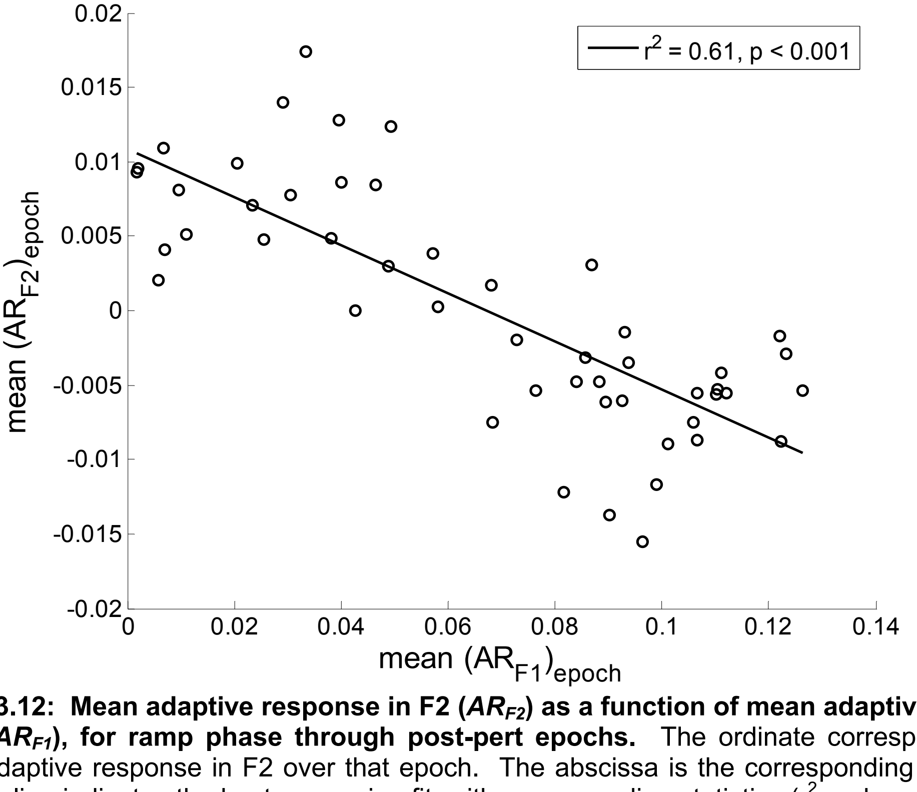

Figure 3.12: Mean adaptive response in F2 (*AR_{F2}*) as a function of mean adaptive response in F1 (*AR_{F1}*), for ramp phase through post-pert epochs. The ordinate corresponds to the mean adaptive response in F2 over that epoch. The abscissa is the corresponding measure in F1. The line indicates the best regression fit, with corresponding statistics (r^2 and p value) shown in the legend.

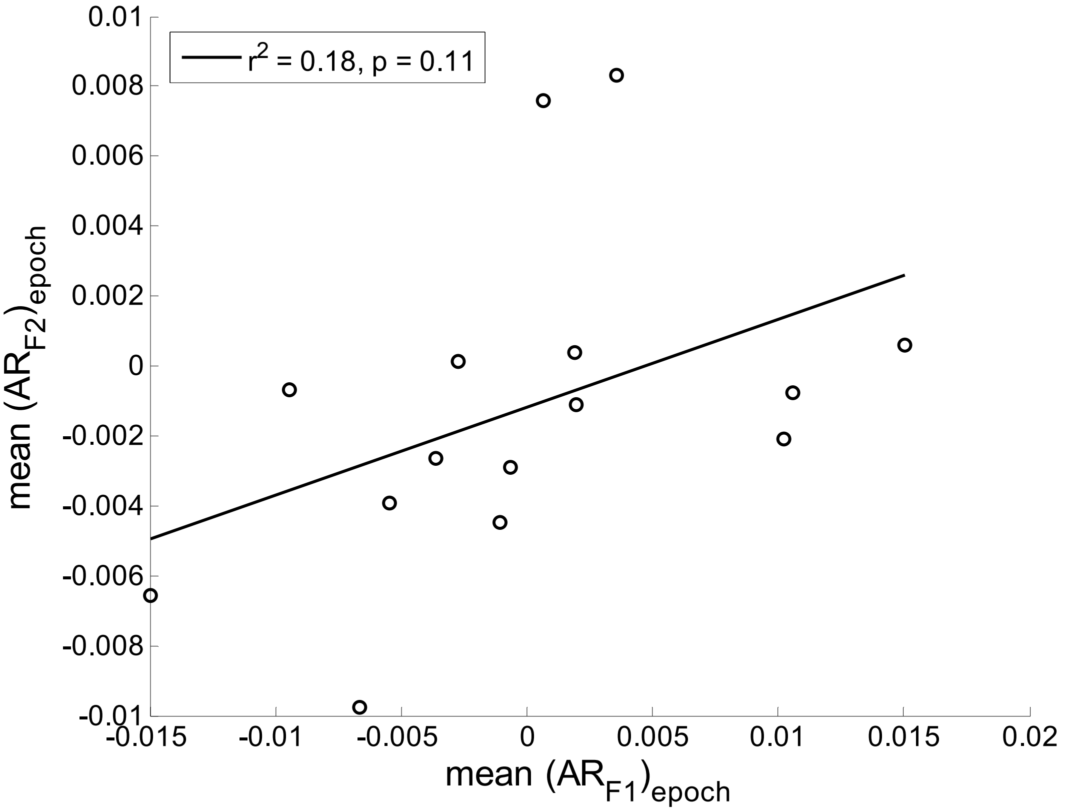

Figure 3.13: Mean adaptive response in F2 (*AR_{F2}*) as a function of mean adaptive response in F1 (*AR_{F1}*), for baseline epochs. This is similar to Figure 3.12, except that only the baseline phase epochs are represented here.

3.4.3. Analysis of –feedback adaptation for the vowel /ɛ/.

The SA wordlist (Table 3.1) contained tokens that were presented without feedback, but which contained the same vowel the subjects heard with full perturbation (/ɛ/). Absent any countering feedback (e.g. somatosensory feedback), the DIVA model predicts that the adaptation learned for /ɛ/ should be maintained even when no acoustic feedback exists. Indeed, Houde and Jordan (2002) demonstrate that such adaptation is maintained, and will generalize to other presentations of the same vowel in different contexts.

In study 1, results –feedback adaptation for /ɛ/ are divided into two groups: -feedback adaptation for the *same context* token, and –feedback adaptation for *different context* tokens. The same context token is the token “pet”, and this refers to the fact that this token is also contained in the +feedback wordlist. The different context tokens are the tokens “get” and “peg”; these tokens were not present in the + feedback wordlist. These results are summarized in Figure 3.14 (same context) and Figure 3.15 (different context), and are depicted in a similar manner to the F1 analysis in 3.4.2.

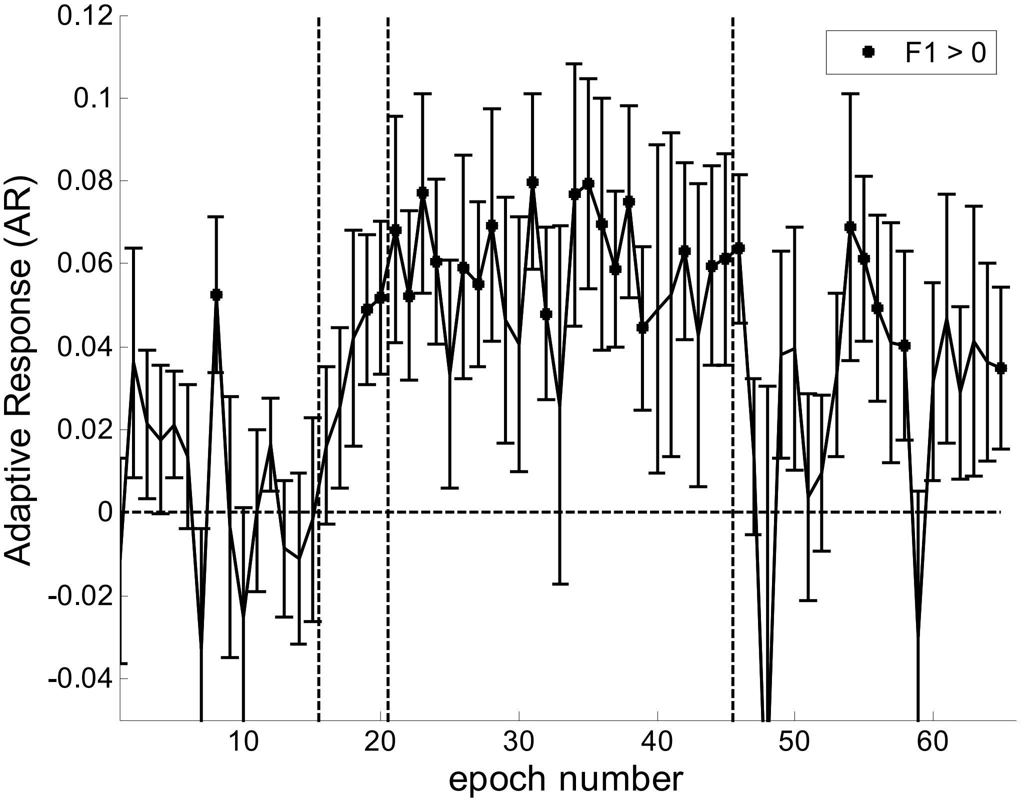

Figure 3.14: Adaptive response (AR) for the first formant of the –feedback token “pet” (the same context token) for all subjects exposed to 0.7 pert in F1. Same context token refers to the fact that “pet” is found in the +feedback wordlist and the –feedback wordlist. Each data point is the mean value of twenty tokens: the one –feedback token “pet” for each of the twenty subjects (ten male, ten female); the error bars depict the standard error about the mean. Refer to Figure 3.10 for further details.

Figure 3.14 indicates that the adaptation learned from the +feedback tokens does indeed transfer to the –feedback tokens with the same vowel, same context condition. The *ARI* for the –feedback “pet” tokens is significantly increased (p < 0.001) from baseline with a value of 0.0579 +/- 0.0055 (refer Table 3.2). This *ARI* value was less (by almost half) of the *ARI* reported F1 in the +feedback tokens: 0.0993 +/- 0.0016 (refer to Section 3.4.2). For better comparison, the

ARI of just the +feedback “pet” tokens was also calculated, and determined to be 0.0984 +/- 0.0044 (also significant with p <0.001)—still greater than the *ARI* of the –feedback “pet” token (refer Table 3.2). The result of lower adaptation in the –feedback tokens confirms a result seen in Houde and Jordan (2002), and is expected if the subject can rely on other sources of feedback that the acoustic perturbation does not immediately influence, such as somatosensory feedback (refer to Section 2.2).

Figure 3.15 shows that the adaptation generalizes to –feedback tokens of the vowel /ɛ/, even when that vowel is contained in a different context from those tokens which received perturbed feedback. The combined *ARI* value found for the “get” and “peg” tokens (different context) is 0.0669 +/- 0.0041 (refer Table 3.2). While this value is less than the *ARI* of +feedback /ɛ/ tokens (confirming the result found above), it is slightly higher than the *ARI* found for the –feedback “pet” token (same context). However, paired t-test analysis of *AR* scores during the full-pert phase was performed between the *same context* scores and the *different context* scores, and showed that the two groups of –feedback tokens did not differ significantly (p > 0.05).

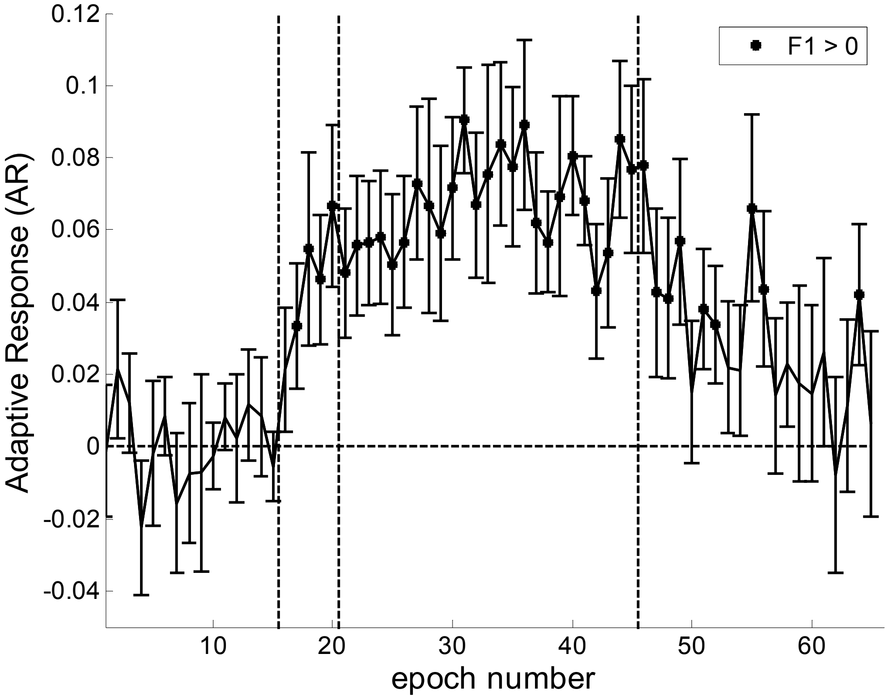

Figure 3.15: Adaptive response (*AR*) for the first formant of the –feedback token "get" and "peg" combined (the *different context* tokens) for all subjects exposed to 0.7 pert in F1. *Different context* token refers to the fact that "peg" and "get" are found only in the –feedback wordlist, though they do contain the vowel /ɛ/, which subjects did hear perturbed in the +feedback tokens . Each data point is the mean value for all subjects for the two –feedback token "peg" and "get"; error bars depict the standard error about the mean. Refer to Figure 3.10 for further details.

The adaptive response index results from Sections 3.4.2 and 3.4.3 are summarized in Table 3.2. For comparison to previous work, comparable measures to the + feedback (F1), -feedback w/ same context, and – feedback w/ different context conditions were derived from the figures contained in Houde and Jordan (1998) by taking the mean across subjects for the *compensation, adaptation*, and *generalization* values reported. As mentioned previously the type of perturbation and thus the metric used to measure response in Houde and Jordan differ from this study. However, this table is informative because both studies indicate the relative order of responses as the following: *+feedback* > *different context –feedback* > *same context –feedback*.

	ARI	std. dev.	Houde & Jordan response (est)
+feedback, F1	0.0993	+/-0.0016	0.55
+feedback, F2	-0.0062	+/-0.0041	*
(below are for F1 only)			
+feedback, same context (pet)	0.0984	+/-0.0044	n/a
-feedback, same context (pet)	0.0579	+/-0.0055	0.32
-feedback, different context (peg and get)	0.0669	+/-0.0041	0.43

Table 3.2: Summary of adaptive response index (ARI) calculated in study 1. ARI calculated according to **Equation 3.5**. This table summarizes all mean ARI values (calculated over the full-pert phase) reported in Section 3.4. The right column displays results derived from figures found in Houde and Jordan (1998). While their results use a different metric than in study 1, the relative orders of the measures are informative.

3.4.4. Analysis of generalized adaptation for multiple vowels.

As indicated in the SA protocol wordlist (Table 3.1), several –feedback tokens contained different vowels from the one subjects received with acoustically perturbed feedback (/ɛ/). These tokens were included in the protocol to establish the degree to which adaptation can generalize to unperturbed vowels. Figure 3.16 - Figure 3.19 summarizes the amount of adaptation found in the following vowels: /I/ (“pit”), /i/ (“pete”), /æ/ (“pat”), /ɑ/ (“pot”), /Λ/ (“put”), and /o/ (“pote”).

The –feedback token /ɛ/ is also displayed for comparison. In these figures, subjects were subdivided into four groups (five subjects each), based on gender and pert level used in the SA protocol (0.7 pert or 1.3 pert). For each vowel, the mean F1 and F2 (in mel scale) are shown for the full baseline (epochs 1-15, labeled as **1**), full pert (epochs 21-45, labeled as **2**) and post-pert (epochs 46-65, labeled as **3**) phases. For convenience, the arrow on each figure shows the direction of the acoustic perturbation. (Note that data presented are separated on the basis of gender because non-normalized formant frequencies are used, and male speakers tend to have lower formants than female speakers.)

Overall, the adaptation generalized to other vowels. This is observed in Figure 3.16 (females) and Figure 3.17 (males) by the shifting of the max-pert phase (**2**) to the right (increased F1) of the baseline phase (**1**) when the acoustic perturbation shifted F1 down. Similarly, Figure 3.18 (females) and Figure 3.19 (males) show that an upwards F1 acoustic perturbation is accompanied by a shift of the full-pert phase (**2**) to the left (i.e. a decrease) of the baseline phase (**1**). On a mel scale, the adaptation seen in the vowels /I/, /æ/, and /ɑ/ was consistently as large, or even larger (see /æ/ and /ɑ/ Figure 3.18 and Figure 3.19).

Exceptions to the generalization of vowel adaptation have been observed. For the vowel /i/, changes in F1 were either small in the female subjects or insignificant—that is, not outside the standard error—in the male subjects. For the vowel /o/, significant adaptation was observed in all conditions except the 1.3 pert male subjects (Figure 3.19). In this same set of subjects, the vowel /Λ/ is observed to change in the same direction as the adaptation, as opposed to a compensatory direction (Figure 3.19). Finally, while the adaptation was specific to F1 in most cases, the 0.7 pert female subjects showed changes in F2 (outside the standard error) for the vowels /Λ/, /o/, and /ɑ/ (Figure 3.16).

The degree to which subjects returned to the baseline vowel positions during the post-pert phase (**3**) was variable, though most vowels that showed an adaptive response also showed at least partial return to baseline. Close to full return to baseline was exhibited in many of the post-pert phase (**3**) vowels—specifically /I/, /ɛ/, /æ/ and /ɑ/—from the subjects shown in Figure 3.19 (1.3 pert males subjects). On the other hand, little return to baseline was evident in several instances: /U/ for 0.7 pert female subjects (Figure 3.16), /æ/ for 0.7 males subjects (Figure 3.17), and the /o/ and /ɑ/ vowels of 1.3 female subjects (Figure 3.18). The remaining vowels returned to baseline to an intermediate degree.

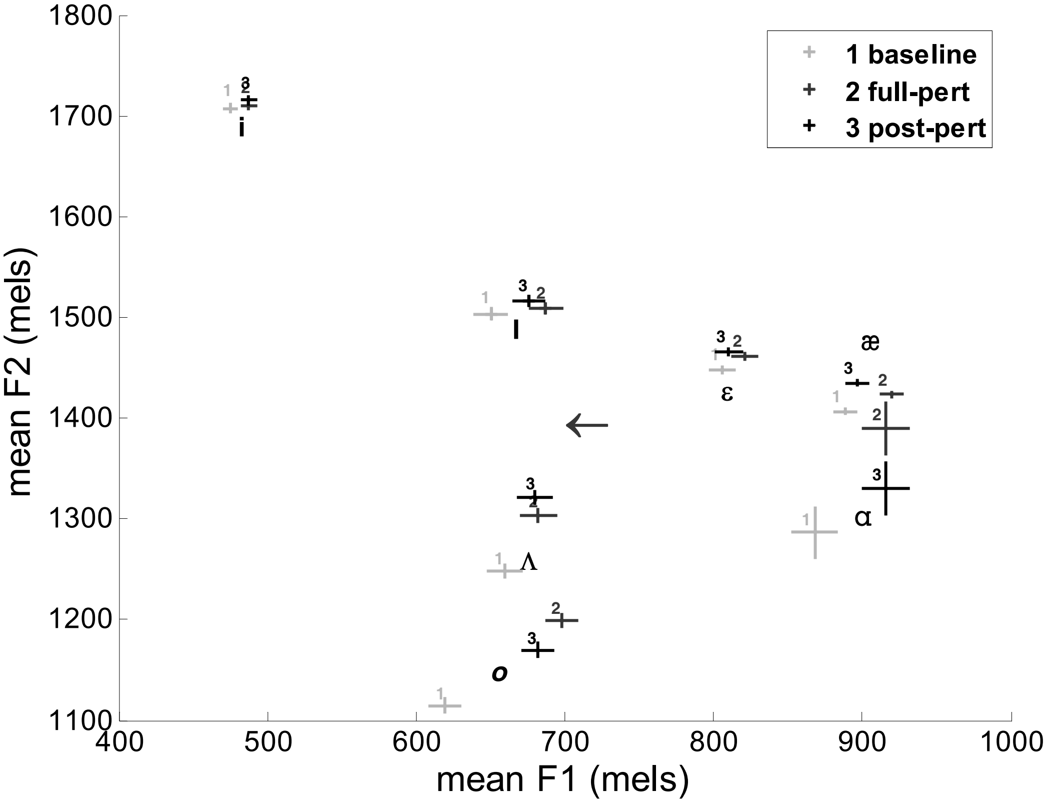

Figure 3.16: Shift in F1/F2 vowel space for all vowels of the -feedback tokens, 0.7 pert female subjects. Shown here are the formant values for the vowels presented without feedback in the "pXt" context. The light colored crosses with the **1** label correspond to the values in the baseline phase (epochs 1-15); the medium colored crosses with the **2** label correspond to the values in the full perturbation phase (epochs (21-45); the dark colored crosses with the **3** label correspond to the mean values in the post perturbation phase (epochs 46-65). The abscissa shows F1 in mels, averaged among five subjects and all the trials within a given phase. The ordinate shows F2 in mels. The vertical and horizontal lines represent standard error about the mean of the formants. The arrow indicates the direction of the perturbation the subjects were exposed to (down shift in F1).

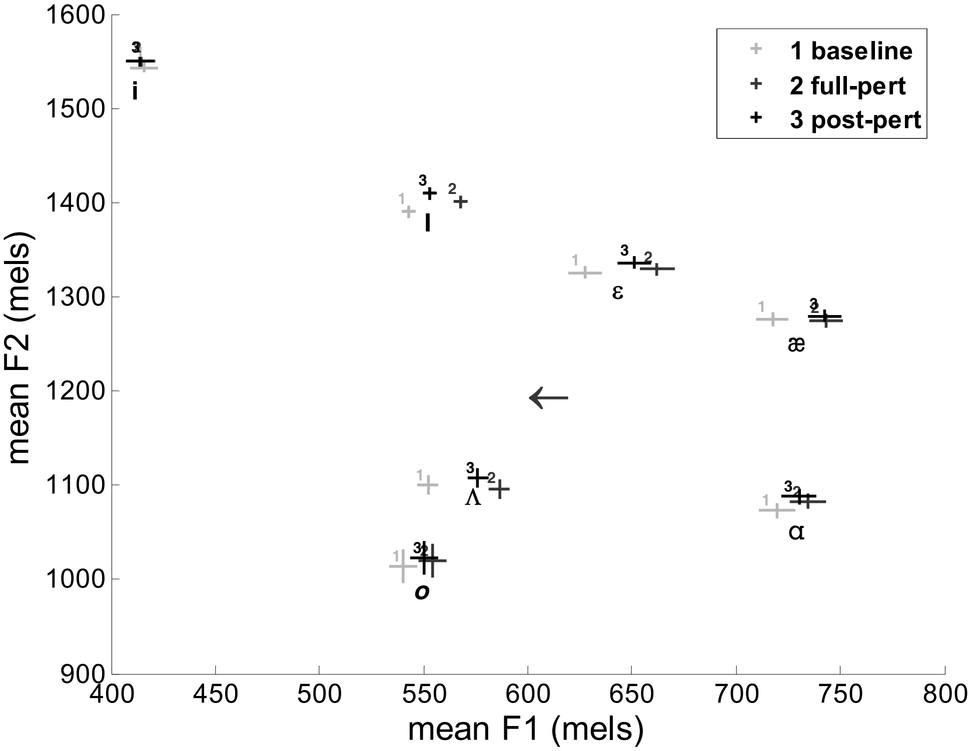

Figure 3.17: Shift in F1/F2 vowel space for all vowels of the -feedback tokens, 0.7 pert male subjects. See Figure 3.16 for figure explanation.

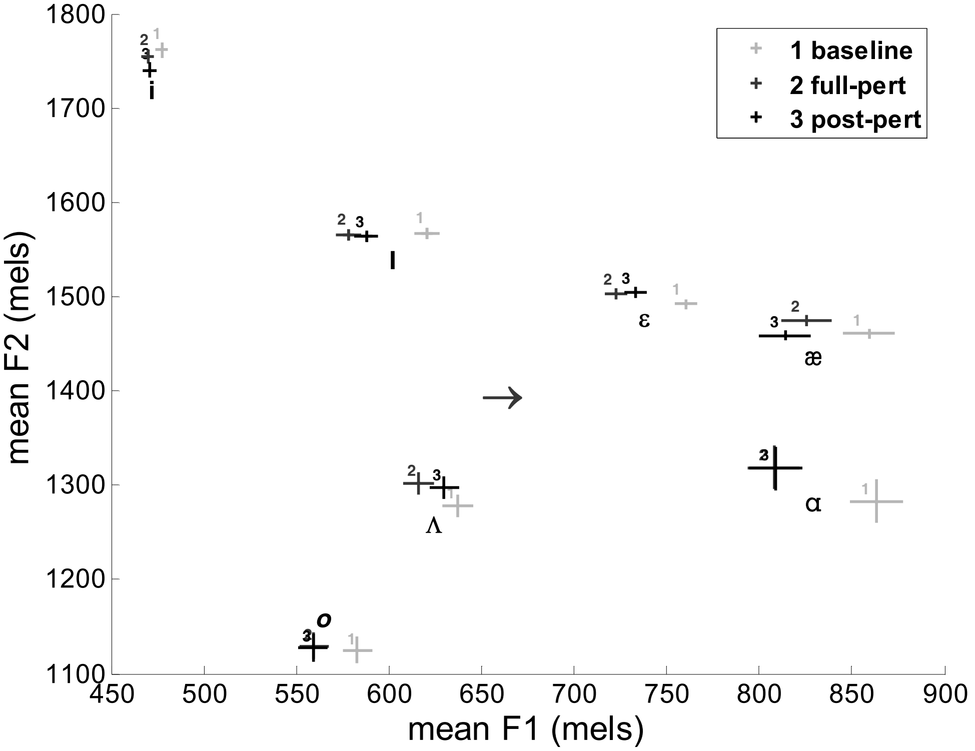

Figure 3.18: Shift in F1/F2 vowel space for all vowels of the -feedback tokens, 1.3 pert female subjects. See Figure 3.16 for figure explanation.

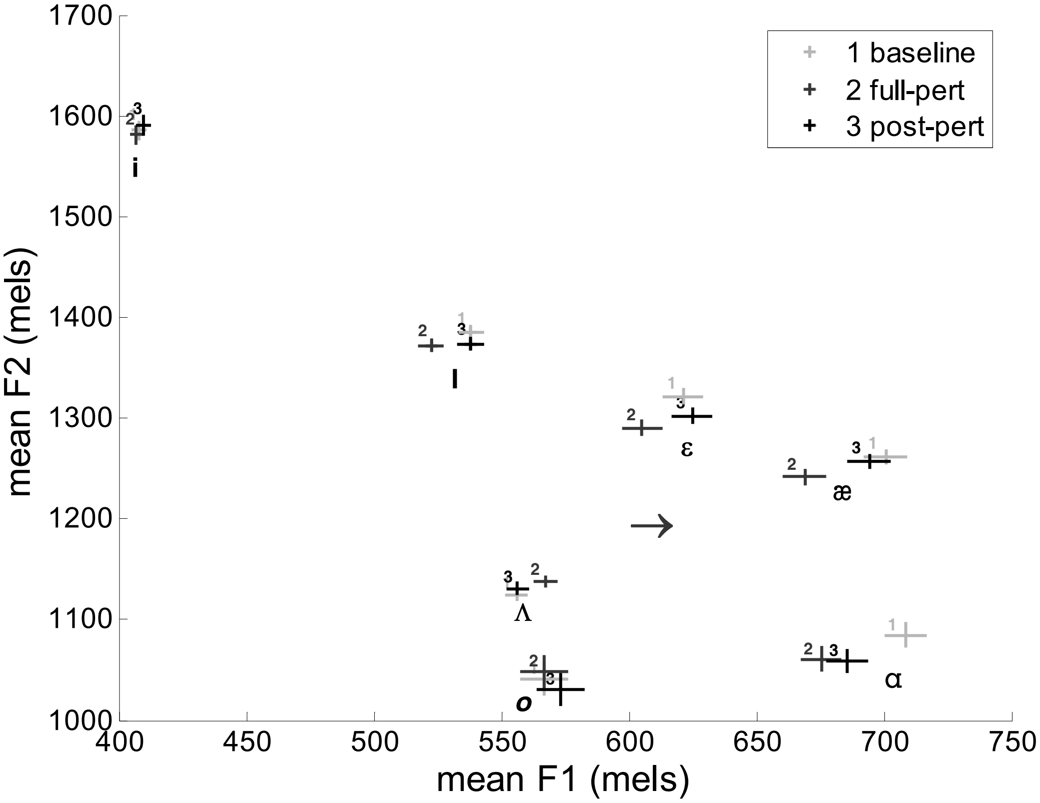

Figure 3.19: Shift in F1/F2 vowel space for all vowels of the -feedback tokens, 1.3 pert male subjects. See Figure 3.16 for figure explanation.

The generalization of adaptation to other vowels suggests that the subjects are not learning to modify a vocal tract configuration that is specific to just the vowel that was perturbed in the SA feedback—the vowel /ε/. Rather, subjects appear to have learned to modify the vocal tract in a way that the adapted response can be applied globally to other vowels. Specifically, changes in the first formant can be accomplished by simply controlling the height of the jaw during vowel production (Stevens, 1998). Moreover, generalization is an advantageous property to have in the speech motor planning system, since people do not often repeat the same words when normally speaking. Applying adaptation learned for one specific context more globally is a behavior that enhances an individual's ability to more quickly react to different acoustic feedback conditions, and maintain intelligibility of the communicated utterances in spite of the altered feedback.

3.4.5. Analysis of the contribution of F0 to adaptation.

Figure 3.20 shows F0 as a function of epoch number, plotted in a similar manner as F1 and F2 were in Figure 3.8: normalized to the mean of the baseline epochs. Figure 3.20 shows that both types of subjects—those exposed to the 0.7 pert shift and those exposed to the 1.3 pert shift—showed a general trend of F0 increasing throughout the SA protocol. Interestingly, subjects exposed to the 0.7 pert shift increased in F0 to a lesser degree (dashed line) than subjects exposed to the 1.3 pert shift (solid line). When factoring out the portion of F0 increase that was common to both pert groups, another trend in F0 was found: subjects tended to produce a shift in F0 that was in the opposite direction of the F1 shift they produced.

This result is not an unsurprising, considering that investigators who conducted a comparable experiment by perturbing F0 in the acoustic feedback (Jones and Munhall, 2000) found a similar trend. They also found F0 generally increased for subjects, regardless of whether they were exposed to the shift-up, shift-down or control protocols. At the same time, Jones and Munhall also found that subjects exposed to the shift down protocol increased in F0 to a greater degree in F0 than the control, while subjects exposed to the shift up protocol increased in F0 to a lesser degree than the control. That is, when the common increase in F0 was factored out, subjects in the Jones and Munhall experiment produced a shift in F0 that was opposite of acoustic F0 perturbation.

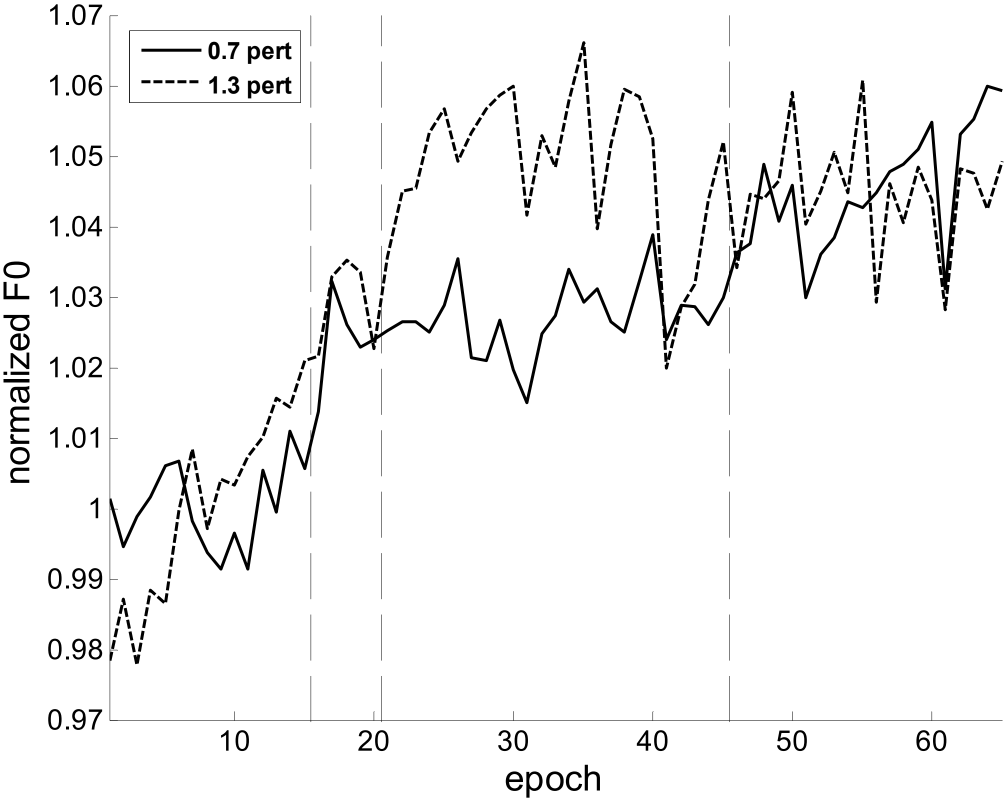

Figure 3.20: F0 normalized to the mean of the baseline epochs (1-15), as a function of epoch number. The solid line represents the mean of the subjects exposed to the 0.7 pert shift, while the dashed line represents the mean of the subjects exposed to the 1.3 pert shift. The vertical lines indicate the transitions in pert level.

In the current acoustic F1 perturbation SA experiment, the additional change in F0 (factoring out the upward trend common to both conditions) seems to be in the opposite direction of the compensatory shift in F1 the subjects produced. Figure 3.21 demonstrates this relation, showing the F0 difference versus F1 difference, with both quantities normalized to the mean of the baseline epochs. F0 difference—defined here as the difference between the subject's normalized F0 and the mean normalized F0 for all subjects in the given epoch—is used to factor out the rising F0 that occurs for all subjects in the experimental session. (For consistency, the F1 difference—defined in the same manner as F0 difference—is used in the ordinate.) This figure demonstrates that a significant (r^2 = 0.55, $p < 0.001$) inverse relation exists between F1 and F0 production, similar to the relation between F1 and F2 (see 3.4.2). When considered separately, the 0.7 pert subjects and 1.3 subjects both showed significant—p<0.01 in each case—negative correlation as well. The inverse relation between F1 and F0 may indicate that subjects perceive, and thus compensate for, a quantity—such the Miller ratio (Miller, 1989)—that incorporates F0 as well as F1.

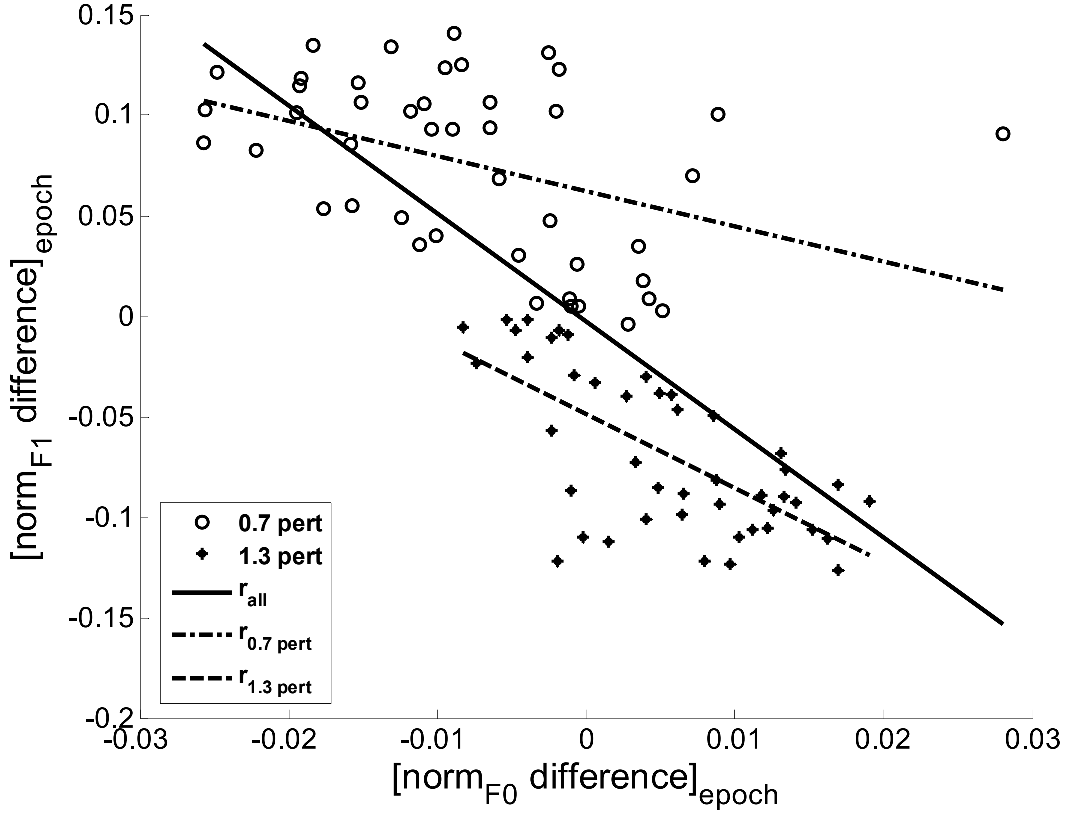

Figure 3.21: Correlation between normalized F0 difference and the normalized F1 difference, over the full pert epochs. The abscissa corresponds to the difference between a subject's normalized F0 and the mean of all subjects' normalized F0, both calculated for a given epoch. The ordinate is the normalized F1 difference, calculated the same way as the F0 difference. The open circles correspond to data from 0.7 pert subjects; the asterisks correspond to data from 1.3 pert subjects. The lines indicate the best regression fit, all of which have significant correlation ($p < 0.001$). The dashed-dotted line corresponds to the correlation of the 0.7 pert data, the dashed line corresponds to the 1.3 pert data, and the solid line corresponds to all data. Only epochs 21 to 65 (full-pert and post-pert epochs) from nineteen subjects are shown; one subject was excluded from this analysis (see text).

3.4.6. Analysis of within token adaptation.

Data from study 1 were reanalyzed to investigate possible evidence of "within token" adaptation (refer to Section 3.2.5). In this analysis, each +feedback token was divided into ten equal-length sections based on the duration of the token:

that is, section 1 represents the first ten percent of the token, section 2 represents the second ten percent of the token, and so on, up to section 10, representing the last ten percent of the token (see Figure 3.22.) Formants were extracted from each segment using the same LPC analysis tool described in 3.3.4, with the major difference being the segment length to which the formant extraction was applied. To allow investigation of how each segment changes relative to epoch number, these sectional F1 values were normalized by the mean baseline F1 value within the corresponding section, and segmental adaptive response values were then determined for +feedback tokens of all subjects (using Equation 3.5). The segments investigated in the following analysis are the *front* segment (defined here as the second and third sections) and the end segment (defined here as the eighth and ninth sections); the first and tenth sections were excluded from analysis to avoid possibly confounding co-articulatory influence from the neighboring stop consonants.

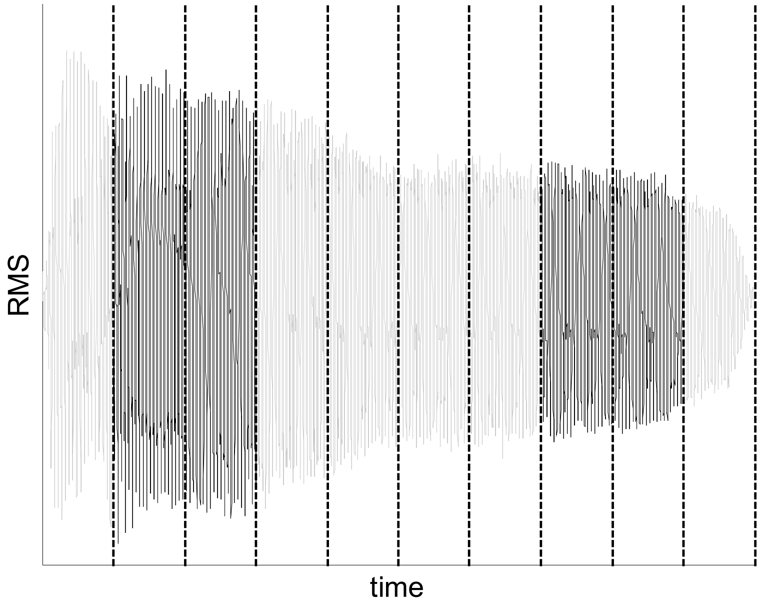

Figure 3.22: Example of time segmentation of tokens for within-vowel adaptation. For within-token analysis, tokens are divided into ten sections of equal duration (vertical lines), from which F1 values are extracted. The darker segments indicate the front and end segments of the vowel which were compared for evidence of within-vowel adaptation. The abscissa is in units of milliseconds.

The adaptive response for the *front* (solid line) and *end* (dashed line) vowel segments throughout the SA experiment are shown in Figure 3.23. In this figure, it is evident that the *front* and *end* segments generally change at the same rate during the experiment, even near the phase transitions (i.e. the beginning of the ramp phase and the beginning of the post-pert phase). Paired, two-tail t-test analysis between *front* and *end* segments performed on an epoch-by-epoch basis showed that the two segments differed significantly only at one epoch (epoch 61).

The lack of any significant adaptative response differences between the front and the end of the vowel may likely result from the design of this protocol. That is, within-vowel differences may only be evident on a time-scale that is shorter than an epoch. However, because each epoch contains tokens of different phonetic contexts, it is difficult to separate within-epoch differences that are due to a lag in compensatory response (as hypothesized in 3.2.5) from those that are due to contextual differences. It should be noted that signficant within-vowel adaptation effects has been noted in another SA experiment that used the same perturbation algorithmn used in this thesis (Tourville et al., 2005).

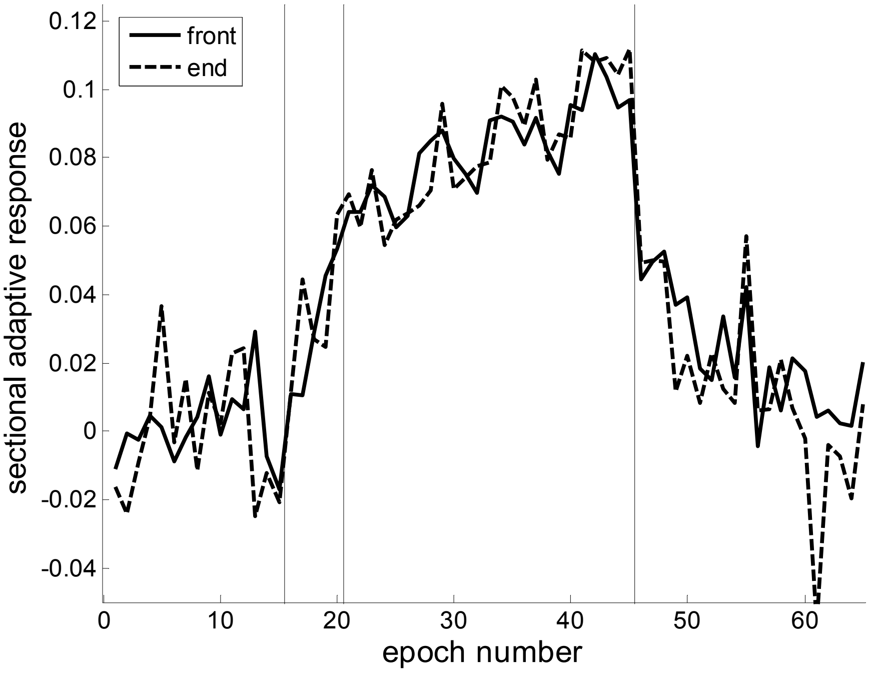

Figure 3.23: Segmental adaptive response for the front and end vowel segments during the entire SA protocol. The *front* segment of the vowel is shown in solid line; the *end* segment is shown in dashed line. The vertical lines indicate transitions in pert level: the leftmost line indicates the start of the *ramp* phase, the middle line indicates the start of the *full-pert* phase, and the rightmost line indicates the start of the *post-pert* phase.

3.5. Study 1 summary.

Results from this study indicate that, in response to perturbations of the first formant in the acoustic feedback of vowel productions, subjects compensate by shifting this formant in a direction opposite to the perturbation. This adaptation persisted even when subjects received feedback blocked by masking noise. Additionally, even though only tokens containing the vowel /ɛ/ received perturbed feedback, the adapted shift in F1 generalized to tokens containing other vowels as well. Subjects also demonstrated that they maintained this adaptation for a brief period after the perturbation was removed. These results are consistent with findings in other sensorimotor adaptation experiments in speech (Houde and Jordan, 1998; Houde and Jordan, 2002; Max et al., 2003).

This study here also suggests findings previously unreported for speech sensorimotor adaptation. That is, while the adaptive response was expressed mainly in compensation of the formant that was perturbed (F1), subjects also demonstrated that the second formant (F2) and even the fundamental frequency (F0) changed in a significant way due to the F1 perturbation. However, it should be noted that the analysis was not able to detect within-vowel differences in adaptation.

The analysis in this chapter focused largely on adaptation properties revealed by treating the entire subject set as a whole. The following study will investigate how degree of adaptation varies from one subject to another, focusing largely on the relation between perceptual acuity and adaptation.

Chapter 4. Cross-correlation comparison between vowel discrimination and SA (study 2).

4.1. Background and specific aims of the perceptual acuity experiment.

The purpose of study 2 is to account for some of the individual variations in the ability of subjects to adapt to the acoustic speech perturbation. Specifically, this study focuses on the relation between individual *acuity*—i.e. ability to distinguish fine details—in the perception of the perturbation and the ability to adapt to it.

4.1.1. Relation between vowel discrimination and adaptation.

Recent work has tested a prediction of the DIVA model on the relation between speech perception and production. A central concept to this relation is the *goal region*—defined here as a bounded set of sensory expectations for the correct production of a given phoneme, and illustrated in Figure 4.1. Vowels with auditory dimensions (*F1, F2*) that fall within the goal region are judged as correct productions of that vowel, while vowels with (*F1, F2*) falling outside the goal region are judged as incorrect productions. In line with the feedback control mechanism discussed in Section 2.3, speakers that judge their own vowel as incorrectly produced are expected to correct for this error. Thus, the size of the sensory goal region—a perceptual phenomenon based on the discrimination of speech acoustics—determines the role of feedback error correction in speech production. As discussed in Section 2.3, the predicted relation—greater discrimination of speech acoustics occurring with greater contrast in speech production—has been observed in cross-subject correlations between speech production and discrimination (Newman, 2003; Perkell et al., 2004b; Perkell et al., 2004a); other evidence for sensory goal regions is discussed in Section 5.1.2.

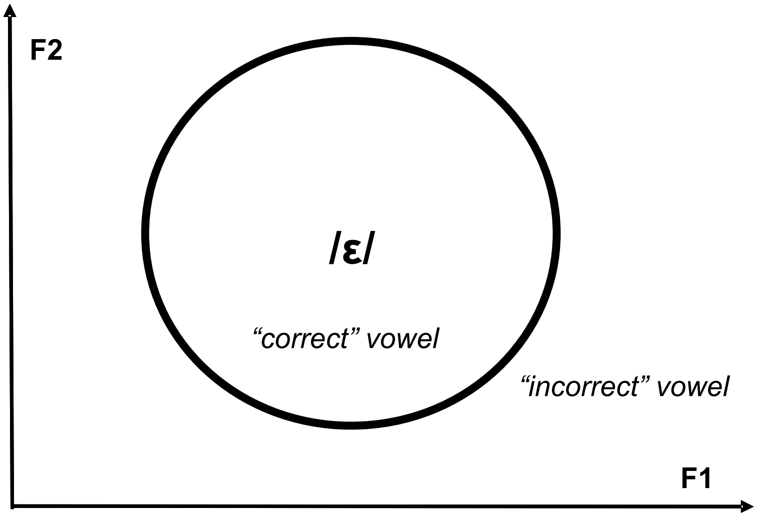

Figure 4.1: The auditory goal region. The "auditory" goal region (circle) for a phoneme (here, the vowel /ɛ/) is shown in a two-dimensional (*F1,F2*) space. Vowels that are perceived to fall within the goal region are judged as "correct" vowel productions, while vowels that are perceived to fall outside the goal region are judged as "incorrect" vowel productions.

One consequence of the prediction relating perception and production is that subjects with more acute speech perception should be able to better adapt their speech to perceived auditory errors (such as those that were introduced by the SA protocol). Figure 4.2 illustrates the auditory goal regions for the vowel /ɛ/ for two hypothetical subject types, and relates goal region size to extent of adaptation (straight lines pointing to the left) due to the perturbation (dotted line pointing to the right). Subjects that are not able to discriminate differences in the vowel acoustics well (*low acuity* speakers) are expected to have larger auditory goal regions representing their vowels; on the other hand, subjects that can discriminate fine changes in the vowel acoustics (*high acuity* speakers) are expected to have smaller auditory goal regions.

In the Figure 4.2 example, both hypothetical subjects are exposed to the same size auditory perturbation, which shifts F1 up. In response to the auditory perturbation, the subject with the smaller auditory goal region will have to adapt to a greater extent (solid line) to cause the production of that vowel to be perceptibly acceptable—that is, within the boundaries of the auditory goal regions—especially when compared to the adaptive response (dashed line) of the subject with a larger auditory goal region. Since the size of the auditory goal regions of speech is dependent on auditory acuity, it follows that subjects that demonstrate better perceptual acuity of speech should show greater SA response. This relationship can be investigated by performing a vowel discrimination experiment on subjects from study 1, and correlating the results of these two studies across subjects.

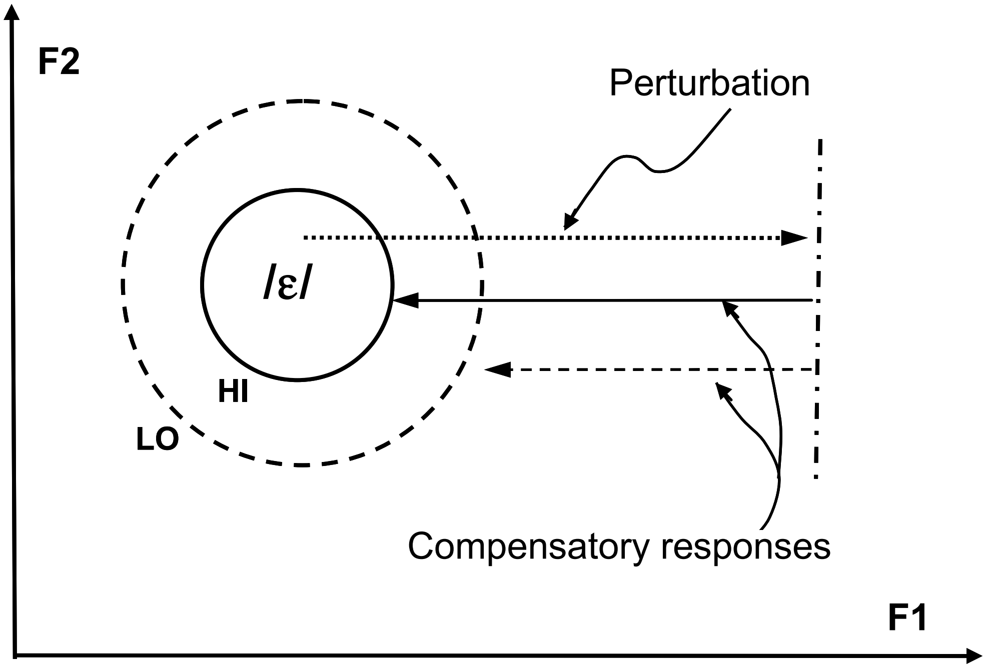

Figure 4.2: Proposed relation between auditory goal region size and adaptive response. The two circles represent the auditory goal regions of the vowel /ɛ/ for two hypothetical subjects: a *high acuity* subject (solid line circle), who has a smaller goal region size; and a *low acuity* subject (dashed line circle), who has a larger goal region. For the same degree of perturbation (black dotted line to the right), the subject with smaller goal region will demonstrate greater adaptive response (solid line to the left), than when compared to the adaptive response of the subject with the larger goal region (dashed line to the left). *Adapted with permission from Perkell, et al (unpublished).*

This series of experiments was designed to study the relation between an individual's ability to adapt to an acoustic perturbation in speech and his/her perceptual acuity of that perturbation. Subjects that participated in study 1 on this project were recalled to participate in a battery of speech perception experiments. Results from these experiments were then correlated with measurements of adaptive response obtained in the experiments described in Chapter 3.

4.1.2. Relation between vowel spacing and adaptation.

Since the SA experiment included baseline (epochs 1-15) tokens of the vowels /æ/, /ɛ/, and /I/ ("pat", "pet", and "pit" –feedback tokens, respectively), the relationship between baseline vowel separation in F1 and adaptive response can also be measured. While this relationship was not taken into account during the design of the SA and perceptual acuity experiments, it is reasonable to expect it exists. Two alternative hypotheses relating vowel spacing and adaptation are considered here.

When a subject hears the perturbed vowel during the full-pert epochs, the subject may compensate by an amount that is proportional to the separation between the perceived (i.e. perturbed) vowel and the target vowel (i.e. unperturbed) vowel. Consider a subject trained on the 0.7 pert SA protocol, which shifts the sound of the vowel /ɛ/ to sound like the vowel /I/ (i.e. shift-down in F1). If that subject's baseline /ɛ/ and /I/ vowels are close together in F1, he may not perceive the need to increase the perturbed F1 greatly to shift his perception of the vowel from an /I/ to an /ɛ/. However, if the subject's baseline F1 of these vowels are separated widely, he or she may attempt a greater correction to shift the perceived vowel back to / ɛ/. This proposed relation is illustrated in Figure 4.3.[8]

An alternative hypothesis suggests that vowel spacing and adaptation are related in the opposite manner: subjects who have vowels spaced further apart in the first formant dimension will adapt less than those with closely spaced vowels. This idea arises from the assumption that, for a fixed perturbation, subjects with closely spaced vowels are more likely to perceive the perturbation than subjects with vowels spaced further apart. This increased likelihood in perception of the perturbation would then lead to a larger adaptive response, in the alternative hypothesis. Considering these competing hypotheses about the relation between produced vowel spacing and adaptation, the following study addresses

[8] This hypothesis implies that subjects with larger vowel spacing will make larger corrections during the perturbation phase, thus leading to larger adaptation than subjects with smaller vowel spacing (who would make smaller corrections).

how perceptual acuity, produced vowel spacing and adaptation relate to one another.

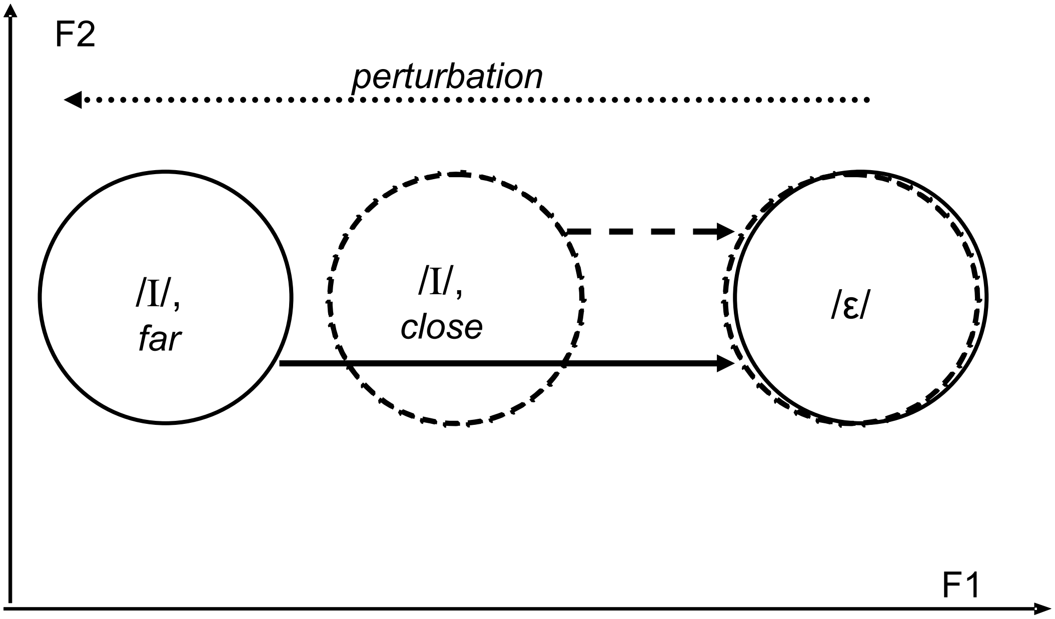

Figure 4.3: Proposed relation between vowel spacing and adaptation. Representation of auditory goal regions of F1 for two hypothetical subjects shown here: one whose baseline F1 for the vowel /I/ is close to the vowel /ɛ/, and one whose baseline F1 for the vowel /I/ is far from the vowel /ɛ/. Here, the auditory goal region for the vowel /ɛ/ is the same in both hypothetical subjects. Each subject experiences the same size perturbation in F1 of the /ɛ/ vowel (dotted line). Assuming both subjects perceive they have spoken the vowel /I/ during the perturbation, one likely correction each subject may undertake (at least initially) is to increase F1 by an amount proportional to the spacing between /I/ (the incorrect vowel) and /ɛ/ (the correct vowel). Thus, the subject with /I/ that is close to/ɛ/ will make a smaller correction (dashed line) than the subject with /I/ that is far from /ɛ/ (solid line).

4.2. Methodology of study 2: the perceptual acuity experiment.

The battery of perceptual acuity experiments was broken down into four steps: speech recording, an adaptive staircase discrimination task, a second discrimination task, and a goodness rating task. From this battery, the just noticeable difference (*jnd*) was determined from the discrimination task, and other perceptual measures were determined from the goodness rating results. The use of a two-stage protocol for measuring *jnd* was based on work from other researchers (Guenther et al., 1999b; Guenther et al., 2004) showing that tihs method results in a more precise measure of *jnd*.

Note that subjects with greater auditory acuity should be able to resolve finer differences; thus, subjects with greater acuity with respect to the perturbation should have smaller *jnd* values.

4.2.1. Participating subjects.

The same set of subjects that were used in the SA study also participated in this experiment. Seven out of the twenty subjects were no longer available at the time the second study was conducted, so the results from the acuity experiment were based on thirteen subjects.

4.2.2. Recording of the subject's speech.

The speech recordings were conducted in a sound attenuating room using a head-mounted piezo-electric microphone (Audio-Technica, model AT803B) placed at a fixed distance of 20 cm from the speaker's lips. Elicited utterances were presented on a monitor. The monitor also displayed cues that induced the subject to speak at a target loudness (85 +/- 2 dB SPL) and word duration (300 msecs)[9]. Subjects were allowed to practice to achieve these targets. Subjects were then instructed to speak ten tokens each of the following words: "bet", "bit" and "bat". The F1 frequency for each "bet" token was measured, and the "bet" token with the median F1 value was selected as the base token.

The following perceptual acuity tests were carried out in the same sound attenuating room that the recordings were made in, though not necessarily on the same day. Subjects heard stimuli over closed back headphones (Sennheiser EH2200), played on a computer controlled by Matlab script.

[9] The displayed loudness cue displayed the SPL as a bar with the ideal range marked off. The duration cue consisted of a change in display background color from white to gray after 300msec from the onset of voicing. These are the same visual cues used to control loudness and word duration in study 1.

4.2.3. Staircase protocol to estimate *jnd.*

The purpose of this staircase protocol is to obtain an approximate estimate *jnd*. The second stage of the discrimination task can yield a better estimate of the subject's *jnd*, but only over a limited range of pert values. By using the estimate from this first stage to determine the range of tokens for the second stage, it is more likely that the second stage of the discrimination task will operate in the subject's most sensitive range.

Three milestone synthetic stimuli were generated from the base token, spaced at 0.85 pert, 1.0 pert (i.e. identical to the base token) and 1.15 pert apart. Around each milestone, an adaptive, 1-up, 2-down staircase protocol was run to estimate the *jnd* for that milestone. In this procedure, pairs of tokens that were either the *same* or *different* from each other were presented to the subject with equal probability. The members of the *same* pairs both consisted of the milestone, while the *different* pairs consisted of tokens straddling the milestone equally spaced in pert. Whenever the subject responded incorrectly to either the *same* or *different* pairs, the distance between the *different* pairs increased. Whenever the subject responded correctly to two presentations of a given different pair, the distance between the different pairs decreased. The separation was unchanged when the subject responds correctly to a *same* pair presentation. The order of the three staircase protocols was randomized for each subject.

The stimuli pairs were separated initially by 0.30 pert from each other. The first four changes in separation were 0.04 pert, followed by changes in pert separation of 0.02 pert after that. Once the tokens got to within 0.10 pert from each other, the separation was only changed by 0.01 pert. After eight reversals (changes in direction of the staircase), the protocol terminated, and the jnd_{est} was calculated as the median value of the last four reversals on the staircase.

Two subjects participating in this experiment had jnd_{est} that were higher than the initial value set at the beginning of the staircase protocol. (That is, the staircase "climbed" rather than "descended".) When this occurred, a new continuum of perturbed tokens was generated from new recordings of the subject's speech, and the entire speech acuity experiment was re-run.

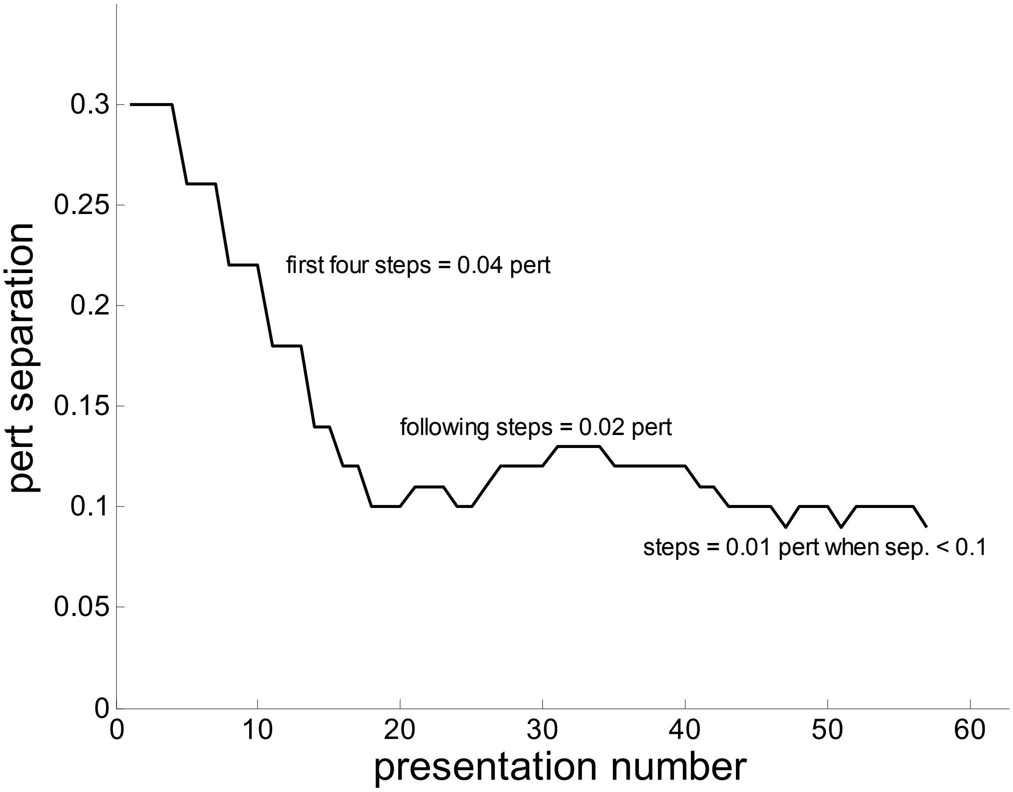

Figure 4.4: Example an adaptive rocedure used to estimate *jnd*. The abscissa shows the presentation number of the given pair, and the ordinate depicts the separation of the *different* pairs in pert. The text within the figure gives conditions for changes in step size. The staircase terminated after eight reversals of the staircase. Refer to Section 4.2.3 for a more detailed explanation of the procedure.

4.2.4. A more precise same-different protocol.

Three blocks (one for each milestone) of a more precise *same-different* protocol were then run on each subject. In this protocol, presented tokens were either the *same* (both = milestones) or *different* (straddling the milestone, refer to Figure 4.5). The *different* pairs were spaced by the following multiples of the *jnd*$_{est}$: +/-0.25, +/-0.5, +/-0.75, +/-1.0 and +/-1.4. The +multiple of the *jnd*$_{est}$ pair was always presented with the corresponding –multiple for a *different* pair presentation, though the order of which token was first presented was randomized. Each unique pair (the one same and five different pairs) was presented to the subject 50 times, for a total of 300 presentations per block. Subjects were given feedback as to the correct response to the pair just presented. Both the order of presentations within each block, and the order in which the blocks occurred, were randomized.

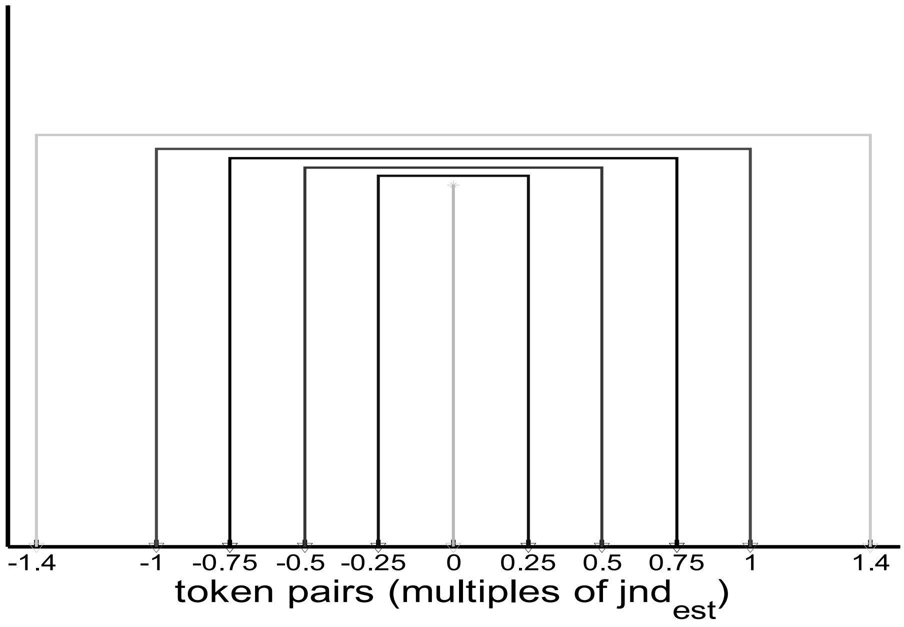

Figure 4.5: Token pairs used within the more precise same-different protocol. The abscissa depicts the separation of the stimuli in the pairs of tokens used within a given block of the more precise same-different protocol, measured as a multiple of the *jnd*$_{\text{est}}$ obtained from the staircase procedure. The milestone (also the *same* pair) is represented by the *0* token. Branches join the tokens that are paired together in a given *different* presentation. Note that the members of each pair are equally spaced from the milestone (when measured in pert), thus the *different* pairs “straddle” the milestone.

4.2.5. Goodness rating task.

A continuum of 41 tokens, evenly spaced in pert and ranging from 0.7 to 1.3 pert, was then generated from the subject’s base token. The subject performed two test blocks—one with 0.7 to 1.0 pert tokens and the other with 1.0 to 1.3 pert tokens—of goodness rating tasks, in which he or she was instructed to rate the token on a scale from 0 to 7, with 7 as the best example of the token /ɛ/.[10] The test blocks contained tokens ranging from either 0.7 to 1.0 pert, or 1.0 to 1.3 pert.

Subjects were allowed to replay the token, and were given a practice block (which went through the entire continuum in random order) before the test block. In the test blocks, the continuum of 21 tokens was presented in five repetitions, and the tokens were randomized within each repetition. These goodness rating scores were ultimately used to determine vowel category width (see Section 4.3.5); in this perceptual acuity measure, smaller category widths are presumed to reflect higher vowel discrimination.

4.3. Analysis and correlation results.

4.3.1. Analysis of d' scores.

The d' score for each pair was calculated using the standard signal detection theory formula (Macmillan and Creelman, 2005):

Equation 4.1: $$d' = z(H) - z(F)$$

where z is the normal inverse function, H is the hit rate (responds "different"|different) and F is the false alarm rate (responds "different"|same). Because z score values of 1 and 0 are undefined, all rates are calculated out of 50.5 (rather than 50 presentations), and rates of zero are increased to 0.5 out of 50.5.

Data consisting of d' score as a function pair separation (in perts) were then fitted with a sigmoid function. A sigmoid function was used in this case because this function is monotonic and best captures the sharp rise of d' in the sensitive region, while also capturing ceiling and floor properties observed in the data.

[10] The continuum for the goodness rating task was divided into two—rather than presenting the entire continuum in one task—to allow increased contrast between the base token and the tokens at the extreme of the continuum. In pilot studies, subjects tended to rate the base token and the extreme tokens closer together when all tokens were presented in one task.

Note that, in fitting the data, the origin (0 pert *jnd*, 0 d'score) is included as a data point.

Some subjects had d' vs. pert separation functions whose maximal d' value was less than 1.0. Consequently, the criterion for the *jnd* used here was the maximal d' value common to all subjects run on the perceptual acuity protocol, in this case, 0.7. Thus, the *jnd* was defined here the pert separation corresponding to a d' score of 0.7, as determined by from the best fit function (refer to Figure 4.6).

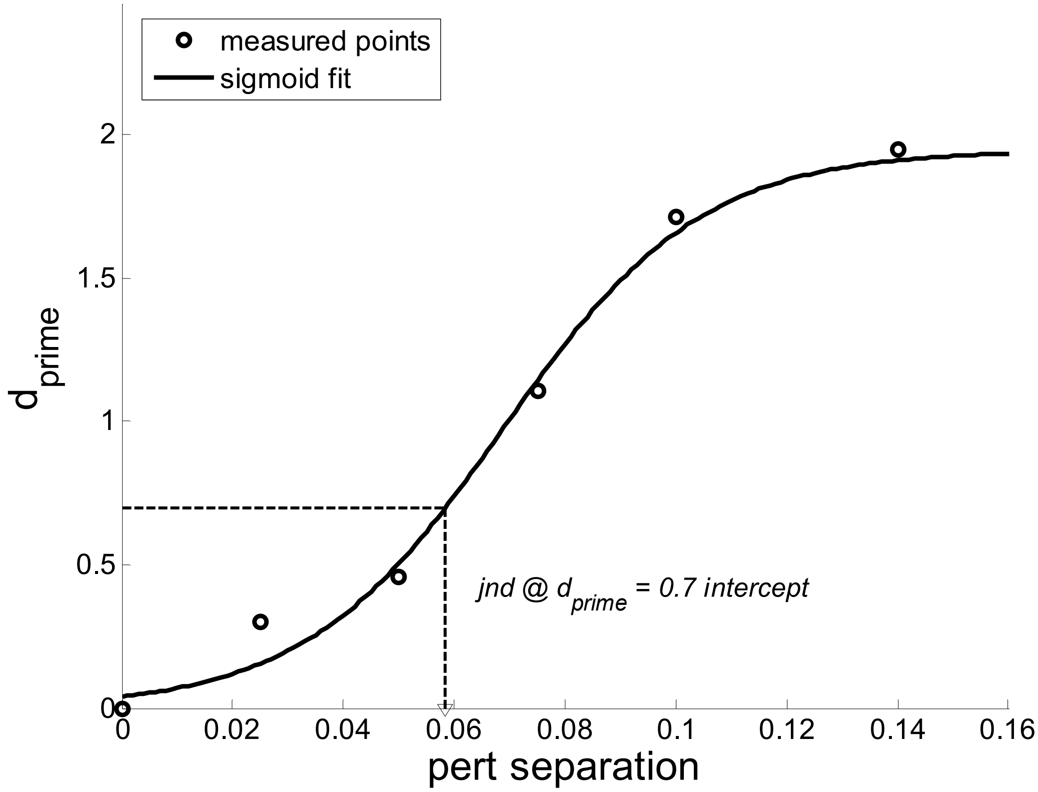

Figure 4.6: Example of calculating *jnd* more precisely from the "same-different" d' scores. This graph portrays d' score (ordinate) obtained for one subject under one milestone condition, as a function of pert separation of the different tokens (abscissa). The open circles correspond to measured d'; the solid curve depicts the best fitting sigmoid curve. The *jnd* is measured as the pert separation corresponding to a d' score of 0.7. (dashed arrow).

4.3.2. Correlation between *jnd* scores and adaptation scores.

The subjects' *jnd scores* were subsequently correlated with their *adaptive response indices*, as shown in Figure 4.7, Figure 4.8, and Figure 4.9. The

milestone = “same” figure (Figure 4.7) shows the *jnd* values at the 0.85 pert milestone for the 0.7 pert trained subjects (open circles) grouped with the *jnd* of the 1.15 pert milestone for the 1.3 pert trained subjects (crosses). The **milestone = “center”** figure (Figure 4.8) presents the *jnd* at the 1.0 pert milestone for the 0.7 pert trained subjects (open circles) and the 1.3 pert trained subjects (crosses). The **milestone = “opposite”** figure (Figure 4.9) presents the *jnd* at the 0.85 pert milestone for the 0.7 pert trained subjects (open circles) grouped with the *jnd* of the 1.15 pert milestone for the 1.3 pert trained subjects (crosses). Each figure shows a regression line, along with r^2 (amount of variation accounted for) and p-value (significance) shown in the legend.

Figure 4.7 to Figure 4.9 all demonstrate the predicted trend: subjects with smaller *jnds* tend to adapt to a greater extent. For the **same** and **opposite** milestones, these correlations account for little of the variation, and neither is significant (defined as p scores < 0.05). On the other hand, relation between *jnd* and adaptive response for the **center** milestone is significant ($p < 0.047$); this relation accounts for 31 percent of the variance.

The hypothesis proposed in Section 4.1.1 states that adaptation should depend on the auditory discrimination of the speech target—the auditory goal region. Since the target vowel for adaptation was the vowel /ɛ/, it follows that the **center** milestone *jnd*—measuring the perceptual discrimination of the vowel /ɛ/--should correlate significantly to adaptive response. Had subjects demonstrated a significant correlation between *jnd* measured on the **same** side milestone, this would have indicated that adaptation is also significantly dependent on the perception of the perturbed speech. However, Figure 4.7 seems to indicate that this is not the case. One explanation for this outcome is that the perturbed speech perceived by each subject was not constant during the SA protocol, since the amount that each subject adapted—which can be seen in the variation in *ARI* scores—affects the perception of the perturbed speech. Thus, it is not surprising that when a constant milestone—the **same** milestone—was used to measure the perception of the perturbed speech, no correlation was found with adaptation.

Further, had subjects demonstrated a significant correlation between the **opposite** milestone *jnd* and adaptive response, this would have suggested that the acoustics related to the subject's produced speech during the perturbation affected adaptation. This is a particularly unlikely outcome since subjects could not have heard their own adapted production, given the perturbed acoustic feedback. The lack of correlation between adaptive response and the *jnds* measured at the non-center milestones reinforces the notion that it is the ability of the subject to perceive a difference from the expected acoustics that drives adaptation.

Finally, the statistical analysis reported here was repeated using *jnd* estimated from the first-stage of the two-stage discrimination task. This analysis (refer to Appendix E) found no significant correlation.

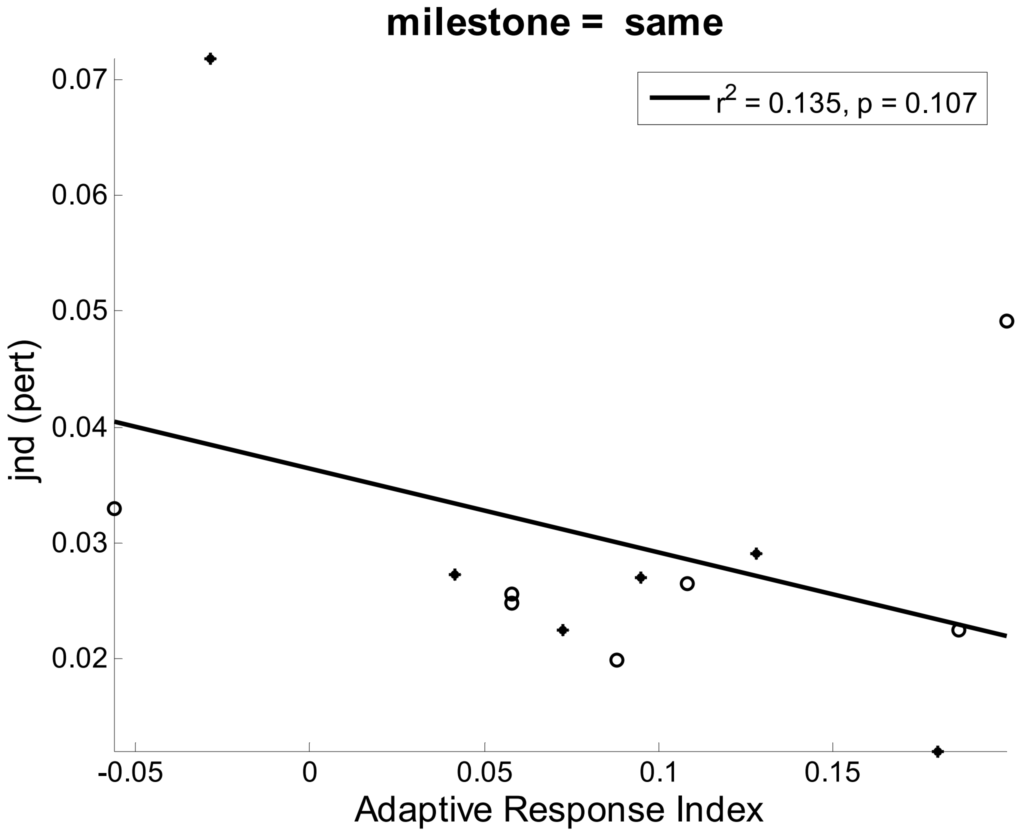

Figure 4.7: Adaptive response index is not correlated with the *jnd* score of the milestone in the same direction as the SA training. The 0.85 pert milestone *jnd* score was used for 0.7 pert trained subjects (open circles), while the 1.15 pert milestone *jnd* score was used for the 1.3 pert trained subjects (crosses). The abscissa shows the adaptive response index, discussed above. The ordinate shows the *jnd* (in pert) for the "same" milestone, as determined in the "same-different" protocol. Statistics for the regression line are shown in the legend; the p-score reported uses a two-tail t-test.

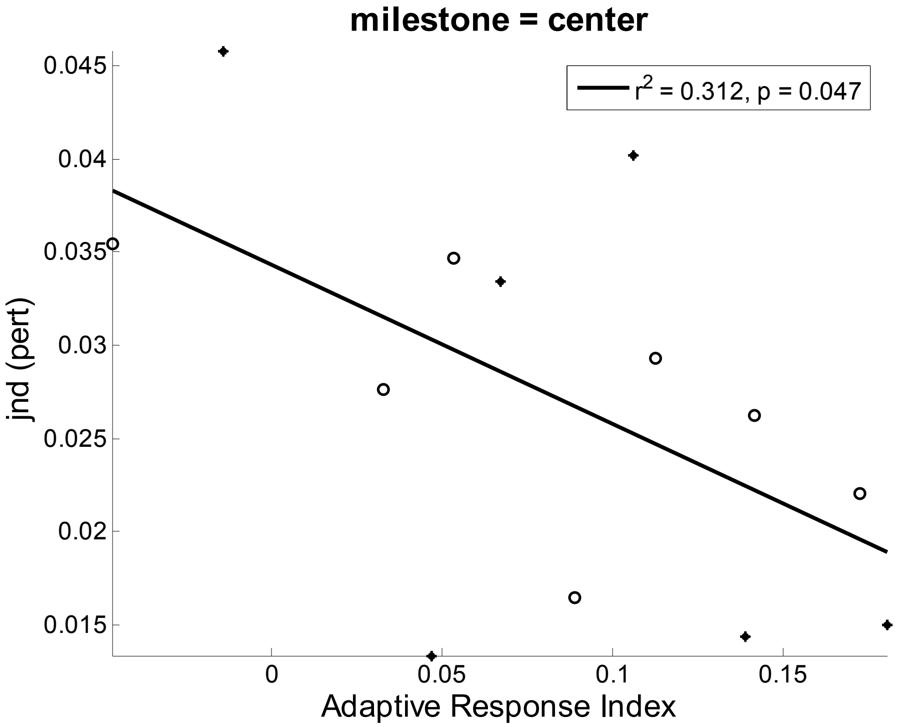

Figure 4.8: Adaptive response index is correlated with the *jnd* score of the center milestone. The 1.0 pert milestone *jnd* score was used for 0.7 pert (open circles) and 1.3 pert (crosses) trained subjects. Refer to Figure 4.7 for axis and legend details.

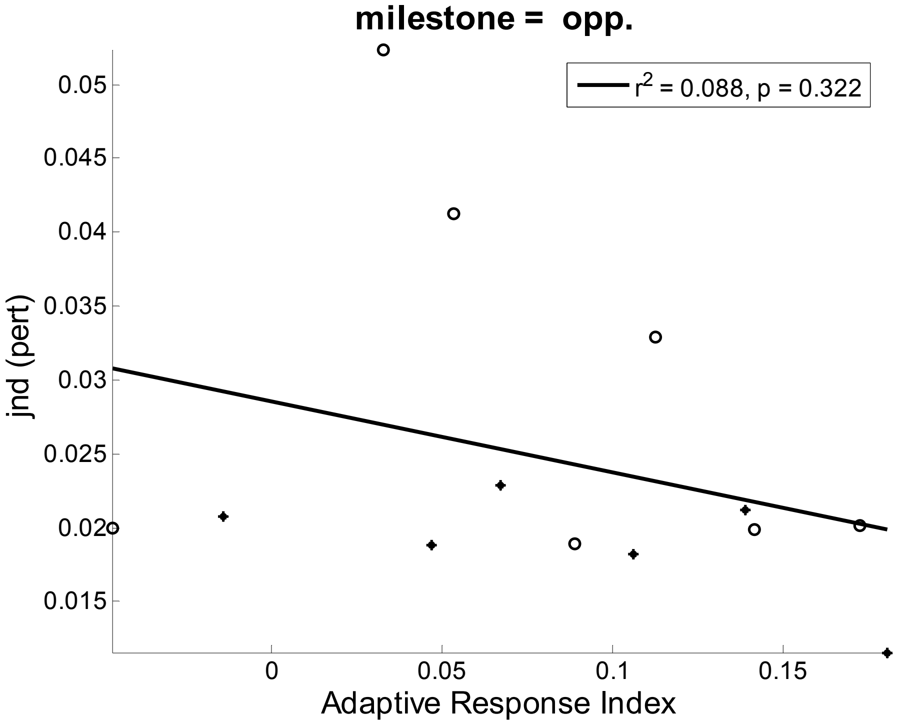

Figure 4.9: Adaptive response index is not correlated with the *jnd* score of the milestone in the opposite direction of the SA training. The 1.15 pert milestone *jnd* score was used for 0.7 pert trained subjects (open circles), while the 0.85 pert milestone *jnd* score was used for the 1.3 pert trained subjects (crosses). Refer to Figure 4.7 for axis and legend details.

4.3.3. Correlation between vowel F1 separation and adaptation scores.

To calculate F1 vowel separation, the following calculations were made. Note that the *F1_separation* values are normalized by the baseline F1 from the word "pet". All F1 values were taken from the baseline phase tokens. Since the tokens "pat" and "pit" were only presented as *–feedback* tokens, F1 values of "pet" were taken from the *–feedback* tokens for consistency.

Equation 4.2:

$$F1\_separation_{pet-pit} = \frac{pet\_F1_{median} - pit\_F1_{median}}{pet\_F1_{median}}$$

$$F1\_separation_{pat-pet} = \frac{pat\_F1_{median} - pet\_F1_{median}}{pet\_F1_{median}}$$

Figure 4.10 and Figure 4.11 show the produced vowel separation as a function of Adaptive Response Index. As with the *jnd* scores in the correlation studies above, Figure 4.10 (same) grouped the *F1_separation*$_{pet-pit}$ from 0.7 pert trained subjects with the *F1_separation*$_{pat-pet}$ from the 1.3 pert trained subjects. Conversely, Figure 4.11 (**opposite)** grouped the *F1_separation*$_{pet-pit}$ from 1.3 pert trained subjects with the *F1_separation*$_{pat-pet}$ from the 0.7 pert trained subjects.

Figure 4.10 shows that subjects with larger vowel separation (on the same side as the perturbation) do tend to adapt to a greater extent. However, this correlation is not large (accounting for only 15 percent of the variance), and does not reach significance (p value = 0.082). The results shown in Figure 4.11 verifies that there is no significant relationship (p value = 0.706) between vowel separation on the opposite side of the perturbation, and adaptation.

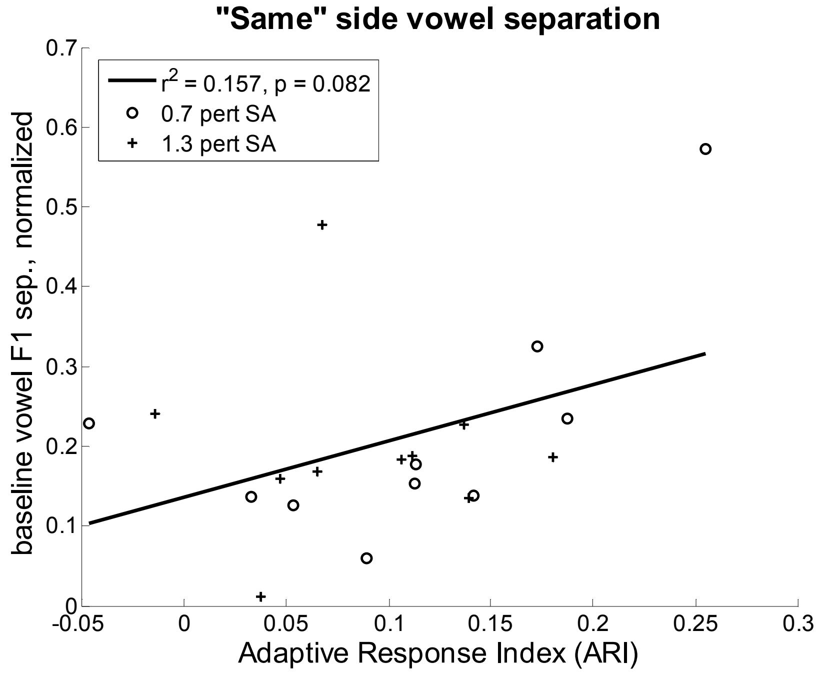

Figure 4.10: Adaptive response index is not correlated with the baseline vowel F1 separation on the same side as the perturbation. The /ɛ/ - /I/ separation was used for subjects run on the 0.7 pert protocol (open circles), while the /æ/ - /ɛ/ separation was used for subjects run on the 1.3 pert protocol (asterisks). The abscissa shows the adaptive response index. The ordinate is the value of the F1 difference between the two vowels, normalized by the median baseline F1 value for /ɛ/ (Equation 4.3). Statistics for the regression line are shown in the legend.

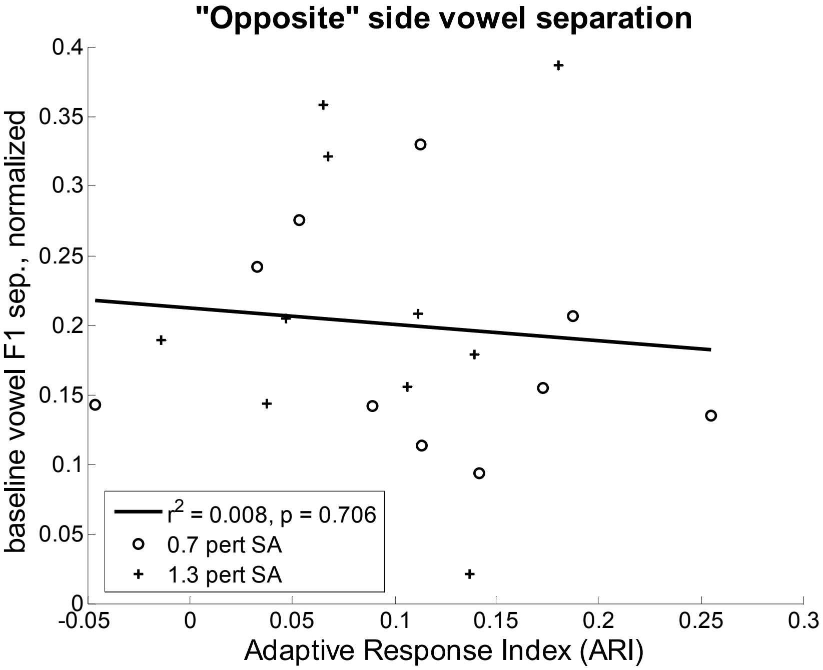

Figure 4.11: Adaptive response index is not correlated with the baseline vowel F1 separation on the opposite side of the perturbation. The /æ/ - /ɛ/ separation was used for subjects run on the 0.7 pert protocol (open circles), while the /ɛ/ - /I/ separation was used for subjects run on the 1.3 pert protocol (asterisks). Refer to Figure 4.10 for axis and legend details.

The correlation coefficient shown in Figure 4.10 incorporates the two subjects who shifted F1 in the opposite direction of compensation (i.e., negative *ARI* scores). When these two subjects are excluded, the correlation between adaptive response and "same side" vowel separation for the remaining eleven subjects is significant ($p < 0.05$) and accounts for 32 percent of the variance (see Figure 4.12). This result supports the hypothesis that subjects with greater vowel spacing adapt to a greater extent (refer to Section 4.1.2).

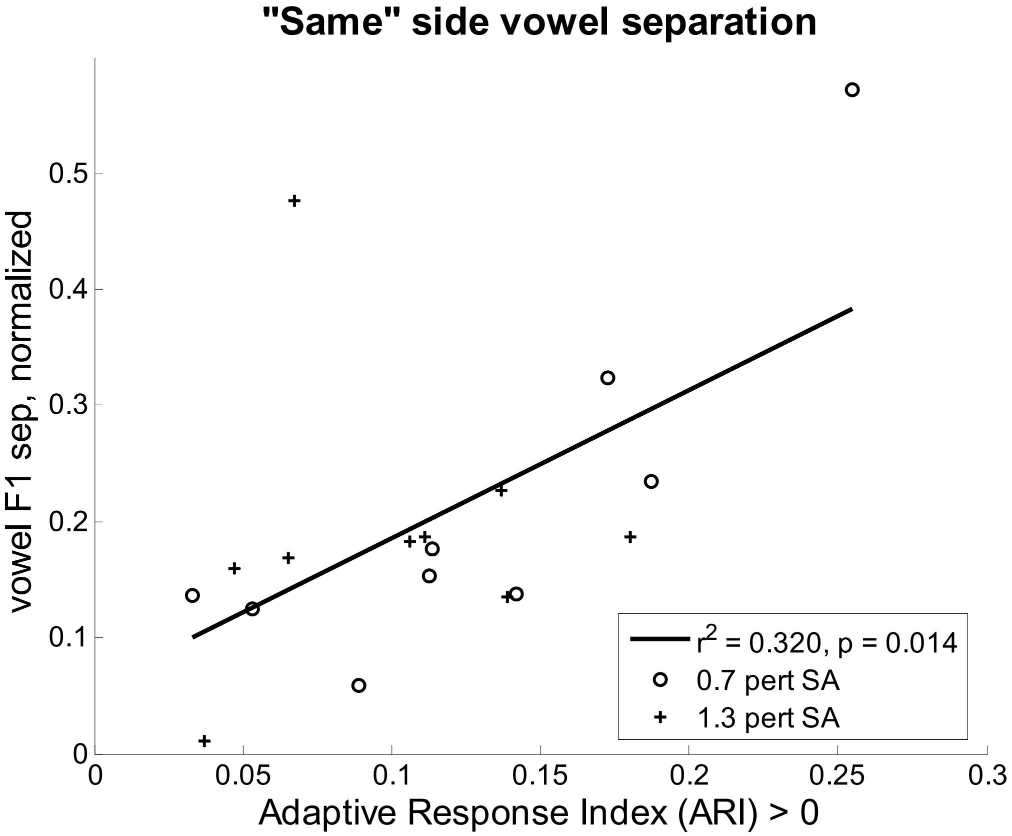

Figure 4.12: Adaptive response index—excluding negative ARI—is correlated with the baseline vowel F1 separation on the same side as the perturbation. This is the same as **Figure 4.10** with the exception that subjects with negative ARI values are not displayed here and were excluded from the correlation coefficient calculation. Refer to Figure 4.10 for axis and legend details.

4.3.4. Correlation between perceptual acuity measure and adaptive response, when adjusting for dependence on vowel separation.

The correlations between *jnd* and adaptive response index (see Section 4.3.2) at the center milestone shows a promising, significant trend, but it still does not account for more than 32 percent of the variance. The relation between *ARI* and baseline vowel separation seen in Figure 4.12 indicates that it could be worthwhile to take F1 separation into account when correlating *ARI* with *jnd*. By examining first order partial correlation coefficients, it is possible to determine the relationship between perceptual acuity and adaptation, when the dependence on baseline vowel separation is adjusted for.

Given three random variables, **x**, **y**, and **z**, the first order partial correlation coefficients are calculated in the following manner:

Equation 4.3:

$$r_{x,y\|z} = \sqrt{\frac{r_{x,y} - r_{y,z}r_{x,z}}{(1-r_{y,z}^2)(1-r_{x,z}^2)}},$$

where $r_{x,y||z}$ is the correlation between x and y, when controlling for z. The p-value is calculated in a similar way for the $r_{x,y}$, expect the degrees of freedom decreases from N-2 to N-3, where N is the number of measured points.

Using the variables adaptive response index (ARI) to measure adaptation, *jnd* to measure perceptual acuity, and normalized F1 separation, these first order partial correlation coefficients were calculated from the zero order ($r_{x,y}$) correlation coefficients. Note that the calculation of p-score is dependent on the number of data points used (N). The correlation coefficient corresponding to the adaptive response and the vowel separation used an N of 20. However, not all 20 subjects from study 1 participated in study 2, p-values from correlation coefficient utilizing *jnd* and other measures used N =13. The partial correlation coefficient analysis also used N=13 in the calculation of their corresponding p-values.

Table 4.1 shows the zero order and first order partial correlation coefficients, utilizing the F1 vowel separation corresponding to the same side as the perturbation that the subject was exposed to. This table demonstrates that there is a significant correlation ($p < 0.01$) between the perceptual *jnd* of the **center** milestone and the adaptive response index, when controlling for normalized F1 separation (shown in Table 4.1 at the **center** set of rows; *jnd, ARI* || *F1 sep.* column). Moreover, this correlation accounts for over **61** percent of the variance and is negative, indicating that smaller *jnd* values (i.e. greater perceptual acuity) are associated with larger adaptation scores. It is also notable that the two other first order partial correlations are significant, though at a higher significance threshold ($p < 0.05$).

The partial correlation coefficients were also calculated for the "same" and "opposite" milestones, to investigate the possibility that the discrimination index (i.e. *jnd*) of these side milestones becomes significantly correlated to adaptation *when* F1 separation is controlled for. Table 4.1 shows that this is not the case; the only significant relation is found between the perception of the the "center" milestone" and the adaptive response index. (Lack of significant correlation between non-**center** milestones and adaptive response was addressed previously in Section 4.3.2.)

		zero order r_{xy}			**first order $r_{xy\|\|z}$**		
milestone		*jnd, ARI*	*F1 sep, ARI*	*jnd, F1 sep*	*jnd, ARI||F1 sep*	*F1 sep, ARI||jnd*	*jnd, F1 sep||ARI*
	r	-0.45		0.01	-0.49	0.42	0.22
same	*r^2*	0.21	*see below*	0.00	0.24	0.18	0.05
	p-score	0.12		0.97	0.10	0.18	0.50
	r	**-0.57**	0.37	0.32	**-0.78**	**0.70**	**0.69**
center	*r^2*	**0.33**	0.13	0.10	**0.61**	**0.50**	**0.48**
	p-score	**0.04**	0.11	0.29	**0.00**	**0.01**	**0.01**
	r	-0.34		-0.20	-0.29	0.32	-0.09
opposite	*r^2*	0.11	*see above*	0.04	0.08	0.10	0.01
	p-score	0.26		0.51	0.36	0.31	0.78

Table 4.1: Partial correlation coefficients, using F1 vowel separation corresponding to the same side of the perturbation. Shown are the correlation coefficients (*r*) between the parameters indicated in the column headings, square of the correlation coefficient (r^2), and the p values for the zero order correlation coefficients (left block) and first order partial correlation coefficients (right block). The top block used the *jnd* values from the milestone = same condition; the middle used *jnd* values from the milestone = center condition; and the bottom block used *jnd* values from the milestone = opposite condition. Significant correlations ($p < 0.05$) are shown in bold.

Table 4.2 is shown below for completeness. It is the same as Table 4.1 but uses the F1 vowel separation corresponding to the *opposite* side of the perturbation that the subject was exposed to. Here, the partial correlation coefficient between the adaptive response and the *jnd* at the **center** milestone, once the F1 separation *opposite of the perturbation* is controlled for, is the only first order partial correlation coefficient that is borderline significant (p = 0.05). However, the p-value for this partial correlation coefficient—p = 0.05—is slightly larger than the p-value for the correlation coefficient when F1 separation was not controlled for—p = 0.04—(see Table 4.1); this indicates that *jnd* and adaptive response likely do not depend on the F1 separation that is on the *opposite* side of the perturbation.

		zero order r_{xy}			**first order $r_{xy\|\|z}$**		
milestone		*jnd, ARI*	*F1 sep, ARI*	*jnd, F1 sep*	*jnd, ARI||F1 sep*	*F1 sep, ARI||jnd*	*jnd, F1 sep||ARI*
same	*r*	*column repeated in Table 5.1*	*see below*	-0.43	-0.53	-0.32	-0.52
	r^2			0.19	0.28	0.10	0.27
	p-score			0.14	0.07	0.32	0.09
center	*r*		-0.06	-0.07	-0.58	-0.12	-0.13
	r^2		0.00	0.00	0.33	0.01	0.02
	p-score		0.81	0.82	0.05	0.71	0.70
opposite	*r*		*see above*	0.22	-0.33	0.02	0.21
	r^2			0.05	0.11	0.00	0.04
	p-score			0.48	0.29	0.96	0.51

Table 4.2: Partial correlation coefficients, using F1 vowel separation corresponding to the opposite side of the perturbation. Shown are the correlation coefficients (*r*), square of the correlation coefficient (r^2), and the p-score for the zero order correlation coefficients (left block) and first order partial correlation coefficients (right block). The top block used the *jnd* values from the milestone = same condition; the middle used *jnd* values from the milestone = center; and the bottom block used *jnd* values from the milestone = opposite condition. Redundant information from Table 1 was omitted from this table. No significant correlations (p < 0.05) indicated.

Since Table 4.1 indicates that a significant relation between adaptation and perceptual acuity exists when the variation due to the produced vowel separation is factored out, *ARI* scores were normalized by dividing by F1 vowel separation. Correlation between this normalized *ARI* and the perceptual *jnd* was then reinvestigated. No significant correlation was found for the “same” (p > 0.4) and “opposite” (p > 0.3) milestones. However, significant correlation was found between the normalized *ARI* and the perceptual *jnd* for the “center” milestone ($p < 0.05$), as shown in Figure 4.13.

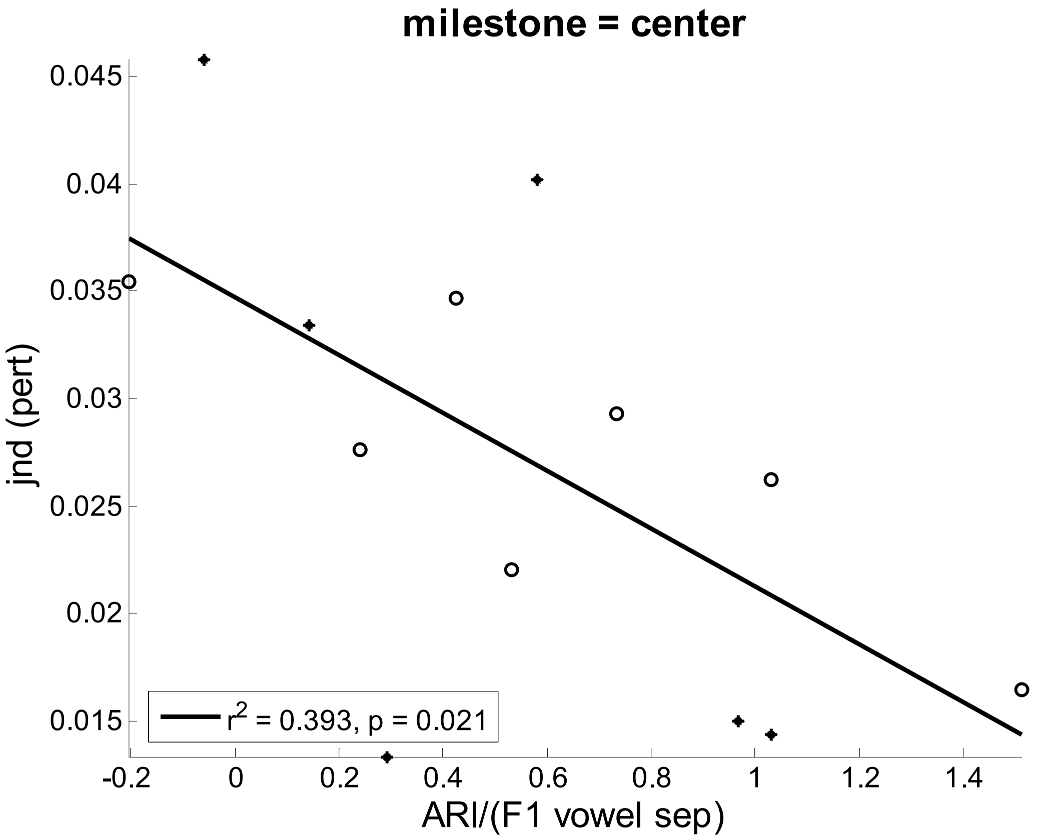

Figure 4.13: Adaptive response index, normalized by produced vowel separation in F1, is correlated with the *jnd* score of the center milestone. That is, the 1.0 pert milestone *jnd* score was used for 0.7 pert (open circles) and 1.3 pert (asterisks) trained subjects. The abscissa is the adaptive response index, divided by the F1 vowel separation, calculated as in **Equation 4.3**. The ordinate is the *jnd* (in pert) for the specified milestone, as determined in the “same-different” protocol. Statistics for the regression line are shown in the legend; the p-score reported uses a one-tail test.

4.3.5. Analysis of goodness rating data.

Scores from the goodness rating task (see Section 4.2.5) were analyzed in the following manner. For each subject, the mean goodness rating value (ranging from 0 to 7) of the five repetitions for each token was calculated. These values were then normalized by the subject’s maximum goodness rating value of the appropriate block: the 0.7 to 1.0 pert block or the 1.0 to 1.3 pert block. A sigmoid curve was then fit to the data results for each goodness rating block of each subject; Figure 4.14 shows an example of this analysis for one subject.

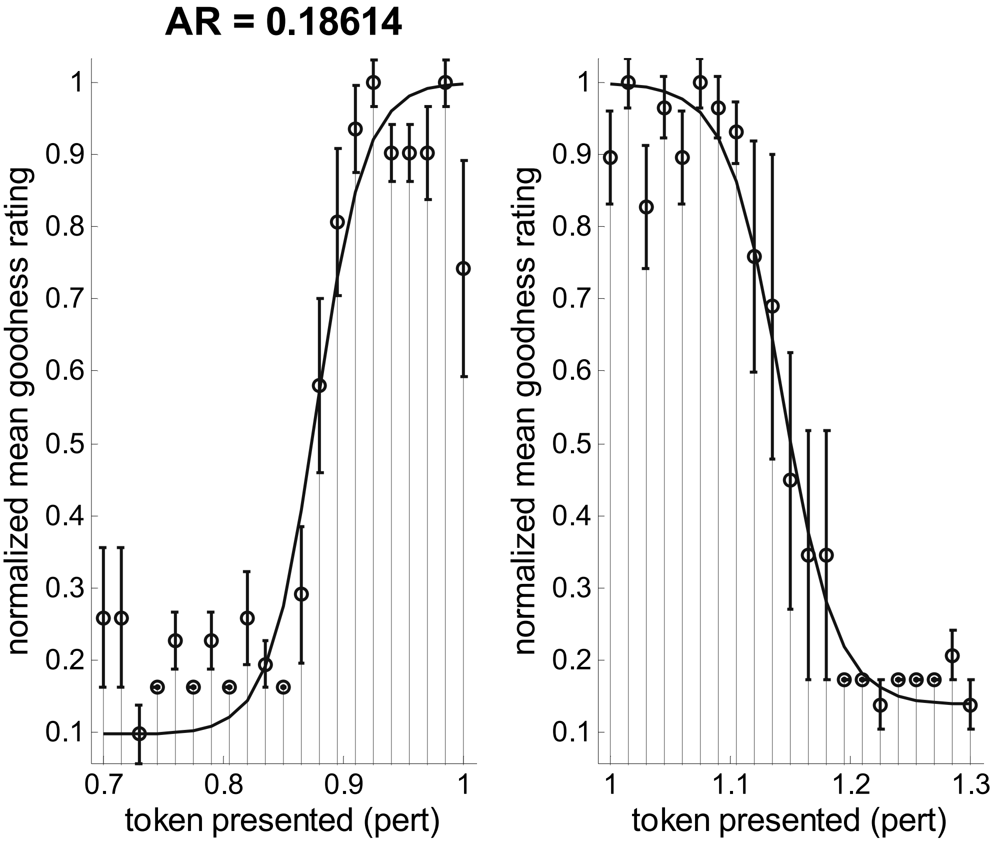

Figure 4.14: Example of the analysis of the goodness rating task in one subject. Shown is the goodness rating score as a function of the token presented (in pert), for the 0.7-1.0 pert block (left) and the 1.0 to 1.3 pert block (right). The goodness rating scores are the mean value over five repetitions, normalized by the maximum mean value within the block. The error bars are the standard error about the mean. The curve represents the best fit to a sigmoid function. The title over the left block indicates the subject's adaptive response index score. The ARI is over the left graph, indicating that this subject was run on the 0.7 pert protocol.

Eleven of the thirteen subjects run on the perception protocol had goodness rating results similar in shape to Figure 4.14. That is, these subjects rated the tokens near or at 1.0 pert as having the highest goodness rating (normalized value = 1.0). Two subjects showed goodness rating curves in which the token rated highest was at the opposite end of the pert continuum as the pert = 1.0 token (see Figure 4.15 and Figure 4.16, left sides). Goodness ratings scores were subsequently re-measured in both subjects, and they still showed the same trend (see Figure 4.15 and Figure 4.16, right sides).

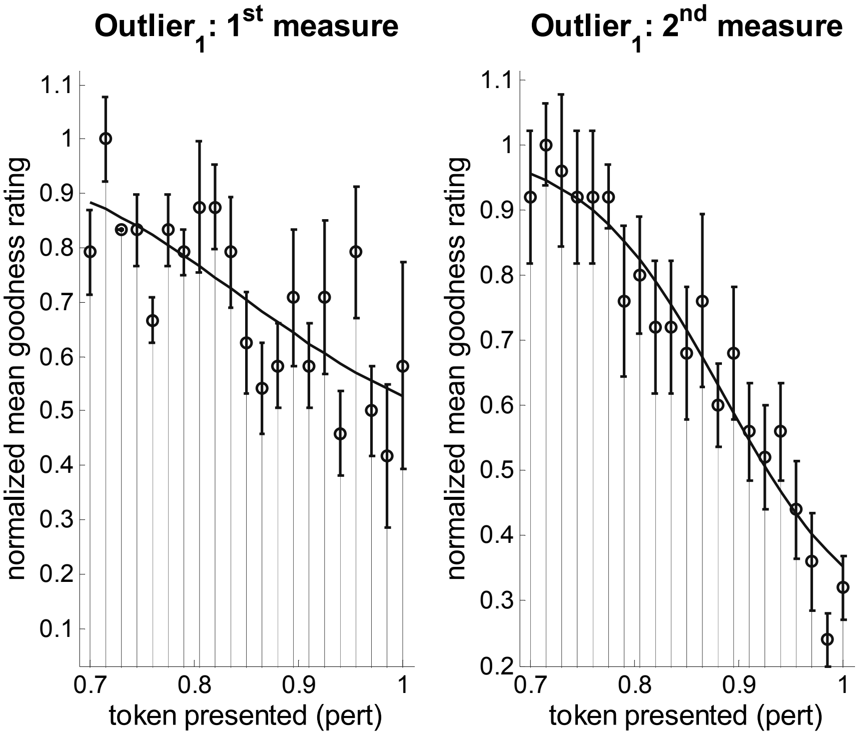

Figure 4.15: Analysis of the goodness rating task for outlier subject 1. Refer to Figure 4.14 for axis and legend details.

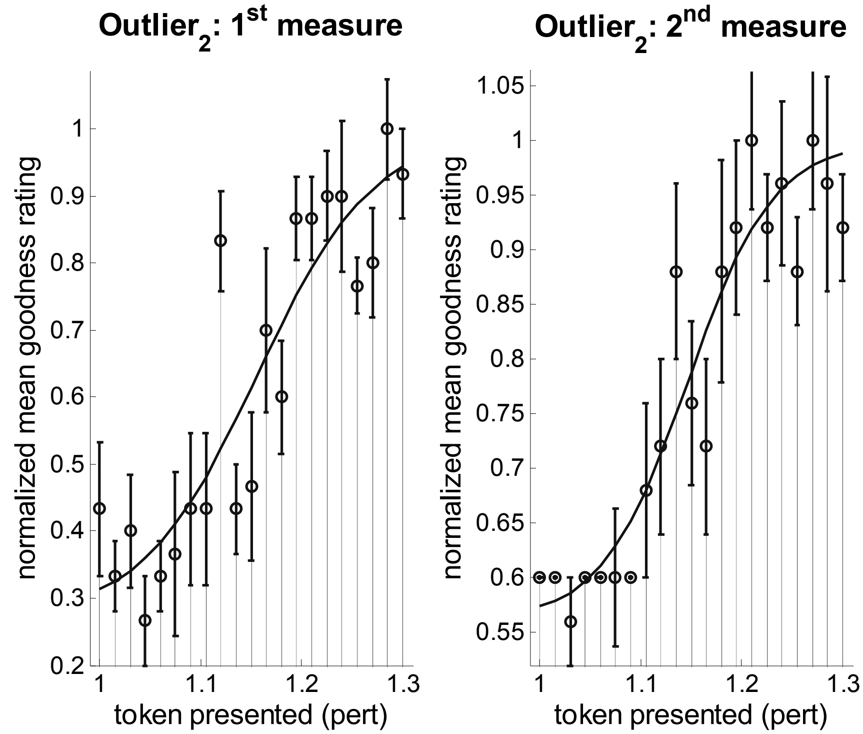

Figure 4.16: Analysis of the goodness rating task for outlier subject 2. Refer to Figure 4.14 for axis and legend details.

Interestingly, outlier subject 2 (Figure 4.16) was also one of the two subjects with a negative adaptive response (*ARI* = -0.02). For this subject, the two anomalous results on the SA and goodness rating tasks may be related. Since this subject perceives perturbed vowels as "better" vowels, this subject apparently shifted F1 in the same direction as the perturbation. This "positive-feedback loop" phenomenon is not generally found in other subjects with anomalous results. That is, the other goodness rating outlier (Figure 4.15) had a positive adaptive response in the SA protocol; the other subject with a negative adaptive response had more typical performance on the goodness rating task (with peak rating near the pert = 1.0 token).

4.3.6. Correlation between goodness rating error and adaptive response.

Measures derived from each subject's goodness rating curves were calculated to examine possible cross-subject relations with adaptive response (in a similar manner to the determination of the relation between *jnd* and adaptive response in Sections 4.3.2 to 4.3.4.) One potential property of the goodness rating curve is category width, defined here as the change in *pert* corresponding to a criterion goodness rating score on the best fit goodness rating curve. Defined as such, category width measures how sharply the category /ɛ/ is represented on a goodness rating scale, with smaller category widths corresponding to more narrow representation of the category. Appendix F shows that, for both goodness rating blocks (the block on the same side and the block on the opposite side of the perturbation) at a variety of criterion goodness scores, no significant correlation was found between category width and adaptive response.

The goodness rating data were also analyzed by examining the amount of variability within each subject's goodness rating responses. Specifically, for the goodness rating block on the same side as the SA perturbation, the standard error in the subject's normalized goodness rating score at each pert value was summed across pert values. The hypothesis here is that subjects with smaller total error (representing variability in goodness rating) should have greater perceptual acuity, and thus larger adaptive response scores (as discussed in Section 4.1.1). In the total error goodness rating analysis, the outliers discussed in Section 4.3.5 were still included (since the direction of their goodness rating curve does not affect the total variability calculation); however, data from the subjects with negative adaptive response scores were not used. Figure 4.17 demonstrates that the adaptive response index is significantly correlated with total goodness rating error (p = 0.05). Moreover, there is a negative relation between the two, which indicates larger ARI scores are correlated with smaller values of total error (confirming the perceptual acuity hypothesis).

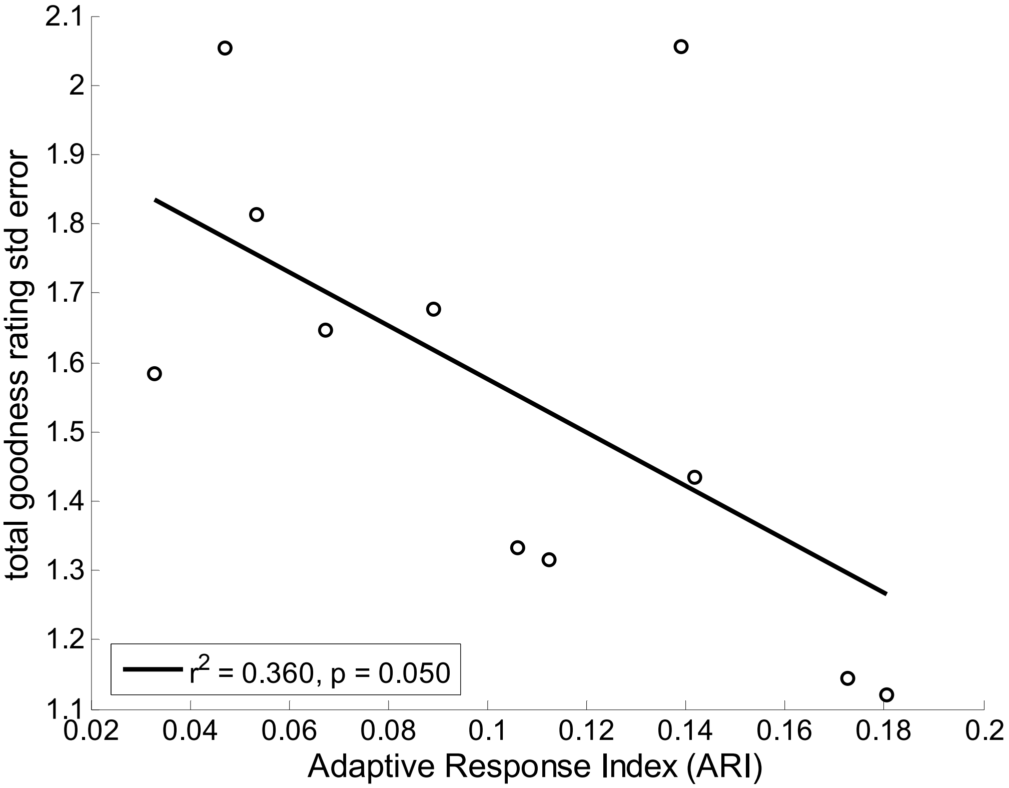

Figure 4.17: Adaptive response index is correlated with total goodness rating standard error. The abscissa is the adaptive response index. The ordinate is the sum of the standard error in the rating of each token presented on the goodness rating block. The goodness rating block used is the one corresponding to the same side as the perturbation the subject experienced in the SA protocol. Statistics for the regression line are shown in the legend.

4.4. Study 2 summary

The results of study 2 show that perceptual acuity and adaptive response to perturbations of F1 are significantly related in the manner predicted in Section 4.1.1: subjects with greater perceptual acuity of the acoustic perturbation demonstrate greater adaptive response. Perceptual acuity of the vowel perturbation was measured in two ways in study 2: by the index of discrimination or *jnd* (refer to Equation 4.1), and by the goodness rating task (refer to Sections 4.3.5 and 4.3.6). The *jnd* measured at the center milestone was found to be significantly and negatively correlated with the adaptive response index (Section 4.3.2); this correlation increased once the parameter of baseline vowel separation was factored out (refer to Section 4.3.4). While the vowel category width calculated from the goodness rating score was not found to correlate with adaptation (refer to Appendix E), the total variability in goodness rating scores was found to be significantly correlated with adaptive response in the negative direction. Taken together, the results of both perceptual tasks provided evidence that a subject's adaptive response increases with greater acuity.

The lack of correlation between vowel category width (as measured with the goodness rating scores) and adaptive response is not surprising, given the inherent subjectivity in rating vowels. For example, two subjects who can equally distinguish the differences vowel acoustics may still rate vowels differently; one subject may make a conscious decision to ignore these acoustic differences, while another subject may focus on these differences during the rating process. In this way, differences in the goodness rating score may not only be due to differences in perceptual acuity, but also due to a higher-level decision of whether or not to ignore perceived differences.

The notion of an auditory goal region is important in relating speech perception—how well one can distinguish differences in the phonemic acoustics—to speech production. This concept is developed further in the DIVA model simulations discussed in study 3.

Chapter 5. SA simulations utilizing the DIVA model (Study 3).

5.1. Outline of the DIVA model and overview of the SA simulations.

Study 3 investigates a series of simulations of the SA study using the DIVA neural network model for speech production. The simulation results were compared to findings from the first study (adaptation with feedback, blocked feedback adaptation, aftereffect adaptation, as well as findings from the second study (dependence of degree of adaptation on the auditory acuity of vowels).

5.1.1. A Functional Outline of the DIVA model

Figure 5.1 illustrates the DIVA model, indicating the relationship between feedback and feedforward control of speech movements in motor cortex.

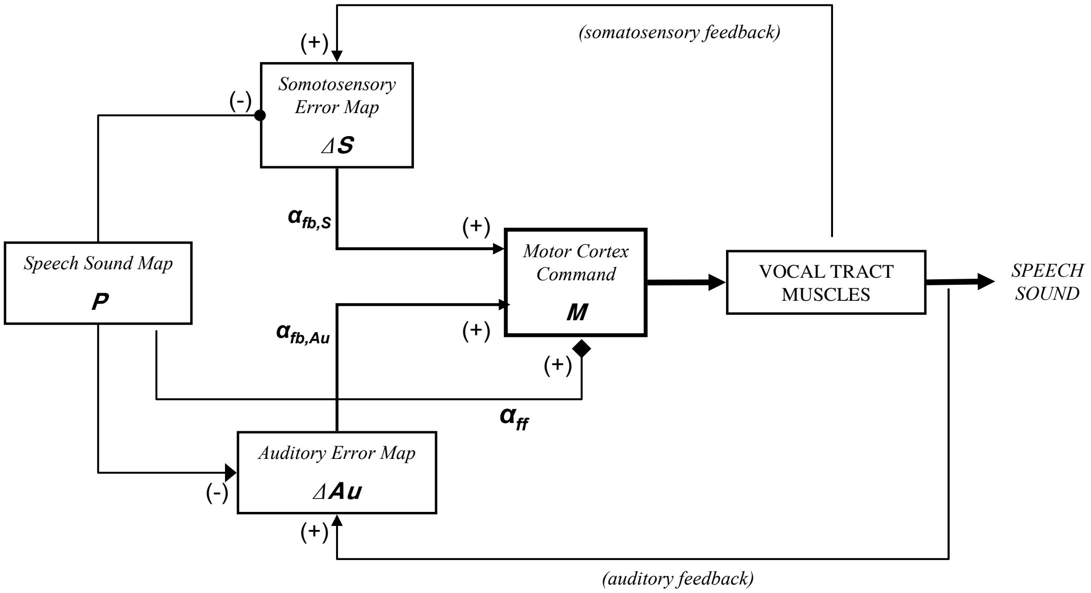

Figure 5.1: A functional outline of the DIVA model. This diagram illustrates the motor control of speech production in the DIVA model. The sensory error maps—*ΔS* and *ΔAu*—compare sensory feedback from the *vocal tract muscles* (somatosensory feedback) or from the acoustic speech sound produced (auditory feedback) to the sensory goals from the *speech sound map* (*P*). The outputs of the sensory error maps comprise the feedback component of the motor command. The *motor cortex M* integrates the feedback-based commands with the feedforward component of the motor command resulting from a direct projection from *P*. The output *M* is the set of motor commands that drive the *vocal tract muscles*, producing the *speech sound*. The diamond ending projection indicates an adaptive projection; the projection with a closed circle indicates that this projection adapts at a slow rate.

The *speech sound map* (symbolized by ***P*** because it is hypothesized to lie in premotor cortex) projects sensory expectations of the speech feedback (weighted by $\boldsymbol{z_{PAu}}$ or $\boldsymbol{z_{PS}}$) to auditory (***ΔAu***) and somatosensory (***ΔS***) error cells, where they are compared to the actual sensory feedback (***Au*** and ***S*** in Equation 5.1). Note that the projections of sensory expectations are learned and continually improve with correct practice (Guenther et al., 2005).

Equation 5.1:

$$\Delta S(t) = S(t) - P(t - \delta_{PS})z_{PS}(t)$$
$$\Delta Au(t) = Au(t) - P(t - \delta_{PAu})z_{PAu}(t)$$

Here, δ_{PS} and δ_{PAu} represent the transmission delays between the premotor cortex to somatosensory and auditory cortices, respectively; in the simulations, these delays are set to 3 msec (Guenther et al., 2005). The weights $\boldsymbol{z_{PAu}}$ encode the auditory expectations (i.e. the goals), which are hypothesized to be learned when an infant hears correct productions of speech from other speakers. On the other hand, the weights $\boldsymbol{z_{PS}}$ encode the somatosensory expectations, and are presumed to be tuned during correct self-productions. It is important to note that Equation 5.1 is modified to account for auditory and somatosensory goals that are not simple point targets, but are goal *regions* (see Equation 5.7 and Equation 5.8).

The signals resulting from the sensory error cells project to the articulatory velocity map, resulting in the feedback component of the motor command**.** These inverse differential kinematics projections are governed by Equation 5.2 (Guenther et al., 2005); here, the gains $\boldsymbol{\alpha_{fb,Au}}$ and $\boldsymbol{\alpha_{fb,S}}$ control how much it contributes to the overall motor command.

Equation 5.2:

$$\Delta M_{fb,Au}(t) = \alpha_{fb,Au} z_{AuM} \Delta Au(t - \delta_{AuM})$$
$$\Delta M_{fb,S}(t) = \alpha_{fb,S} z_{SM} \Delta S(t - \delta_{SM})$$

δ_{AuM} and δ_{SM} represent the transmission delays between auditory and somatosensory cortices and motor cortex, and are again set to 3msec in the simulations. The weights $\boldsymbol{z_{AuM}}$ and $\boldsymbol{z_{SM}}$ transform the sensory error signals into corrective motor, and represent pseudoinverse of the Jacobian relating articulator position (***M***) to the appropriate auditory (***Au***) or somatosensory (***S***) state (Guenther et al., 1998). It is hypothesized that these weights are learned in infancy by babbling—i.e., by making speech motor movements and learning the sensory consequences of those actions.

The speech sound map ***P***—aside from giving rise to the sensory expectations—also projects directly to motor cortex, giving rise to the feedforward component of the motor command ΔM_{ff} (Equation 5.3). By averaging over previous attempts to produce the given speech sound, this motor command is improved over time (Guenther et al., 2005). In the following equation, the feedforward commands are encoded by the weights z_{PM}.

Equation 5.3: $$\Delta M_{ff}(t) = P(t) z_{PM}(t) - M(t)$$

The feedforward and the two feedback components of the motor command are integrated together to form the set of motor commands ***M***, which specifies the desired positions of the speech articulators. Specifically, motor cortex positional cells are governed by
Equation 5.4 (Guenther et al., 2005). Note that the speaking rate signal or "Go" signal (Bullock and Grossberg, 1988)—represented in this equation by ***g(t)***—is present in this equation for completeness, but is outside of the scope of this study. Instead, the function ***g(t)*** is simply set to 1 while speaking. Additionally, ***M*****(0)** represents the configuration of the vocal tract at the time that speaking commences.

Equation 5.4:

$$M(t) = M(0) + \alpha_{ff} \int_{o}^{t} \Delta M_{ff}(t') g(t') dt' + \alpha_{fb,Au} \int_{o}^{t} \Delta M_{fb,Au}(t') g(t') dt' + \alpha_{fb,S} \int_{o}^{t} \Delta M_{fb,S}(t') g(t') dt'$$

The motor commands represented by ***M*** in turn drive the articulators of the vocal tract, producing the speech sound; this production provides sensory feedback to the motor control system. In the DIVA model, the motor commands ***M*** are sent to an articulatory-based speech synthesizer—the Maeda synthesizer—to produce speech sounds (Maeda, 1990).

When first learning to speak (corresponding to infant babbling and early word production), the feedback component of speech control dominates, since the model has not yet learned feedforward commands for different speech sounds. With continued speech training, the feedforward projections from the speech sound map ***P*** improve in their ability to predict the correct feedforward commands. In trained (e.g. adult) speech in normal conditions, feedforward control dominates the command signal for ***M*** cells, since the error signal resulting from the auditory (***ΔAu***) and somatosensory (***ΔS***) error cells is small due to accurate feedforward commands. In the context of the proposed study, alterations in auditory feedback cause the feedback control signal (specifically the auditory component) to increase and significantly influence the overall control of speech motor cortex. Adaptation occurs in this model as the feedforward projections remap to account for the acoustic perturbation.

In the current SA protocol, only the auditory component of the sensory feedback is perturbed; the somatosensory feedback is left unperturbed. Because of somatosensory feedback, the model predicts that adaptation should not fully compensate for purely auditory perturbations. That is, modified feedforward commands will begin to mismatch with previously learned somatosensory goals, so that the somatosensory error signal counteracts (though not completely) the effects of the auditory error signal. This prediction is explored further in the simulations.

5.1.2. Sensory goal regions and auditory acuity in the DIVA model.

One important property of the DIVA model is its reliance on sensory goal *regions*, rather than *points* (Guenther et al., 1998; Guenther, 1995). The notion of sensory goal regions explains a number of phenomena related to speech production. These properties, which result from *auditory* goal regions, include motor equivalent articulatory configurations (Guenther, 1995; Guenther et al., 1998) and their use in reducing acoustic variability (Guenther et al., 1998; Guenther et al., 1999a; Nieto-Castanon et al., 2005), as well as anticipatory coarticulation, carryover coarticulation, and effects related to speaking rate (Guenther, 1995).

Auditory goal regions also allow the DIVA model to predict the relation (confirmed by the experimental results in Chapter 4) that subjects with greater acuity—and thus smaller goal regions—should adapt to a greater extent (see Section 4.1.1). For computational simplicity, previous versions of the DIVA model used a very simple notion of the auditory goal regions that were strict "all or nothing" regions. A more realistic form of the auditory goal regions—one which avoids strict boundaries—is defined here and used in most of simulation results described in Section 5.2; simulations results using the "all or nothing" auditory goal regions are analyzed in Section 5.2.5.

In the new version of auditory goal regions, both the auditory goals ***G*** and the auditory feedback ***F*** are modeled as Gaussian distributions (represented by weights $\boldsymbol{z_G}$ and $\boldsymbol{z_F}$, respectively) acting on error cells $\boldsymbol{x_i}$ (which are each tuned to a preferred frequency) as indicated in Equation 5.5.

Equation 5.5:

$$z_G(x_i) = \exp\left[-\frac{(x_i - \langle G \rangle)^2}{2\sigma_G{}^2} \right]$$

$$z_F(x_i) = \exp\left[-\frac{\left(x_i - \langle F \rangle\right)^2}{2\sigma_F{}^2} \right]$$

The auditory acuity of a simulation can be controlled by varying the standard deviations $\boldsymbol{\sigma_G}$ and $\boldsymbol{\sigma_F}$. These values are linearly related to each other, as specified in Equation 5.6:

Equation 5.6: $$\sigma_G = k_\sigma * \sigma_F, \qquad where \;\; k_\sigma > 1$$

The assumption inherent in Equation 5.6—that people with greater discrimination (smaller $\boldsymbol{\sigma_F}$) will have smaller auditory goals (smaller $\boldsymbol{\sigma_G}$)—is a reasonable one, given that individuals rely heavily on their perception of the acoustic feedback when learning their auditory goals. The assumption that $\boldsymbol{\sigma_G}$ is greater than $\boldsymbol{\sigma_F}$ effectively encodes the concept that the goals are regions, rather than single points, in auditory space; that is, more than one value of auditory feedback is encoded within the goal. Example activation distributions are shown in Figure 5.2.

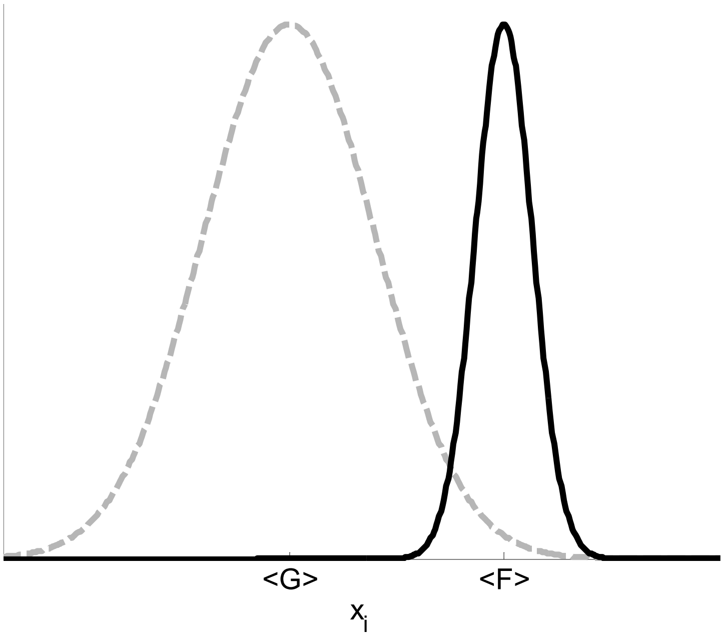

Figure 5.2: Example of the hypothetical activation distributions, in an auditory dimension. The curves z_F (solid) and z_G (dashed) represent the activation—as a function of x_i (preferred frequency in an auditory dimension)—resulting from the actual feedback and the goal.

Equation 5.7 describes the manner in which the distributions from Equation 5.5 are incorporated in the auditory error calculation. The output activity of a given cell (term within the numerator summation) consists of the difference between the activity of the feedback and the goal distributions, with rectification such that negative values are set to zero; this component makes the output dependent on the variance of the feedback and goal regions. Such a function could be thought of as excitatory inputs $\boldsymbol{z_F}$ and inhibitory inputs $\boldsymbol{z_G}$ acting on a given neuron $\boldsymbol{x_i}$, with the rectification acting as a threshold value necessary to excite $\boldsymbol{x_i}$. The auditory error **ΔAu** consists of the sum over all of these cells, and is normalized by the size of the total activation from the feedback (z_F)[11].

Equation 5.7:

$$\Delta Au = \frac{sign(\langle F\rangle - \langle G\rangle)\sum_i [z_F(x_i) - z_G(x_i)]^+}{\sum_i z_F(x_i)}$$

$$where$$

$$[k]^+ = \begin{cases} k, & if \quad k > 0 \\ 0, & otherwise \end{cases}$$

$$and$$

$$sign(k) = \begin{cases} 1, & if \quad k > 0 \\ -1, & otherwise \end{cases}$$

The *sign* function in Equation 5.7 simply yields the direction of the error, based on the difference between the center frequencies of the feedback **<*F*>** and the goal **<*G*>**. The specific value of σ_F for each subject was determined from the *jnd* to adaptive response correlation discussed in Section 4.3.2, under the assumption that the σ_F value is linearly proportional to the subject's *jnd* for the center milestone. The relation between σ_F and adaptive response index is shown below in Figure 5.3. The regression line was used to calculate σ_F from a subject's adaptive response if the *jnd* was not measured, by spacing the missing values (3 for the 0.7 pert group and 4 for the 1.3 pert group) equally along the range of σ_F values. (Recall that auditory acuity data were not collected for 7 of the 20 subjects.) Note that these standard deviation values below refer only to F1; while the standard deviations for higher formants (F2 and F3) varied similarly, they were made larger to roughly account for Weber's law—i.e. the difference threshold or *jnd* is expected to be larger when baseline value (in this case, formant frequency) increases.

[11] To avoid undefined values, ***ΔAu*** was set to 0 rather than using this calculation in blocked feedback trials.

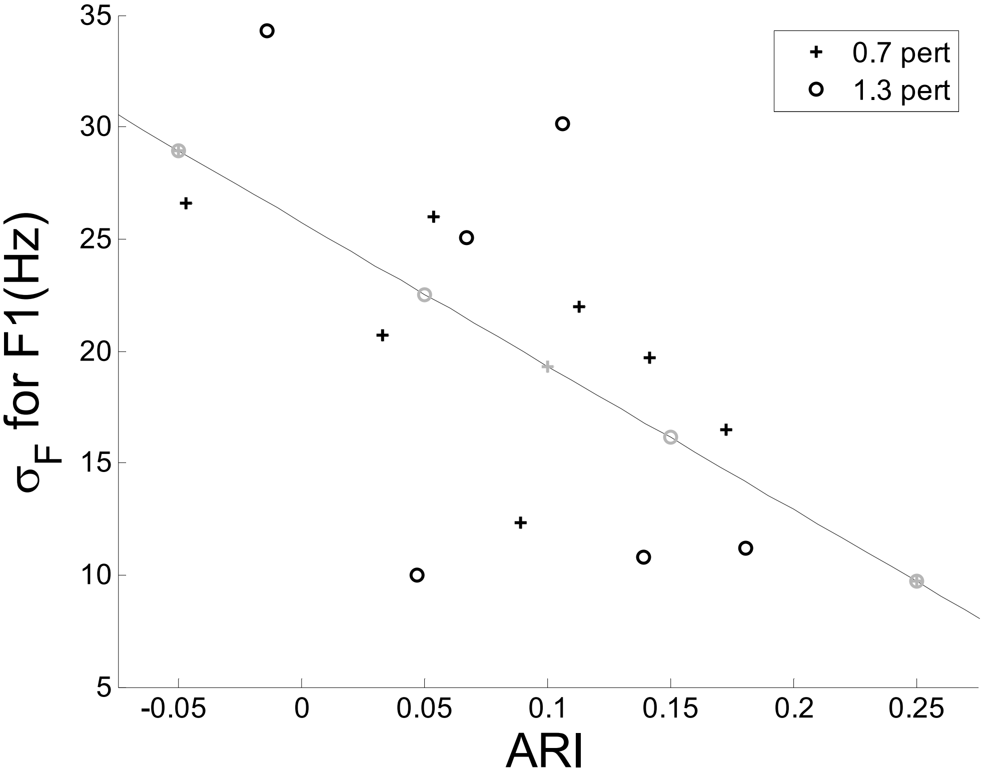

Figure 5.3: Relation between subject adaptive response index (ARI) and model σ_F value. This plot is similar to Figure 4.8, but the ordinate is rescaled from *jnd* values on the *pert* scale to standard deviation values for the auditory activation distributions in Hertz. The cross-labeled values refer to 0.7 pert condition subjects, while the open circles refer to 1.3 pert condition subjects. (Two points, both lying on the regression line, overlapped.) For subjects in which *jnd* was not measured (gray data points), σ_F. was distributed evenly along the range of σ_F. from the regression line.

While the above discussion addresses the calculation of auditory error, the DIVA model also includes a similar set of calculations for the somatosensory error cells. However, the focus of the model simulations presented here is to address adaptation to auditory perturbations, and its relation to auditory acuity. Additionally, measures were not made regarding subject acuity with regard to somatosensory dimensions. Thus, somatosensory error is conceptualized here using a much simpler framework, which has been shown (Guenther et al., 2005) to replicate human data from experiments utilizing somatosensory perturbations, such as lip perturbations (Abbs and Gracco, 1984) or jaw perturbations (Kelso et al., 1984). Specifically, the somatosensory space is composed of dimensions representing proprioceptive information of the current position of the articulators in antagonistic pairs, as well as dimensions representing palatal and labial tactile information. The somatosensory error ***ΔS*** is simply the difference between the goal (***zPS***) and the actual feedback (***S***); for tactile dimensions, this error is algorithmically adjusted so that no error results if the actual feedback falls within a target region (Equation 5.8)[12].

Equation 5.8:

$$\Delta S_{propioceptive} = S_{propioceptive} - zPS_{propioceptive}$$

$$\Delta S_{tactile} = \begin{cases} S_{tactile} - zPS_{tactile}, & if \ \left|S_{tactile} - zPS_{tactile}\right| > threshold \\ 0, & otherwise \end{cases}$$

This somatosensory error calculation drives corrective movements which resist changes in the feedforward command, since such changes will cause somatosensory error and corresponding corrective movements via the somatosensory feedback control. Thus the model will not completely compensate for an auditory perturbation, since the somatosensory feedback will resist compensatory changes to the feedforward command.

5.1.3. Design of the SA simulations within the DIVA model.

The SA experiment was simulated in the DIVA model as a series of trials under varying levels of perturbation to the auditory feedback, with one trial in the DIVA simulation representing one attempt of the DIVA model to produce the given speech token. To simplify the simulations, the target token the DIVA simulations produced was solely the phoneme /ɛ/. Also, the auditory dimensions used in these simulations were the first three formant frequencies, in units of Hertz[13].

Each SA simulation was preceded by a 10 trial speech acquisition period, which allowed the model to learn the baseline speech target. Following this acquisition period, the following simulation trials were divided into four phases, similar in design to the human subject SA experiments: *baseline*, *ramp*, *full-pert*, and *post-*

[12] This threshold represents roughly 2 to 3 percent of the tactile cell's dynamic range.

[13] An alternative representation of the auditory space—using formant ratios—was also considered. However, the use of these auditory dimensions resulted in unintelligible speech productions in pilot studies.

pert. Like the human subject experiments, the perturbation used in the *full-pert* phase is either 0.7 or 1.3 pert.

After acquisition, auditory feedback was turned on and off to replicate the *+feedback* and *-feedback* SA results. For the vowel /ɛ/, the human SA experiment was composed of nine +feedback tokens and three –feedback tokens. To maintain this ratio, one epoch in the simulation was composed of four trials: three trials with feedback turned on, followed by one trial with feedback turned off.

Table 5.1 lists DIVA parameter settings relevant to the SA simulations. While this table briefly describes these settings, these parameters deserve a little more discussion.

- $\boldsymbol{\alpha_{ff}}$: This gain controls the contribution of the feedforward command according to Equation 5.4.
- $\boldsymbol{\alpha_{fb,Au}}$ and $\boldsymbol{\alpha_{fb,S}}$: These gains control the relative contributions of sensory error from auditory and somatosensory error cells to the overall feedback motor command, as according to Equation 5.2. Setting the contribution from somatosensory error to be smaller than the auditory contribution is an assumption that should be valid for vowels (e.g. (Guenther et al., 1998).
- $\boldsymbol{zPAu_{learning\_rate}}$: This learning rate parameters control how fast the auditory expectations (i.e. goals) change. The learning rate of ***zPAu*** is set to 0, meaning that the auditory goals are invariant once a person has learned them (presumably early on in life).
- $\boldsymbol{zPS_{learning\_rate}}$: This learning rate parameters control how fast the somatosensory goals change. Setting $\boldsymbol{zPS_{learning\_rate}}$ to a small value (e.g. 0.001) indicates that the somatosensory goals are expected to change very little over the course of a 1.5 hour experiment; the fact that the somatosensory goals do not change all that much plays an important role in allowing the SA simulations to recover to baseline in the post-pert

phase (see Section 5.2.1). Somatosensory targets are expected to change slowly over a person's lifetime to account for developmental changes in the vocal tract (Callan et al., 2000).

- $zPM_{learning\_rate}$: This learning rate parameters control how fast the feedforward commands are updated. Setting $zPM_{learning\_rate}$ to 0.25 (as opposed to a larger value) allows the feedforward commands to be learned gradually.
- The inertial dampening terms smooth out sharp movements (which are likely physiologically unfeasible) by performing the operation in Equation 5.9 at each time step.

Equation 5.9: $$value(t) = value(t-1) * INERT + (1 - INERT) * value(t)$$

α_{ff}	1.00	*gain for the feedforward command to the overall motor command*
$\alpha_{fb,Au}$	0.95	*gain for the auditory component of the feedback command*
$\alpha_{fb,S}$	0.15	*gain for the somatosensory component of the feedback command*
$zPAu_{learning\_rate}$	0	*controls how fast the auditory goals are updated*
$zPS_{learning\_rate}$	0.001	*controls how fast the somatosensory goals are updated*
$zPM_{learning\_rate}$	0.15	*controls how fast the feedforward commands are updated*
k_{σ}	5.0	*linear relation between* σ_G *and* σ_F
FB_{inert}	0.40	*inertial dampening of the feedback command*
M_{inert}	0.80	*inertial dampening of the motor output*

Table 5.1: Relevant DIVA parameter for the SA simulation. Listed here are the relevant parameters, the values used, and a brief description of the parameter.

Results of the following SA simulations are typically shown as the first formant of each trial, normalized to the mean of the baseline F1. Some of the following DIVA model simulations deviated from the standard model parameters outlined here, as noted in the following text.

5.2. DIVA SA simulations results, with comparison to human subject experiments.

5.2.1. DIVA simulations compared with human subject experiments in the +feedback condition.

Results for the DIVA simulations of the SA protocol from *+feedback* trials are compared to human subject SA data in Figure 5.4. The simulations were composed of twenty individual experimental runs, divided into two sets of pert conditions (either 0.7 or 1.3, just as in the human SA experiments). For a given set of pert conditions, the only parameter varied was the acuity parameter σ_F—using the subjects' measured or interpolated *jnd* (see Figure 5.3).

Figure 5.4--shown in normalized first formant values—demonstrates that the SA simulations account for the human SA data, with F1 changing due to the acoustic perturbation, then returning to the baseline during the post-pert phase. In this comparison between SA simulations and human subject experiments, the SA simulations were able to replicate the full-pert phase of the human subject results, and in the post-pert phase, the simulations returned by to baseline at a similar rate to the human subject results. However, at the ramp-phase, the human SA results seem to show a faster adaptive response than the simulation results, though this difference is not statistically significant (see below).

Comparing the 0.7 pert group to the 1.3 pert group, it is interesting to note that there is a slight asymmetry between the two groups, seen in both the simulations and the human subject results. This is not surprising, given that the inverse of the perturbation—which represents the maximal response expected—is a larger change from baseline for the 0.7 pert condition than for the 1.3 pert. To determine if the simulation results were significantly different than the human subject results, a pooled, two-tail t-test was performed on an epoch-by-epoch basis between the two results; significant differences are indicated in Figure 5.4 by the open circles. This figure indicates that the simulations differed significantly from the subject data in only a few baseline epochs. Also, by comparing the high acuity (solid lines) to the low acuity (dashed lines) simulations, this figure explicitly demonstrates how acuity and the extent of adaptation are positively related in the model.

Note that human subjects tended to gradually increase F1 throughout the baseline (i.e. before the perturbation). The F1 baseline rise is likely a tendency that research subjects exhibit in the abnormal speaking conditions of the experimental setup—(c.f. (Jones and Munhall, 2000). Since the model does not include this tendency, a constant baseline is produced by the model, resulting in the significant differences between the subjects and the model in the baseline phase.

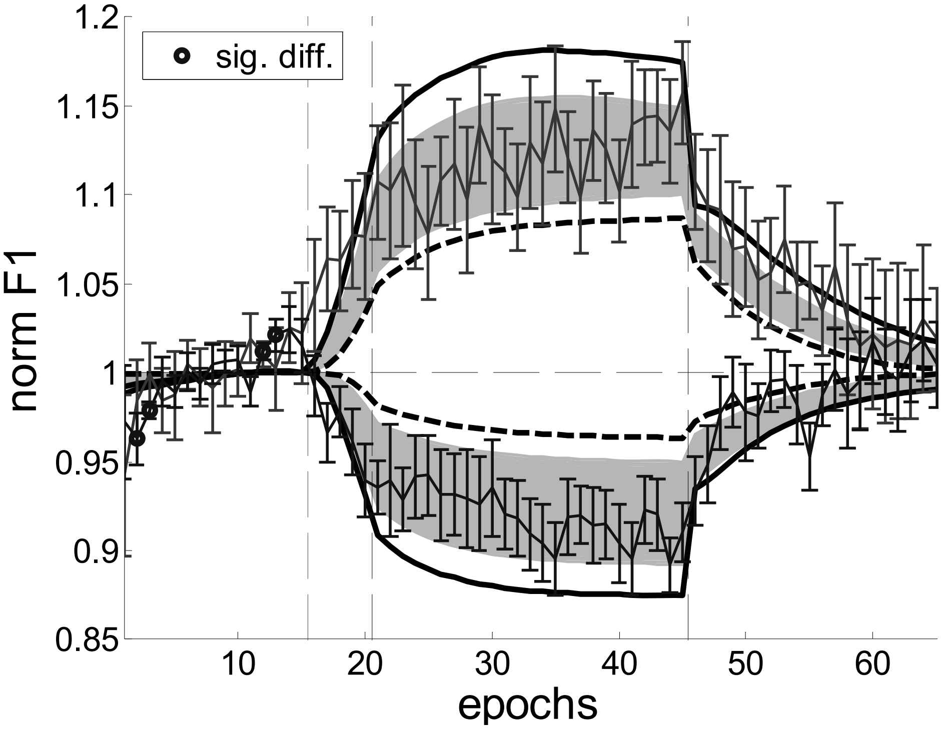

Figure 5.4: Normalized F1 during the SA protocol (with feedback), DIVA simulations compared to human subject results. The ordinate corresponds to the adaptive response in the first formant. The abscissa corresponds to the epoch number. The thin lines shown with standard error bars correspond to the human subject SA data (twenty subjects). The lighter shaded region corresponds to the DIVA simulations, and represents the 95% confidence interval about the mean. The vertical dashed lines show the experimental phase transitions, and the horizontal dashed line indicates the baseline. The open circles indicate epochs in which the data and the simulation results are significantly different. The black solid curves correspond to high acuity (i.e. low σ_F) simulations, while the black dashed curves correspond to low acuity simulations.

Simulation and human subject results from the two pert conditions were then combined by plotting these in *adaptive response* units, similar to what was done in study 1 (see Figure 3.10). Shown in Figure 5.5, the simulation results from the DIVA model compare favorably (as a whole) with human data. Note that only in one epoch during the ramp phase do the simulation and human data differ significantly from one another.

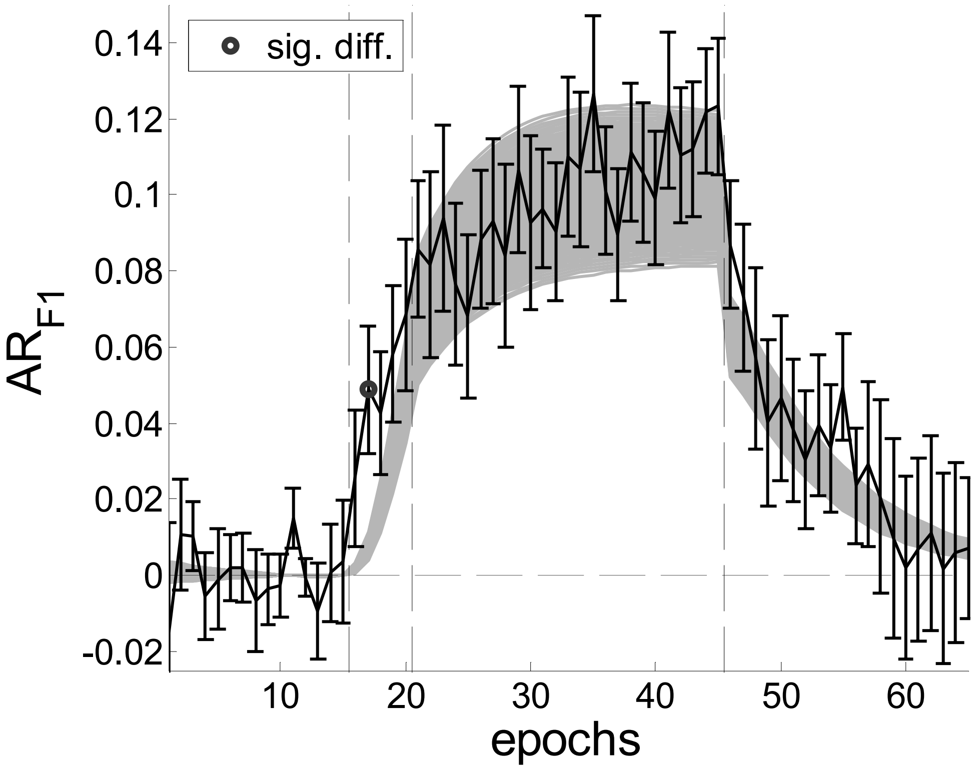

Figure 5.5: Adaptive response (AR) in F1 during the SA protocol (with feedback), DIVA simulations compared to human subject results. The ordinate corresponds to the adaptive response in the first formant. The abscissa corresponds to the epoch number. The soild lines shown with standard error bars correspond to the human subject SA data (all twenty subjects). The lighter shaded region corresponds to the DIVA SA simulations, and represents the 95% confidence interval about the mean. The vertical dashed lines show the experimental phase transitions, and the horizontal dashed line indicates the baseline. The open circle indicates the only epoch in which the data and the simulation results were significantly different.

5.2.2. DIVA simulations changes with changes in simulation parameters.

The SA simulations shown in Figure 5.5 showed near full recovery to baseline in the post-pert phase, similar to the human data results. This property depends in part on setting *$zPS_{learning\_rate}$*—the learning rate of the expected somatosensory states—to a small value (0.001). This slow learning rate for *zPS* allows the expected somatosensory state of the vowel to remain unchanged throughout the experiment; when the perturbation is removed in the post-pert phase, the model thus returns to articulating the vowel as in the baseline phase because it is driven to minimize both auditory *and* somatosensory error. To demonstrate the counter-example, *$zPS_{learning\_rate}$* was increased to 0.005 in a set of similar simulations (Figure 5.6). The increased learning rate in the somatosensory expectations has the effect of allowing *zPS* to change more over time as a result of compensation to the perturbation, rather than act completely resistive. These changes in *zPS* prevent F1 from recovering fully (note how *AR_{F1}* is elevated above baseline in the post-pert phase.

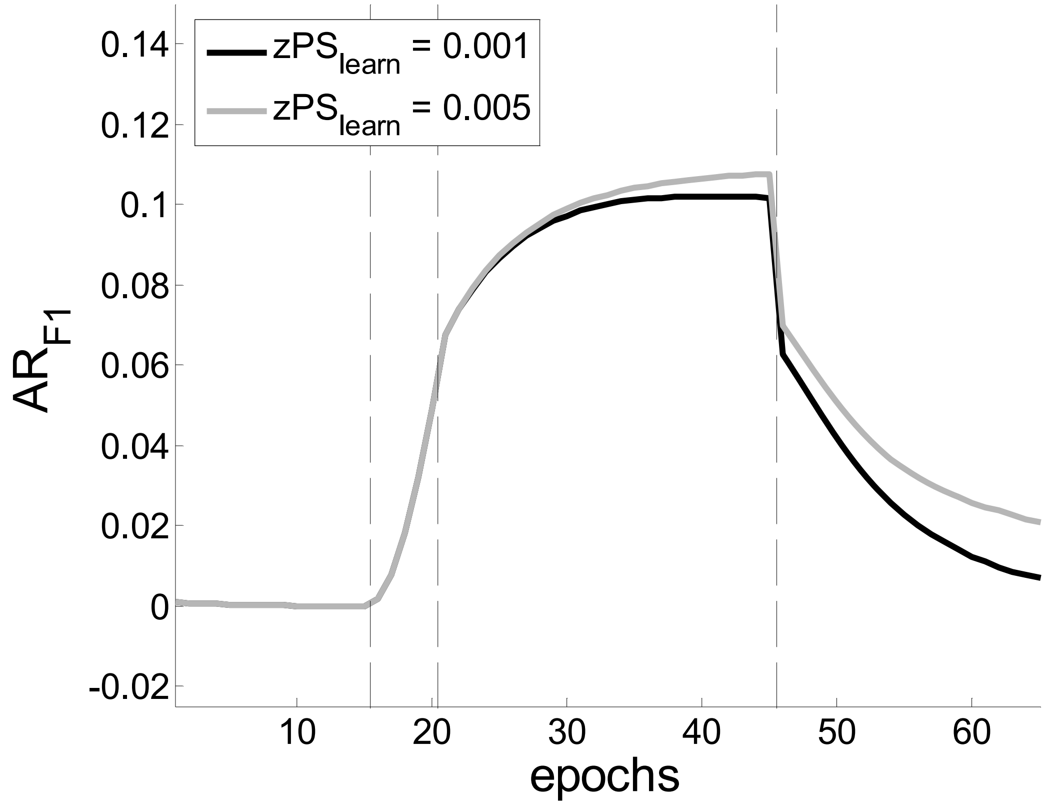

Figure 5.6: Adaptive response (AR) in F1 if the learning rate of the somatosensory goal zPS is increased. This is similar to Figure 5.5, except that adaptive response between simulations with *$zPS_{learning\_rate}$* = 0.001 (black) and *$zPS_{learning\_rate}$* = 0.005 (gray) are compared. Each curve corresponds to the mean over 20 subjects. Refer to Figure 5.5 for axes details.

While the amount of adaptation in the simulations described thus far was controlled solely by the acuity parameter $\boldsymbol{\sigma_F}$, it is also possible to alter the degree of adaptation by changing the relative contributions of the feedback from the somatosensory ($\boldsymbol{\alpha_{fb,S}}$), or auditory ($\boldsymbol{\alpha_{fb,Au}}$) error cells. For example, the extent of adaptation can be decreased by increasing $\boldsymbol{\alpha_{fb,S}}$ (from 0.25 to 0.5 as in Figure 5.7, left side) or by decreasing $\boldsymbol{\alpha_{fb,Au}}$ (from 0.9 to 0.5 as in Figure 5.7, right side). These simulation results suggest that somatosensory measures should be made in future SA experiments—e.g. (Wallace and Max, 2004)—so that the relative contribution between somatosensory and auditory feedback can be better accounted for.

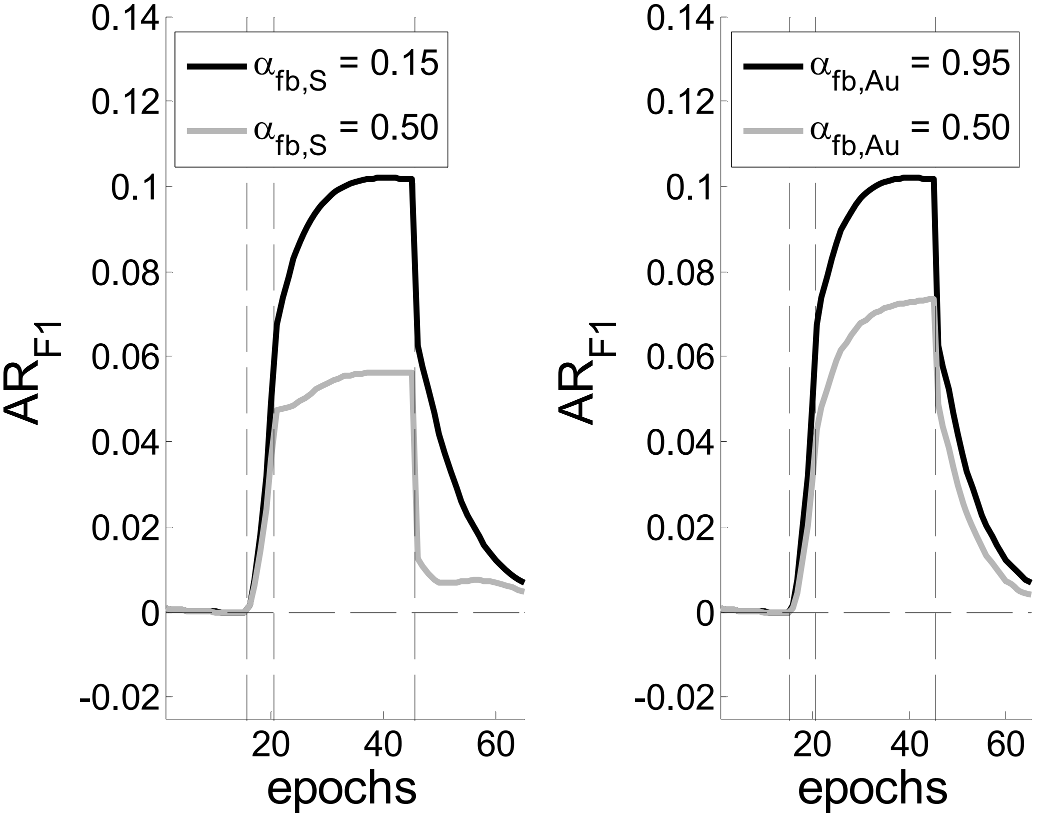

Figure 5.7: Adaptive response (AR) in F1 decreases if the contribution of auditory feedback relative to somatosensory feedback is decreased. These simulations are similar to those shown in Figure 5.5, except that $\alpha_{fb,S}$ is increased from 0.25 to 0.50 (left) or $\alpha_{fb,Au}$ is decreased from 0.90 to 0.50 (right). Each curve corresponds to the mean over 20 subjects. The simulations using the original parameters are shown in the dark curves; the simulations using the changed parameters are shown in the lighter shaded curves. Note that adaptive response decreases with both of these parameter changes. Refer to Figure 5.5 for axes details.

5.2.3. Changes in the second formant frequency found in the DIVA SA simulations.

To understand how the DIVA simulations model the human changes observed in the second formant, adaptive response values in F2 for the simulations and human results are compared in Figure 5.8. The adaptive responses in the second formant for the DIVA simulations were small, obvious by comparing scale of Figure 5.8 to that of Figure 5.5, which shows adaptive response in F1. Moreover, the simulations exhibited changes in F2 that were on the same scale as seen in the human data. However, the trend of F2 changing in the opposite direction of F1—observed in the human results (see Section 3.4.2)—was not observed in these simulations. That is, F2 changed in the positive direction during the full-pert, which is the same direction as the adaptive response changes for F1.

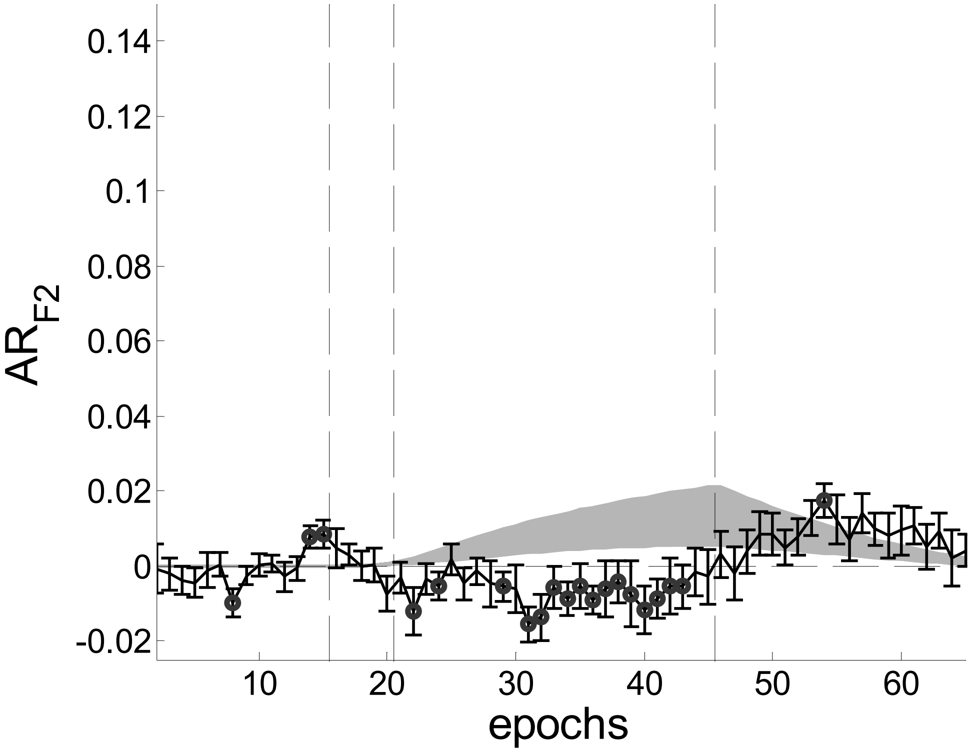

Figure 5.8: Adaptive response in F2 during the SA protocol (with feedback), DIVA simulated subjects compared to human subject results. This is similar to Figure 5.5, but for the second formant adaptive response. The scale of the ordinate is the same as in Figure 5.5.

As mentioned earlier, the dimensions for the auditory goals were represented by formant frequencies, in units of Hertz (see Section 5.1.3). It is possible that representing the auditory goal regions in an alternative auditory space would better account for properties related to F2 changes. SA simulations were run with the auditory spaced represented in Miller formant ratios (Miller, 1989); this space is define in Equation 3.1. These simulations showed changes in F1 (see Figure 5.9) that did not follow the human subject results as closely as the simulations using normal formant auditory dimensions (refer to Figure 5.5). However, it is interesting to note that F2 for these simulations changes in the same direction as the human results; that is, in the opposite direction of the F1 changes (see Figure 5.10). Formant ratios have been suggested as a way of presenting acoustic signals for the same speech sound across speakers; the present simulation results suggest that a speaker-normalized auditory representation may explain the F2 results better than the standard formant representation (Callan et al., 2000).

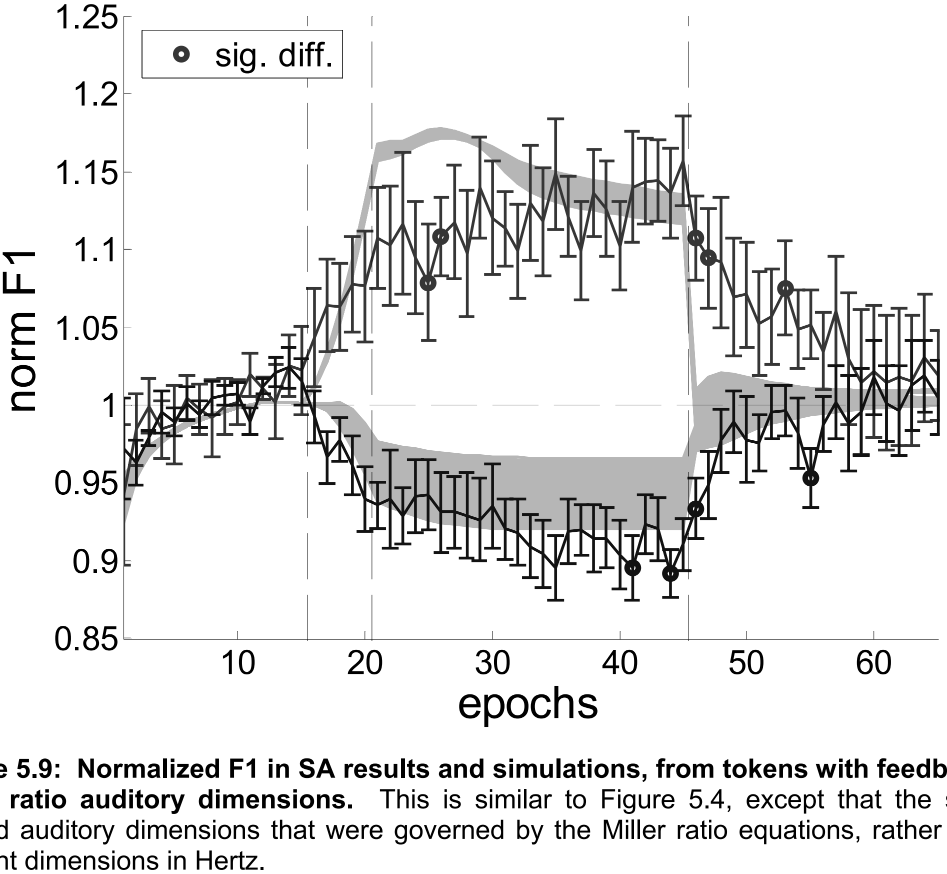

Figure 5.9: Normalized F1 in SA results and simulations, from tokens with feedback, using Miller ratio auditory dimensions. This is similar to Figure 5.4, except that the simulations utilized auditory dimensions that were governed by the Miller ratio equations, rather than using formant dimensions in Hertz.

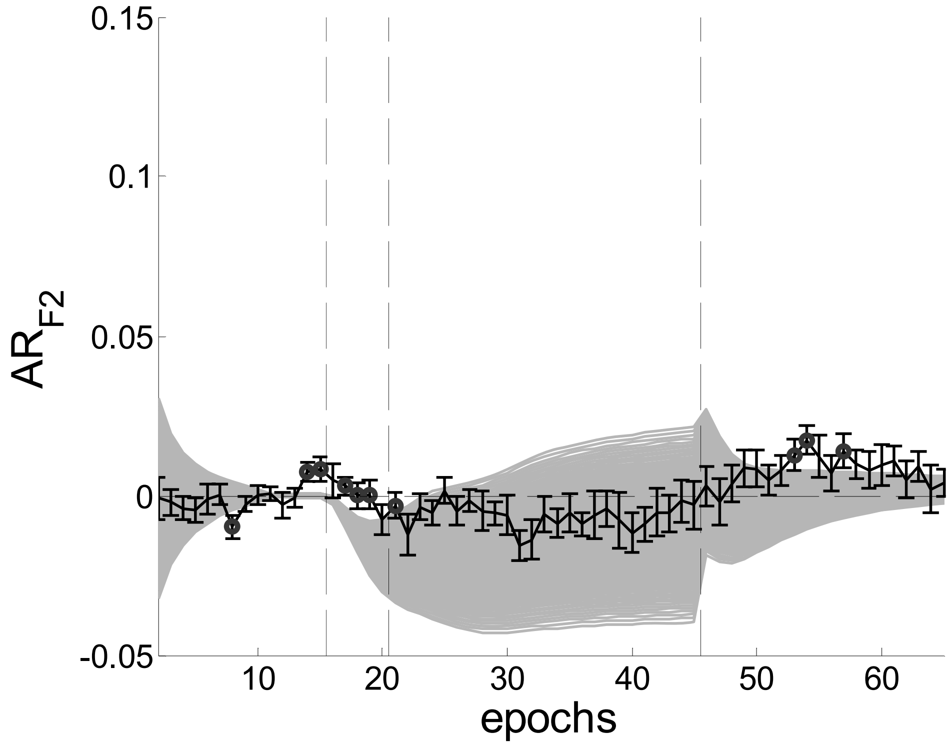

Figure 5.10: Adaptive response of F2 in SA results and simulations, from tokens with feedback, using Miller ratio auditory dimensions. Unlike Figure 5.8, in which the simulations used auditory dimensions of formant values in Hertz, the simulations represented here used auditory dimensions governed by the Miller ratio equations.

5.2.4. DIVA simulations compared to human subject results in the blocked feedback condition.

Since the series of simulations included blocked feedback trials, -feedback SA results for the simulations and human data (refer to Section 3.4.3) were also analyzed (Figure 5.11). The SA simulations exhibit adaptive response that was similar in extent to that seen in human data from –feedback tokens. In the model, the extent of blocked feedback adaptation is controlled by the learning rate of the *zPM* (the feedforward commands). This is because the feedforward component of the total motor command is the only source of information of the perturbation when auditory feedback is blocked. Figure 5.12 shows adaptive response in blocked feedback tokens decreasing when the learning rate of ***zPM*** is decreased (from its current setting of 0.15 to 0.05); when ***zPM*** is increased (from 0.15 to 0.20), adaptive response increases at a faster rate before reaching the same plateau.

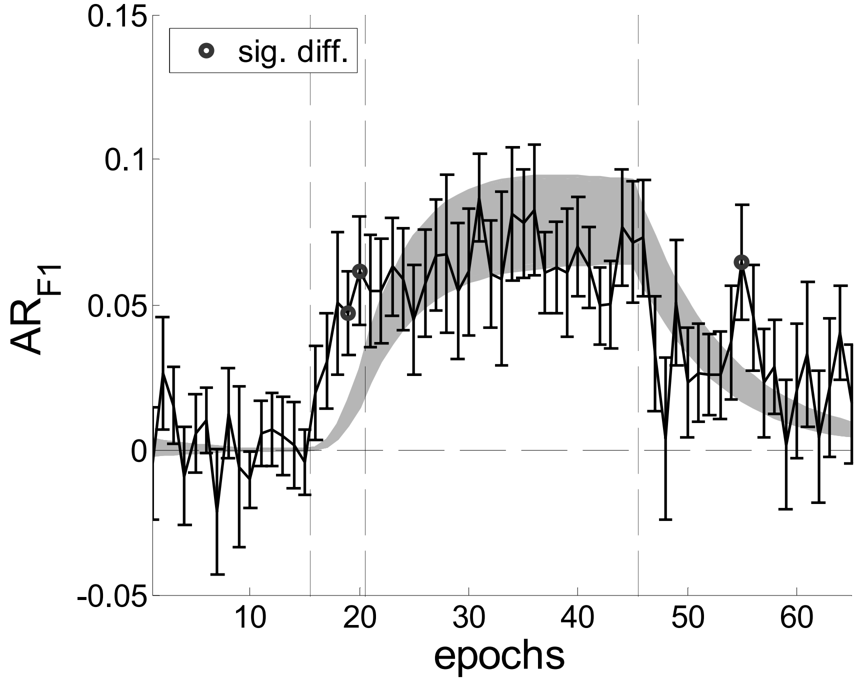

Figure 5.11: Adaptive response (AR) in F1 for blocked feedback trials, DIVA simulated subjects compared to human subject results. This figure is similar to Figure 5.5, but for blocked feedback trials/tokens (rather than +feedback trials/tokens). The scale of the ordinate is the same as in Figure 5.5.

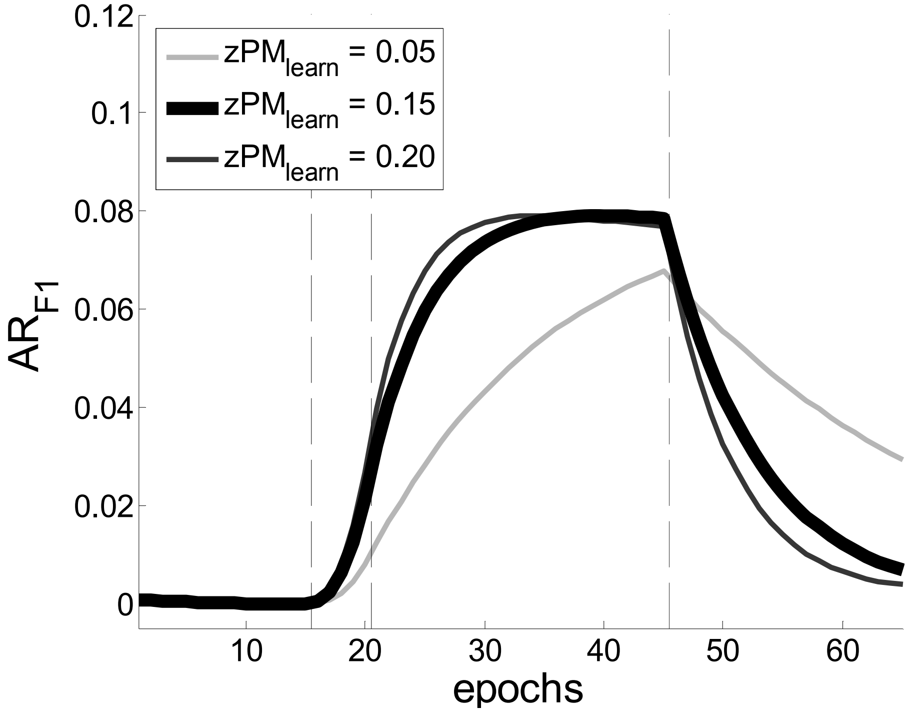

Figure 5.12: Adaptive response in *blocked* auditory feedback tokens changes with changes in *$zPM_{learning\_rate}$*. Each curve corresponds to the mean over 20 subjects. The thick curve shows the default setting for the learning rate of ***zPM***. Blocked feedback adaptation decreases by decreasing this learning rate (light gray curve), while it increases by increasing this learning rate (dark gray curve).

5.2.5. Comparison with a simple conceptualization of the auditory goal regions (the "all or nothing" approach).

Previous versions of the DIVA model implemented a much simpler conceptualization of auditory goal regions (Guenther, 1995; Guenther et al., 1998; Guenther et al., 2005), in which *no* auditory feedback error resulted if the actual feedback fell within the goal region (i.e. the goal region acted as a "dead zone" with respect to feedback error). Algorithmically, this concept of the auditory goal region can be implemented in DIVA as according to the following equation:

Equation 5.10: $$\Delta Au = \begin{cases} LB - Au, & LB > Au \\ UB - Au, & UB < Au \\ 0, & otherwise \end{cases}$$

The action of the auditory error cells in this version of the DIVA model corrects for sensory errors only up to the boundaries of the goal region, rather than all the way up to the center of the goal region (as is the case for the Gaussian targets described in Section 5.1.2) . As shown in Figure 5.13, having the target boundaries widely separated (dotted line) results in a smaller magnitude auditory error signal (and thus smaller $\boldsymbol{\Delta M_{fb,Au}}$) when compared to more narrowly separated boundaries (solid line). In the following simulations, subjects of varying auditory acuity were simulated by varying the separation of the boundaries of the auditory goal regions. The half-width of the goal regions used in these simulations were also based on subject *jnd* scores, and were 0.8 times the $\boldsymbol{\sigma_G}$ values used in the previous simulations.

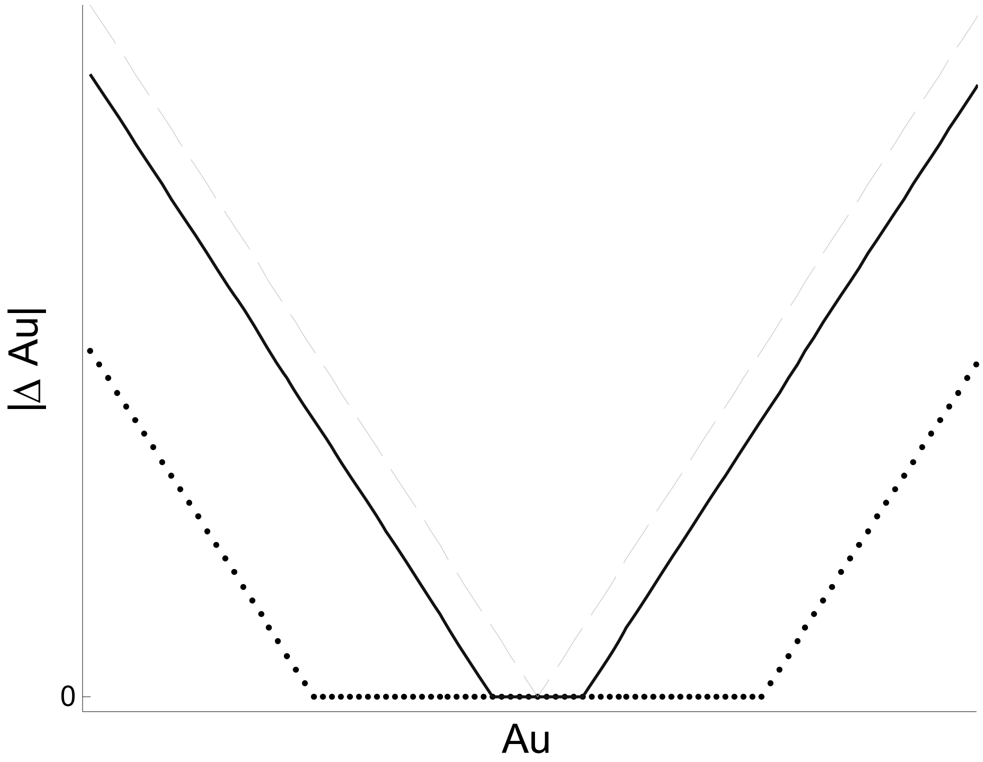

Figure 5.13: Dependence of the output of auditory error cells on the size of the auditory goal. Shown here is the auditory feedback error (***ΔAu***) as a function of the auditory feedback (***Au***), both in one-dimension. The solid line represents the output of ***ΔAu*** from a small goal region, while the dotted line represents the output from a large goal region. For reference, the dashed line represents the output for an auditory point target.

The results of DIVA simulations using these auditory goal regions are shown in Figure 5.14; note that the remaining model parameters (see Table 5.1) were unchanged from the DIVA simulations described in Section 5.2.1. In comparing Figure 5.14 to Figure 5.4 (which used auditory goals regions as described in Section 5.1.2), the two versions of DIVA simulations show striking similarity. Indeed, plotted on the shown scale, the only major differences between the two simulations are that the “all or nothing” goal region simulations appear to have a wider range of responses (exhibited by the wider confidence interval) for the 1.3 pert simulations, and that one epoch during the full-pert phase of the “all or nothing” simulations was significantly different from the human subject results.

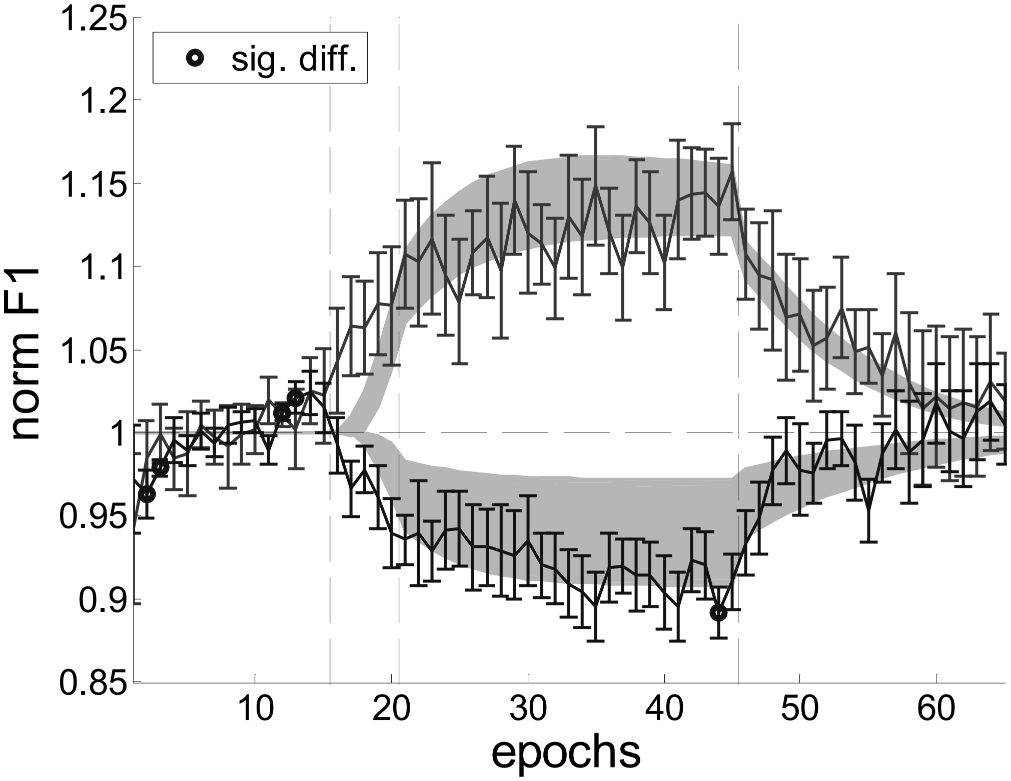

Figure 5.14: Normalized F1 during the SA protocol (with feedback) using "all or nothing" auditory goal regions. This figure is similar to Figure 5.4, except that the simulations shown here used "all or nothing" auditory goal regions, according to Equation 5.10.

One part of the SA protocol in which there would be a predicted difference between the two auditory goal conceptualizations is during small perturbations. Simulations using "all or nothing" auditory goals are expected to show no adaptive response if the actual feedback falls within the auditory goal; the same is not expected of simulations using Gaussian auditory goals. The simulations do in fact demonstrate this behavior, as shown in Figure 5.15; the "all or nothing" simulations show less change in F1 than the Gaussian auditory goal simulations at the early epochs of the ramp phase. Indeed, for epochs 16 and 17 in the 1.3 pert simulations, no change in F1 is seen in the simulations on the right, indicating that the perturbation is not large enough to cause the actual auditory feedback to fall outside the goal region. Given the large adaptive response seen in the ramp phase of the human SA data, it is likely that auditory goal regions resemble the Gaussian distributions rather than the simple "all or nothing" regions in the tendency to start adapting to even very small perturbations.

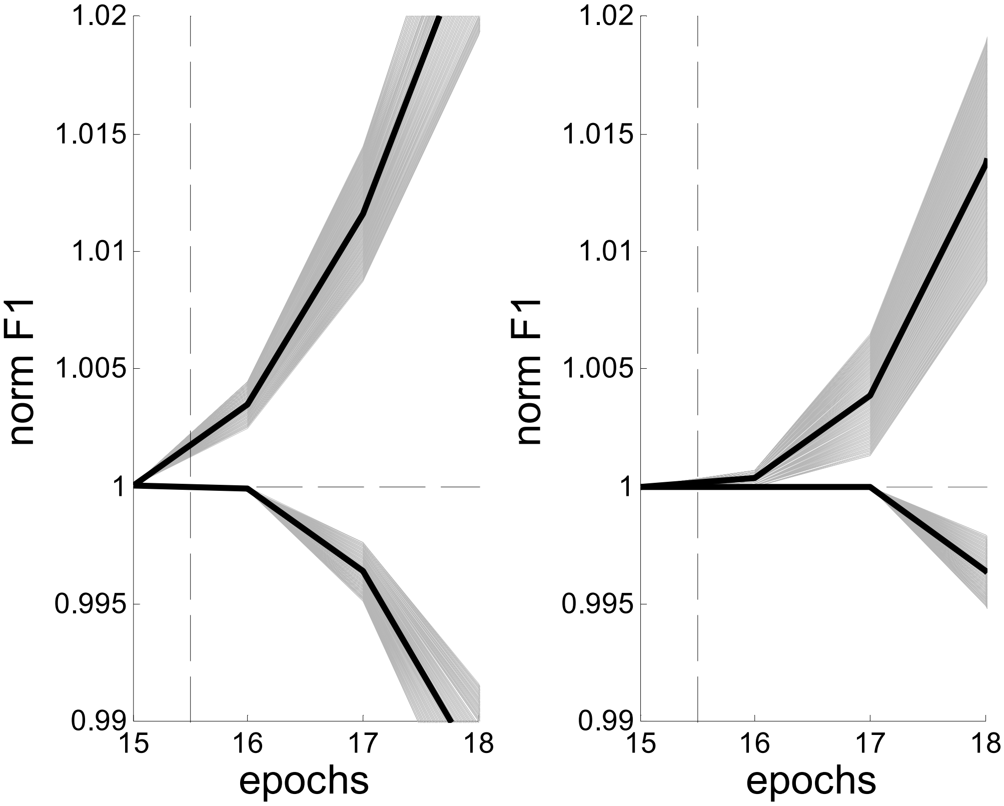

Figure 5.15: Comparison of normalized F1 during the early part of the ramp-phase between simulations using goal regions that are Gaussian (left) or "all or nothing" (right). The solid lines indicate the mean normalized F1 value for 0.7 pert simulations (upper) and 1.3 pert simulations (lower). The shaded regions indicate +/- one standard error. The vertical dashed line indicates the start of the ramp phase, while the horizontal dashed line indicates the baseline**.**

5.3. Study 3 Summary.

In the series of simulations presented here, the DIVA model was able to quantitatively account for a number of characteristics of the human subject SA studies. The DIVA simulations demonstrated adaptation to acoustic perturbations (Figure 5.4 & Figure 5.5). This adaptive response was retained when feedback was turned off in a similar manner to human SA data (Figure 5.11) and demonstrated greater specificity for F1—the formant perturbed in the SA protocol—than for F2 (Figure 5.8). Individual auditory acuity for vowels is accounted for in DIVA by the auditory goal regions, which are smaller in individuals with greater acuity.

Differences between the DIVA simulations and human subject data have suggested possible ways in which DIVA may be modified to better model the speech production system. For example, the simulation results suggest that the interaction between somatosensory feedback and auditory feedback will significantly affect the degree of adaptation (see Figure 5.7). However, the current DIVA simulations were run using the assumption that the relative weight of somatosensory and auditory feedback ($\boldsymbol{\alpha_{fb,S}}$ and $\boldsymbol{\alpha_{fb,Au}}$) are constant from subject to subject, an assumption that may not necessarily be valid and should be measured. Additionally, results from the Miller ratio simulations (Figure 5.10) suggest that changes to the model's auditory representation to account for speaker normalization may provide a better explanation for the direction of change of F2 in response to perturbations in F1.

An additional discrepancy between the simulation results and the human subject results is during the ramp-phase: human subjects appear to react more quickly to the perturbation than the simulations do, though this difference did not reach statistical significance in most epochs. There may be a number of methods to improve the model's performance to small perturbations. The manner in which auditory goal regions are implemented in the model may need to be modified. For example, the shape of the activation distributions $\boldsymbol{z_G}$ and $\boldsymbol{z_F}$ could be changed (they are currently modeled as Gaussian functions) to another function that may allow greater adaptive response to small perturbations than was seen in Figure 5.15. Another possibility is that the auditory error calculation occurs as a two-stage process, rather than the one-stage process described here. Earlier versions of the DIVA model hypothesized that projections from sensory error cells to motor cortex had cortico-cortical components (as described in Section 5.1.1), as well as cerebellar ones (Guenther and Ghosh, 2003). A two-stage feedback control process, with each stage differing in sensitivity to changes in phoneme acoustics, may be able to account for the sensitivity to small acoustic perturbations demonstrated by subjects participating in study 1. However, it should be noted that fMRI experiments studying the regions of the brain that are active during unexpected auditory perturbations (Tourville et al., 2005) did not find regions of the cerebellum active during perturbations, thus supporting the hypothesis that sensory error cells utilize only the cortico-cortical pathway.

Chapter 6. Overall summary and future directions.

6.1. Overall research summary.

The intent of the research in this thesis was to study the auditory feedback component of speech motor control with an experimental protocol that caused subjects to adapt to perturbations in their auditory feedback. Study 1 extensively investigated the responses of human subjects in a speech sensorimotor adaptation protocol, addressing issues such as adaptation specificity (changes in unperturbed auditory dimensions such as F0 or F2); adaptation persistence when feedback is blocked and when the perturbation is removed; and generalization to untrained vowels or phonetic context. In study 2, perceptual acuity for some of the study 1 subjects was measured in two ways: in a discrimination protocol and in a goodness rating task. Analysis of the acuity measures showed that subjects with greater acuity for the acoustic perturbation demonstrated greater adaptive response, and this relation was statistically significant. DIVA model simulations of the sensorimotor adaptation experiments were able to accurately capture many aspects of the human subject results (study 3).

The analysis of this thesis research illuminated a number of assumptions that the DIVA model simulations used to replicate the results of the SA experiment. The variations of the sensorimotor adaptation experiment proposed here are designed to better understand the validity of these assumptions, as well as to allow for further refinement of the DIVA neural network model. Possible ways the DIVA model may be improved are discussed in the following.

6.2. The role of somatosensory feedback.

In the previous DIVA simulations, the weight of somatosensory feedback control ($\alpha_{fb,S}$) relative to auditory feedback control ($\alpha_{fb,Au}$) was presumed to be the same across subjects. This is not necessarily a valid assumption; moreover, since somatosensory feedback can influence the extent of adaptation in DIVA simulations (see Section 5.2.1), it is possible that differences in somatosensory feedback can account for some of the inter-subject variation seen in adaptation.

One possible way to determine the relative contributions of somatosensory and auditory sensory information to the overall feedback motor control command is in an experiment which incorporates conflicting perturbations in both sensory dimensions. Colleagues have developed a jaw-perturbation apparatus (henceforth referred to as the "Perturbatron"), which consists of a solenoid-driven air cylinder that delivers pneumatic pressure to a small balloon placed between the subjects molars (Tourville et al., 2004). Jaw height can be used to control first formant frequency: vowels with a high F1 (such as /æ/) are articulated with a low jaw height while low F1 vowels (such as /I/) are articulated with a high jaw height. By using the Perturbatron in conjunction with F1 formant shifted acoustic feedback such that subjects get contradictory somatosensory and auditory feedback concerning F1, it would be possible to measure the degree to which the jaw perturbation inhibits adaptation to acoustic perturbations. The extent of this inhibition can give insight into how auditory feedback and somatosensory feedback interact in speech motor control. It would also be interesting to study subject acuity to somatosensory feedback, in a manner analogous to the way auditory acuity was studied in Study 2. As mentioned in Section 5.1.2, somatosensory error in the simulations was calculated in a simpler manner than auditory error because subject somatosensory acuity data did not exist.

6.3. SA experiments using acoustic perturbations of other acoustic cues.

Shifts in vowel F1 (as used in this specific acoustic perturbation algorithm) correspond to tongue body height movements (Stevens, 1998). Specifically, shifting F1 about /ɛ/—a [-high, -low] vowel—altered the sound towards /æ/—a [-high, +low] vowel—for F1 increases, or altered it to sound like /I/—a [+high, -low] vowel. A similar SA experiment might be carried out which studies subject responses to second formant (F2) shifts, with the hypothesis that subjects should demonstrate adaptive responses in F2 in an equivalent manner that was shown in study 1. However, this experiment lacks the symmetry in phonetic representation of F2 shifts that exists for shifts in F1 of /ɛ/. Whereas shifting F2 up for a [+back] vowel can cause it to be perceived as a [-back] vowel, shifting F2 down for the same vowel does not lead to a perception of different vowel perception (Stevens, 1998). Indeed, the fact that F2 is already low in [+back] vowels may present a constraint for subjects in their adaptive response. (Note that a similar problem is posed for F2 shifts in [-back] vowels

Another future SA experiment could use a similar F1 shift, but centering the shift on the [+back] vowel /o/; /ɛ/ is a [-back] vowel. Again, the hypothesis is that subjects should demonstrate adaptation in the same way as shown in study 1. This SA experiment would require modification to the F1 perturbation algorithm to improve F1 detection, since [+back] vowels have low F2 values that have the potential of being falsely detected as F1. Further, this acoustic perturbation algorithm might also be used to study adaptive responses to third formant (F3) perturbations in the phoneme /r/—which is acoustically distinctive by a drop in F3 (Boyce and Espy-Wilson, 1997). The approach could also be broadened by introducing acoustic perturbations of the acoustics of consonants.

Taken together, such SA experiments would test the robustness of the hypothesis that speech motor planning makes use of sensory goal regions.

6.4. Neuroanatomic loci of sensory error cells.

Aside from functionally describing the speech motor control system, the DIVA model also predicts the anatomic locations of the neural cells that make up this system (Guenther et al., 2005; Guenther and Ghosh, 2003). Functional magnetic resonance imaging (fMRI) techniques have been useful in identifying the areas of brain (both cortical and cerebellar) active during overt speech production (Hickok and Poeppel, 2000); such an fMRI study of simple syllable productions has found supporting evidence for a number of the model's anatomic predictions (Guenther et al., 2005). Recent research utilizing the aforementioned Perturbatron with fMRI techniques has been used to determine areas of the brain that may act as somatosensory error cells (Tourville et al., 2004). The results of this experiment corroborate the model's prediction of somatosensory error cells located in the supramarginal gyrus. Further, recent fMRI work uses an acoustic perturbation processor comparable to the one used in Study 1 to determine areas of the brain that may act as auditory error cells during unexpected auditory perturbations (Tourville et al., 2005). Again, the model's prediction, this time of auditory error cells in the posterior superior temporal gyrus were supported. Findings from other imaging studies support this hypothesis, including the activity of this same region during both speech perception and production (Buchsbaum et al., 2001).

Functional imaging will continue to be an important tool to testing hypotheses of the speech production model. For example, a current imaging study is investigating the activity of the brain during *sustained* (as opposed to unexpected) auditory perturbations, and utilizes the same acoustic perturbation processor. Also, if imaging data could be obtained in conjunction with the combined articulatory and acoustic perturbation experiment (proposed in Section 6.2), the activation in each sensory error cell region may provide better insight into the relation between somatosensory and auditory feedback.

6.5. Proposed enhancements to the DIVA model.

Some of the human subject results in study 1 (Chapter 3) were not replicated in the SA simulations, suggesting ways that the DIVA model can be enhanced or expanded to account for these results. Additionally, differences between the simulations and the human subject results (Chapter 5) suggest other ways the DIVA model may be modified to better model human data.

The model currently represents different phonetic strings in distinct sound map cells (Guenther et al., 2005), implying that adaptation will not carry over to speech sounds that did not experience perturbation. This is clearly not the case in human subjects: when trained—via a series of words receiving perturbed feedback—to adapt the vowel /ɛ/, this adaptation generalized to untrained words containing this vowel (Section 3.4.3), as well as to words containing untrained vowels (Section 3.4.4). One way to resolve this issue is to allow interaction between the sound map cells of different speech sounds, with the amount of interaction dependent on the amount of similarity between the two speech sounds.

The fundamental frequency (F0) contour is not controlled by the model; instead, F0 is given a steady value of 100 Hz throughout all simulations. In-progress research with the model is focused on allowing the model to vary F0 as an auditory dimension. Such modification will allow the model to replicate results from sensorimotor adaptation experiments involving F0, as well as moving the model toward accounting for the control of prosodic aspects of speech. Additionally, the SA simulations utilizing Miller formant-ratio theory (see Sections 3.2.3 and 5.2.3) may be more successful in replicating human results if F0 is allowed to vary, since one of the Miller ratio dimensions involves F0 (see Equation 3.1).

In its current form, the model is a deterministic one; that is, having no random variables, the same simulation run multiple times will result in the same outcome—produced speech sound—every time. Speech production and perception are to some extent stochastic processes, evident in variation in F1 produced during the baseline of the SA experiment (see Figure 3.8) and in the probabilistic nature of subject responses during discrimination tasks (see Figure 4.6). Transforming DIVA into a stochastic model will allow it to better reflect human speech.

Appendix A. Summary of terms used in this thesis.

The following are different manifestations of sensorimotor adaptation, as measured in this thesis, compared with the equivalent terminology used in the Houde and Jordan SA experiment (Houde and Jordan, 2002).

Terminology used in thesis	Definition	Equivalent term used in Houde and Jordan (2002)
+feedback adaptation	Compensatory change to an acoustic perturbation, as measured in tokens presented with acoustic feedback turned on	*Compensation*
-feedback adaptation	Compensatory change to an acoustic perturbation, as measured in tokens presented with acoustic feedback blocked by noise	*Adaptation*
Generalized adaptation	Compensatory change to an acoustic perturbation found in vowels or other phonetic contexts that were only presented with the acoustic feedback blocked by noise	*Generalization*
Aftereffect adaptation	Compensatory change to an acoustic perturbation that persists after the acoustic perturbation is removed	not measured
Within vowel adaptation	Compensatory change measured during the token presentation (used in +feedback tokens) that demonstrates a lag in adaptive response	not measured

Appendix B. Use of the LPC coefficients to determine and shift F1.

The result of the autocorrelation LPC routine in the formant shifting algorithm (see **Figure 3.2**) is an 8th order polynomial that represents of original speech segment:

Equation B.1:
$$A(z) = 1 - \sum_{i=1}^{8} a_i z^{-i}$$

where the relation between *A(z)* and the original, pre-emphasized[14] speech segment *X(z)* is defined in the following manner:

Equation B.2:
$$X(z) = \frac{G}{A(z)}$$

That is, the LPC analysis method assumes that *X(z)* can be accurately represented by a gain factor *G* and the polynomial *A(z)*, which describes only the poles of *X(z)*. Thus, the assumption in LPC analysis is that the analyzed speech segment contains no zeros and can be described by an "all-pole" model (Markel and Gray, 1976).

Equation B.1 can alternatively be written with the roots of *A(z)* stated explicitly, as in the following:

Equation B.3:
$$A(z) = \prod_{i=1}^{4} (1 - c_i z^{-1})(1 - c_i^* z^{-1})$$

Since *X(z)*, and thus *A(z)* are real, the roots of *A(z)* described in Equation B.3 occur in complex conjugate pairs (e.g. c_l and c_l^*). Equation B.3 is a much more useful form of *A(z)*, since the absolute value of the angles of the roots correspond to the formants of the analyzed speech segment (Markel and Gray, 1976). Specifically, a given formant F_n can be determined from the root c_n (or alternatively its complex conjugate c_n^*) using the following equation:

[14] A pre-emphasis filter is applied to the speech segment to transform the speech excitation function, *G(z)*, to a constant gain, *G*.

Equation B.4: $$F_n = \frac{2\pi}{F_S}\left|angle(c_n)\right|, \quad where \;\; F_S = sampling \;\; rate$$

Since the autocorrelation LPC analysis yields the polynomial form of *A(z)* (Equation B.1), the roots must be determined using a root-finding algorithm, such as the Hessenberg QR method (Press et al., 2002). The first formant corresponds to the root with the smallest absolute angle (Equation B.4). Moreover, the shifted F1 formant can be determined by altering the angle of the F1 complex roots. Since the order of the LPC polynomial used in the formant shifting algorithm is 8th order, and its roots occur in complex conjugate pairs, the maximum number of formants resolved in this application is 4.

The synthesis of the perturbed speech can be accomplished by "zeroing" out the poles of the original speech segment defined by *A(z)* and introducing the new poles corresponding to the perturbed speech segment (defined as *A'(z)*):

Equation B.5: $$Y(z) = \frac{A(z)}{A'(z)}X(z)$$

Figure B.1 shows a graphical representation of this synthesis, and demonstrates that the poles of 1/*A'(z)* and the zeros of *A(z)* corresponding to the unshifted formants cancel each other out. Therefore, whereas the LPC analysis yielded an 8th order polynomial, the synthesis can be accomplished with only a second order filter representing *A(z)* and *A'(z)* in Equation B.5. Specifically, consider that the original F1 can be represented by the following complex conjugate root pair, with *Θ* corresponding to F1 as in Equation B.4:

Equation B.6: $$\begin{aligned} c &= r\cos\theta + jr\sin\theta \\ c^* &= r\cos\theta - jr\sin\theta \end{aligned}$$

The root pair corresponding to the shifted formant F1' can also be represented by substituting Equation B.6 with c', c*' and *Θ'*. Using this representation of the complex roots of *F1* and *F1'*, Equation B.5 can be rewritten in the following manner:

Equation B.7:

$$\begin{aligned} Y(z) &= \frac{(1-cz^{-1})(1-c^{*}z^{-1})}{(1-c'z^{-1})(1-c'^{*}z^{-1})}X(z) \\ &= \frac{1-2r\cos\theta z^{-1}+r^{2}z^{-2}}{1-2r\cos\theta' z^{-1}+r^{2}z^{-2}}X(z) \end{aligned}$$

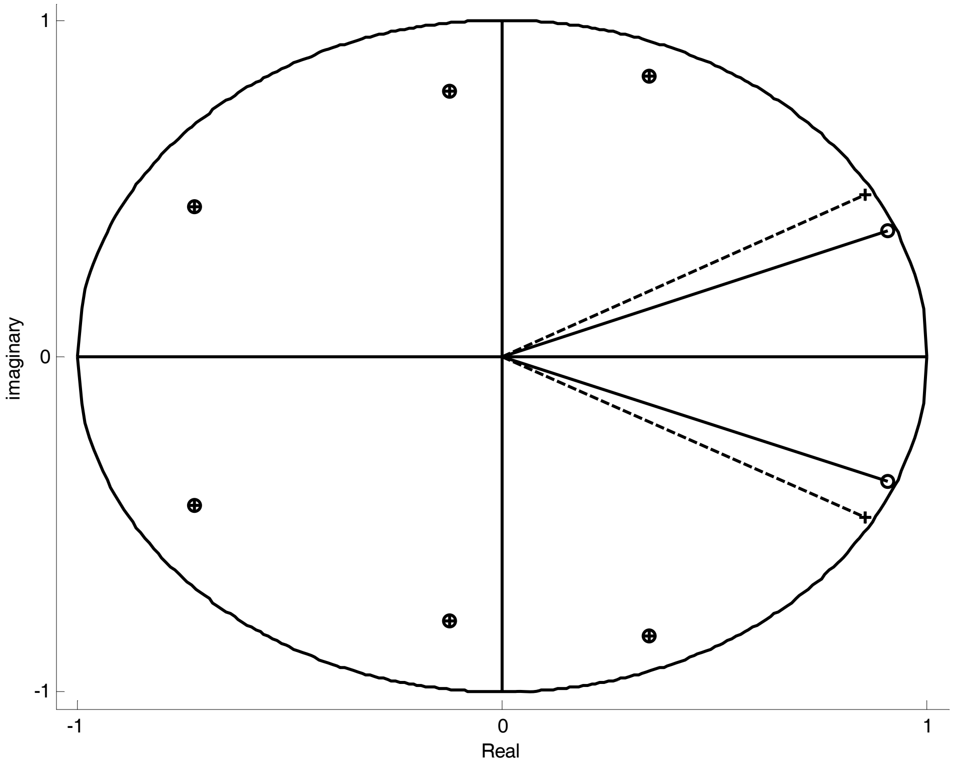

Figure B.1: Graphic depiction of the roots (polar form) corresponding to the original and perturbed speech segments. Each root is shown in polar form, with the complex conjugate pairs mirrored about the *Im=0* axis. The perturbed speech synthesizer removes the original formants by zeroing out its corresponding roots *A(z)* ("o" in the figure). The shifted formants are introduced as the poles of *A'(z)* ("+" in the figure). This figure shows that, since only F1 is altered, the poles of 1/ *A'(z)* cancels the zeros of *A(z)* for every complex conjugate root pair except those corresponding to F1. The solid line shows the angle of the roots corresponding to the original, unshifted F1; the dashed line shows the angle of the roots corresponding to the shifted F1 (here, shifted up).

The formant shifting algorithm implements the filter described by Equation B.7 using a direct form II transposed structure (Oppenheim and Schafer, 1999). The time domain difference equation corresponding to Equation B.7 is as follows:

Equation B.8:

$$y[n] = x[n] + (2r\cos\theta)x[n-1] + r^2 x[n-2] \\ -(2r\cos\theta')y[n-1] + r^2 y[n-2]$$

Typical examples spectral analysis of the unperturbed and perturbed (0.7 pert) vowel /ɛ/ are shown for comparison in Figure B.2 and Figure B.3, respectively. The shift of F1 from 535 Hz to 370 Hz represents a change in F1 of 0.69 pert[15], demonstrating that the perturbation algorithm is effectively shifting F1 as designed. Additionally, the amplitude of the original F1 peak is reduced in amplitude by 12.5 dB compared to the new (perturbed) F1 peak (see Figure B.3); this demonstrates that the formant shifting algorithm can adequately attenuate the original F1 value.

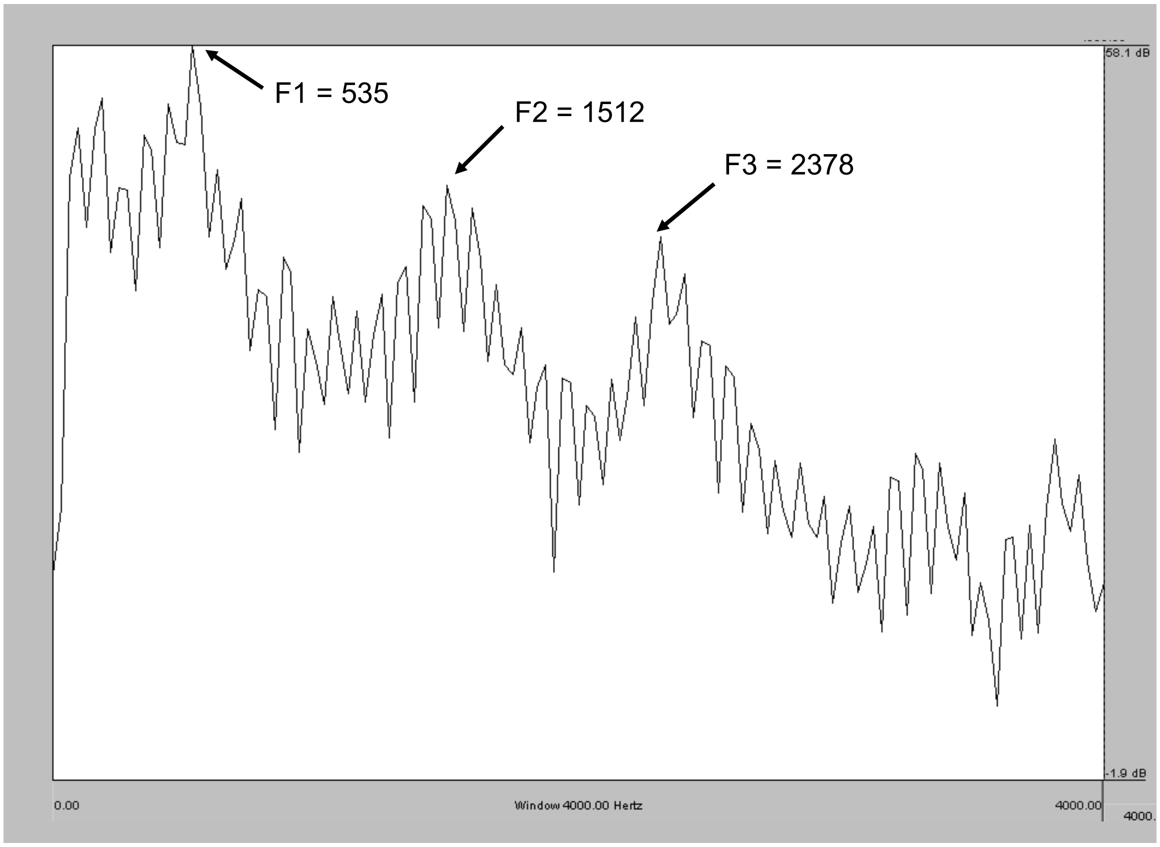

Figure B.2: DFT spectrum within an example /ɛ/ vowel, unperturbed. This spectrum was taken from within the vowel of a speech token digitized directly and recorded from the microphone (pre-DSP perturbation). This analysis was carried out via Pratt v 4.2.17—a speech analysis software package—using the following parameters: Hanning window shape with length of 32 msec, and 6 dB/octave pre-emphasis. The ordinate is in units of dB; the abscissa is in units of Hz. The first three formants are labeled.

[15] Formant values were obtained from LPC analysis of each spectra.

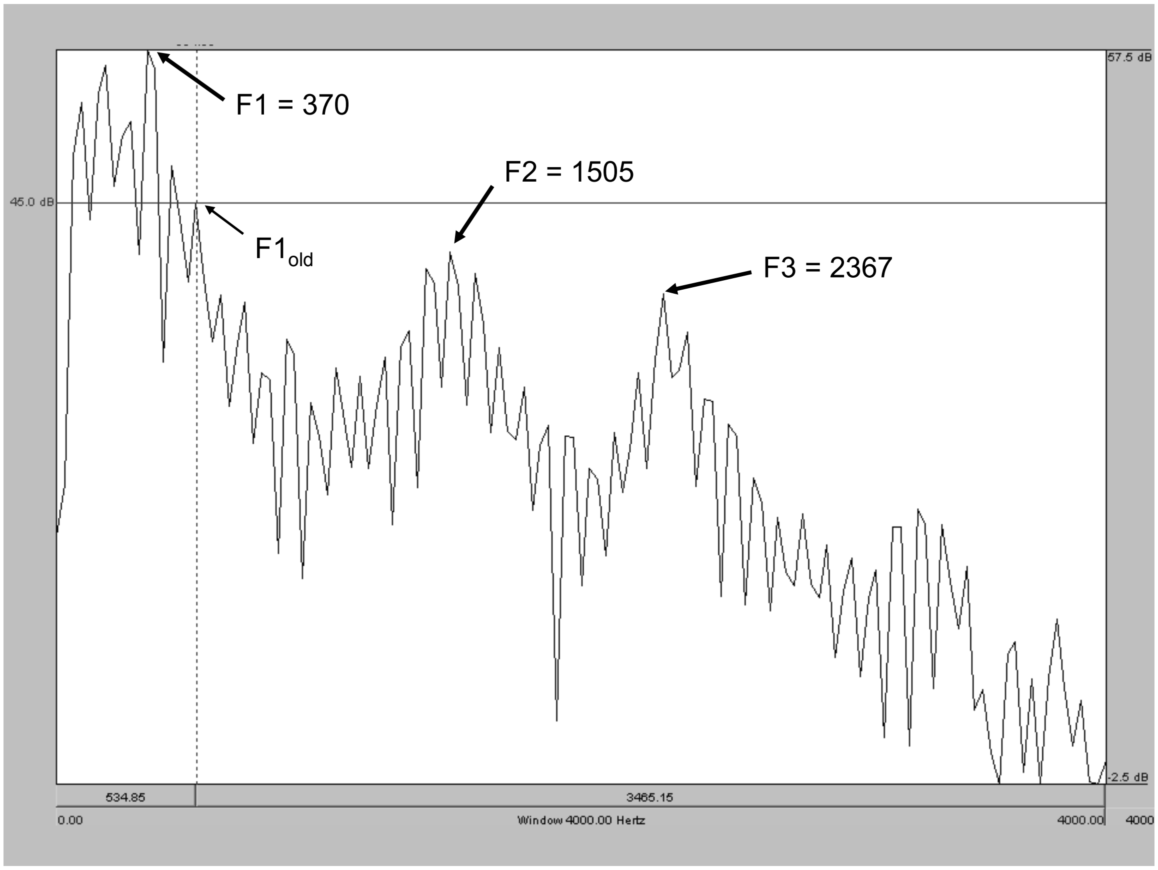

Figure B.3: DFT spectrum within an example /ɛ/ vowel, perturbed. This spectrum was taken from within the vowel of a speech token directly digitized and recorded at the output of the DSP board, perturbation level set at 0.7 pert. The first three formants, as well as the location of the unperturbed F1 (F1$_{old}$), are labeled. Refer to Figure B.2 for axes details.

Appendix C. Individual adaptive response during the sensorimotor adaptation protocol.

The following figures demonstrate the performance of each subject (id numbers 1-20) run on the sensorimotor adaptation protocol (study 1). Performance is measured by calculating Adaptive Response (see Equation 3.5) as a function of epoch number. Tokens used to calculate AR only include the + feedback tokens. For convenience, each subject's ARI value is shown in the corresponding title.

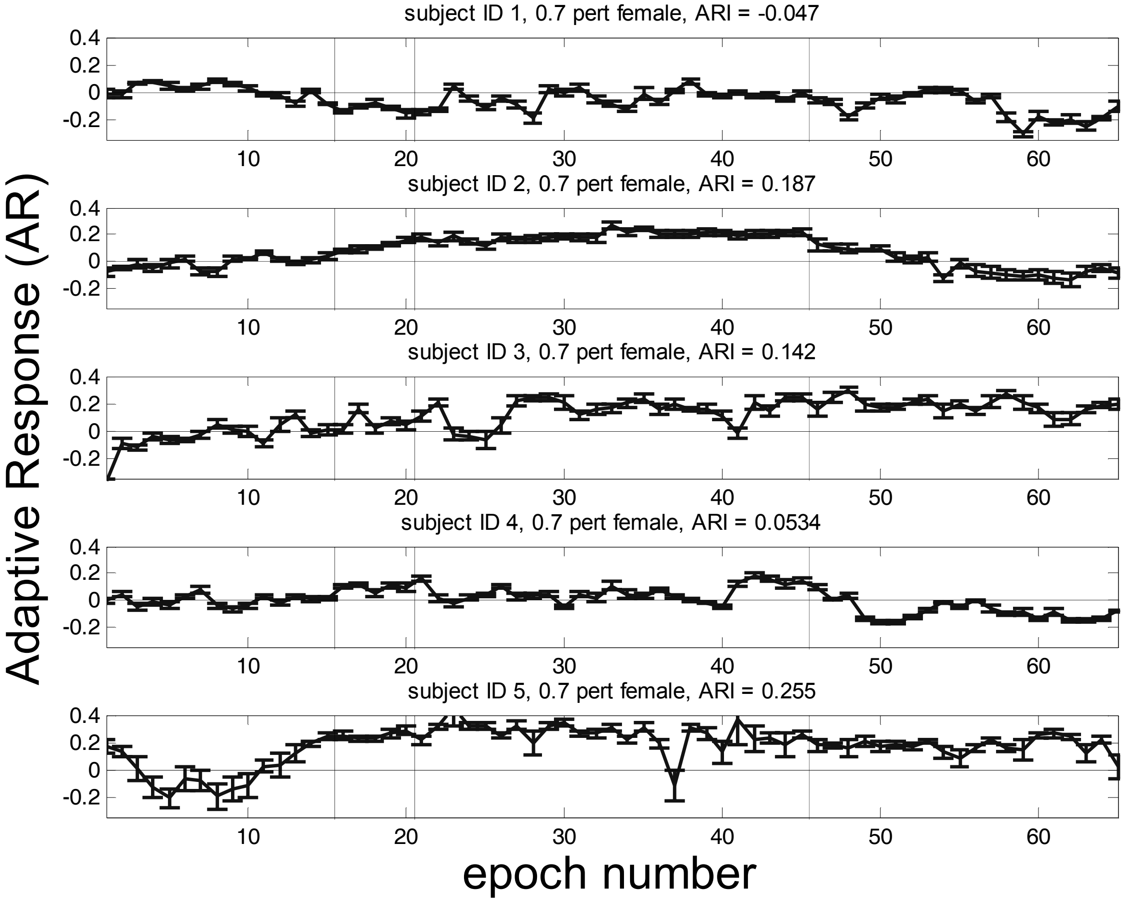

Figure C.1: Individual adaptive response as a function of epoch number for 0.7 pert SA protocol, female subjects. The ordinate corresponds to the adaptive response, which is the formant (in Hz) normalized to the mean value of epochs 6-15 within the baseline phase, then transformed to highlight changes about the baseline of 1.0 (see 3.4.1 for details). Each data point is the mean value of the nine +feedback words; the error bars depict the standard error about the mean. The horizontal dashed line shows *AR* = 0.0. The vertical lines show transitions in phase of the SA protocol.

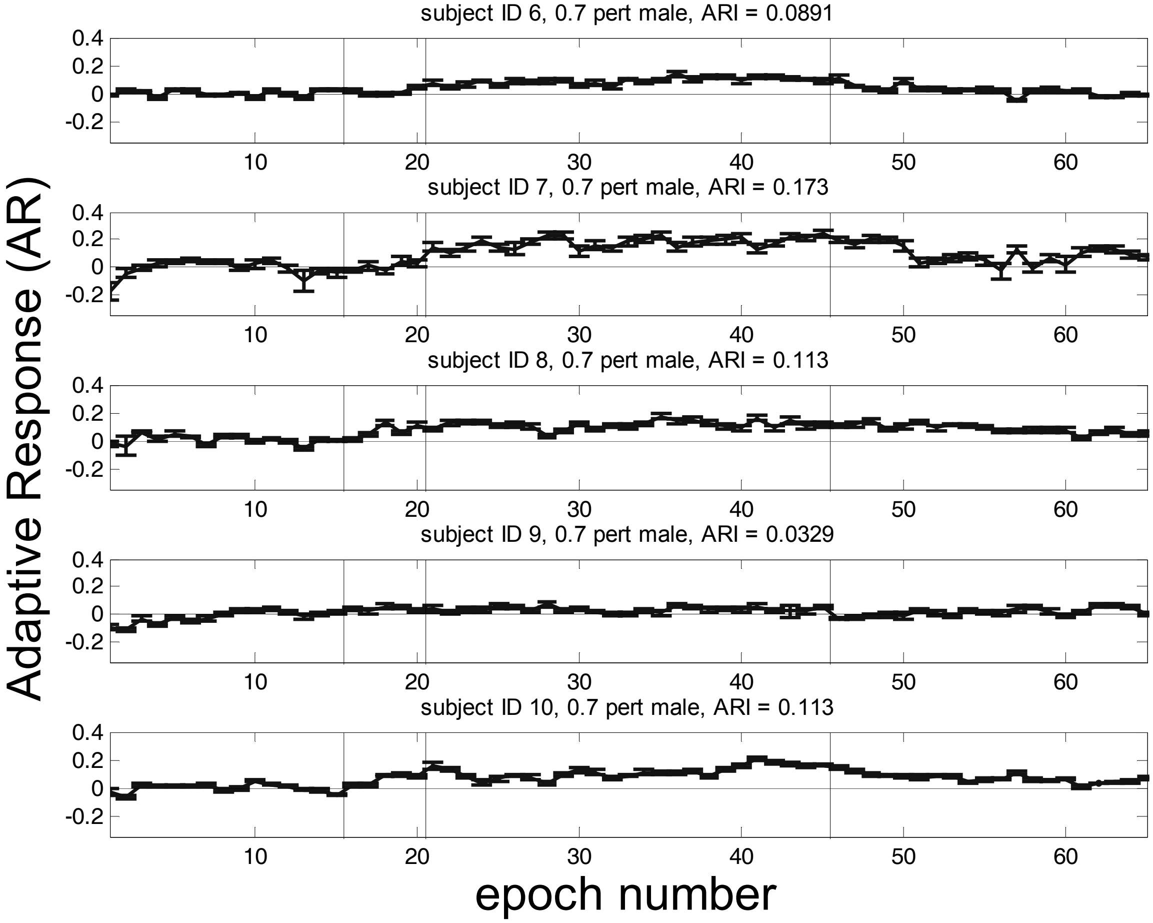

Figure C.2: **Individual adaptive response as a function of epoch number for 0.7 pert SA protocol, male subjects.** Refer to Figure C.1 for axes details.

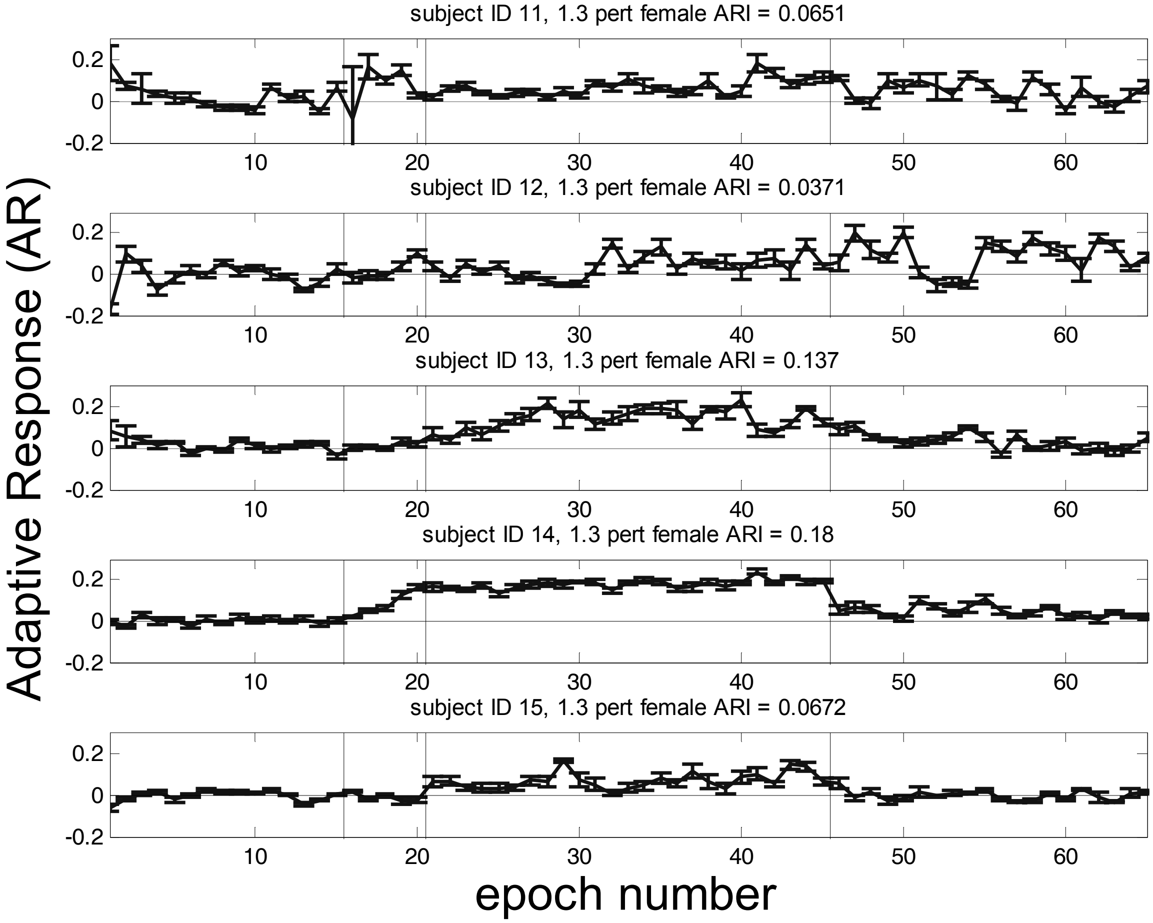

Figure C.3: **Individual adaptive response as a function of epoch number for 1.3 pert SA protocol, female subjects.** Refer to Figure C.1 for axes details.

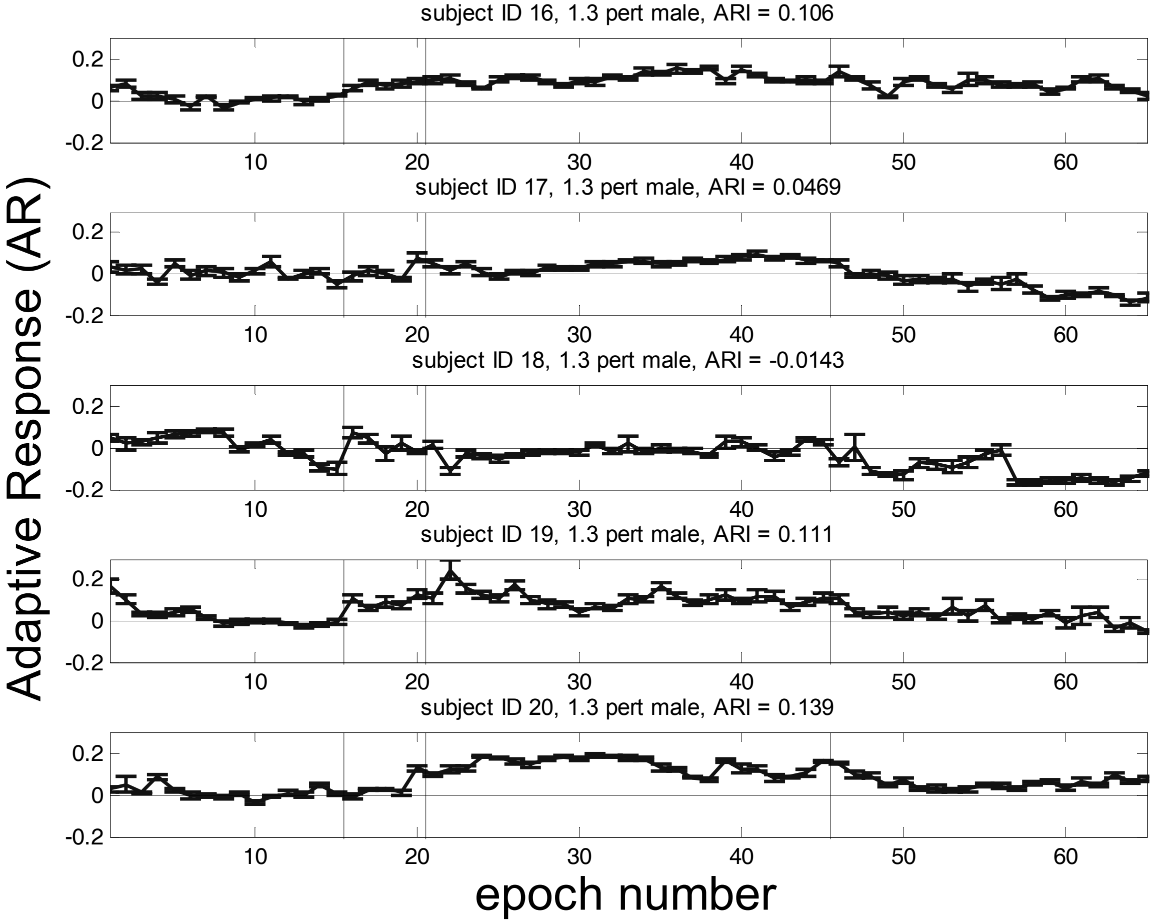

Figure C.4: **Individual adaptive response as a function of epoch number for 1.3 pert SA protocol, male subjects.** Refer to Figure C.1 for axes details.

* * * * * * * * * *

Individual subjects generally showed an increase in *AR* due to the perturbation, followed by a gradual decrease after the perturbation was removed. The notable exceptions to this trend were subjects 1 and 18, both of whom showed negative adaptation. These figures show that there was still wide variation in the extent of adaptation in all subjects, as well as in the rate of adaptation (how fast subjects adapted), and in their rate of recovery (how fast subjects reverted to baseline after the perturbation was removed).

Appendix D. Investigation of the influence of the perturbation algorithm on the second formant.

Results from Section 3.4.2 suggest that, while small, there is a significant change in the second formant (F2) that is related to changes that the sensorimotor adaptation protocol causes in the first formant (F1). This Section is included to investigate the possibility that the F2 changes were a result of the signal processing from the perturbation algorithm (as opposed to actual changes in F2 produced by the subject). If the perturbation algorithm did introduce changes in F2, then it could be that the inverse relation between F1 and F2 changes seen during the SA protocol actually resulted from the feedback signal out of the DSP board, rather than from constraints related to human speech production or perception.

Certain tokens from the pre-experiment phase of the SA protocol were run with the perturbation algorithm set at full-pert value, but with the subjects *not* wearing the insert earphones (so that the subjects could not hear the perturbed feedback). In these tokens, F1 and F2 were extracted from both the input signal to the DSP board (unshifting in F1) and the output signal from the DSP board (shifted in F1). Changes in F1 caused by the DSP board (calculated as $F1_{out}/F1_{in}$) were tested for statistical significance to changes in F2 ($F2_{out}/F2_{in}$).

The result of this analysis is that *no* significant correlation between F1 and F2 changes was seen in tokens resulting from the 1.3 pert shift in F1 ($p = 0.18$), nor in tokens from the 0.7 pert shift ($p = 0.5624$). This is evidence that the significant relation between F1 and F2 changes seen during the SA experiments resulted from actual subject production

Appendix E. Correlation between adaptive response and *jnd* obtained from staircase protocol only.

The use of a two-stage protocol for measuring *jnd* was based on the work of other researchers (Guenther et al., 1999b; Guenther et al., 2004). However, running this two-stage protocol is time-consuming; on average, the second stage of the discrimination task took four to five times longer than the first stage (the adaptive staircase method). Because of this time cost, this analysis investigates whether the *jnd* estimated from the first stage is sufficient to find the significant relations determined when using the more precise (two-stage protocol) *jnd* measure.

As Figure E.1 demonstrates, the correlation between *jnd* and adaptive response which was significant using the data shown in Figure 4.8 is not significant when using the one-stage *jnd* estimate. Furthermore, Table E.1 shows that the correlation statistics between *jnd* and ARI measured at all three milestones worsens when using the one-stage estimate of *jnd.* Thus, while time-consuming, these results indicate that the second stage of the discrimination task is necessary to measure *jnd* precisely.

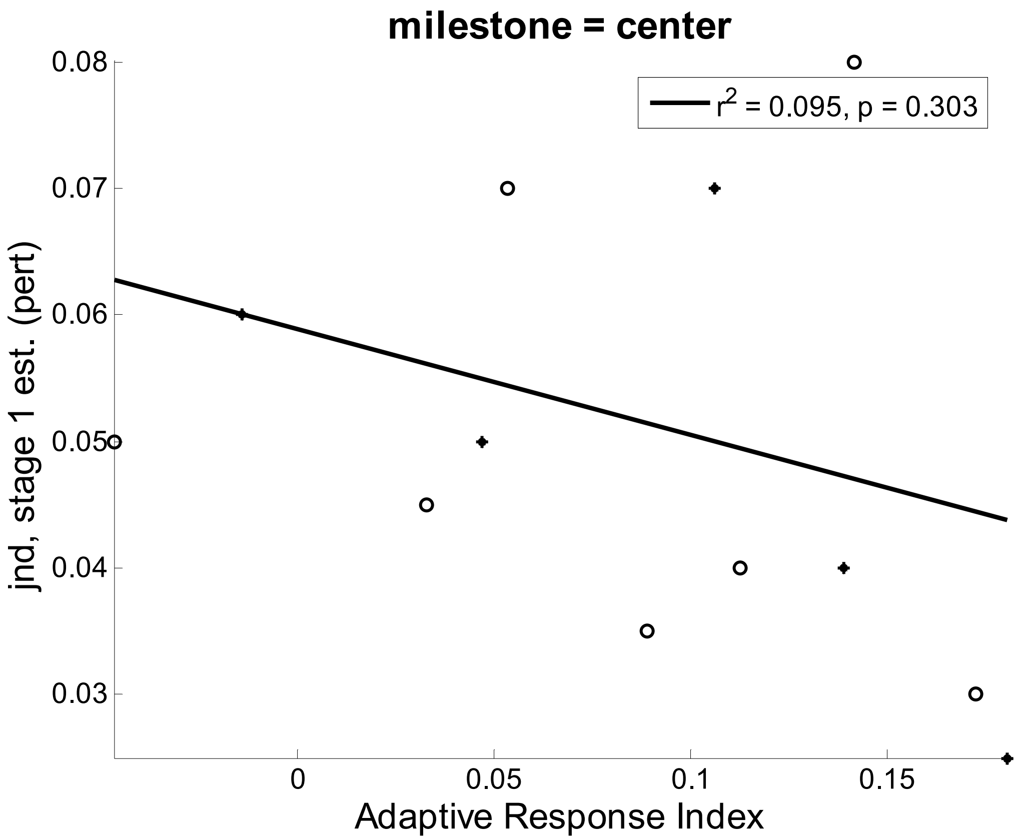

Figure E.1: Adaptive response index is not correlated with the 1-stage estimate of the *jnd* for the center milestone. This plot is similar to Figure 4.8 (which showed a significant correlation). The difference is that the jnd score used here was estimated from the first stage (the adaptive staircase) of the two stage protocol. The abscissa shows the adaptive response index, discussed above. The ordinate is the 1-stage estimate of the *jnd* (in pert) for the "center" milestone. The statistics for the regression line are shown in the legend; the p-score reported uses a two-tail t-test.

		one-stage protocol	two-stage protocol
same	r^2	0.192	0.189
	p-score	0.133	0.136
center	r^2	**0.095**	**0.312**
	p-score	**0.303**	**0.047**
opposite	r^2	0.084	0.088
	p-score	0.335	0.322

Table E.1: Statistics of correlation between ARI *and jnd*, one-stage protocol estimate of *jnd* compared to two-stage protocol *jnd* measure. The statistics reported are the r^2 (square of the correlation coefficient) and the p-score resulting from a one-tail t-test. The center column reports statistics resulting from the correlation between ARI and the one-stage protocol (adaptive staircase) *jnd* estimate. The right column reports statistics for correlation between ARI and the two-stage protocol *jnd* measure.

Appendix F. Relation between category width and adaptive response.

The goodness rating scores determined from the perceptual acuity protocol (refer to 4.3.5) are used here to determine a measure of the category width for the unperturbed tokens. Category width is defined here as:

Equation F.1: $$category\_width = \begin{cases} 1 - pert_{goodness=0.7}, & \textit{if SA pert} = 0.7 \\ pert_{goodness=0.7} - 1, & \textit{if SA pert} = 1.3 \end{cases}$$

Here, the criterion goodness rating score for all subjects is set at 0.7, since 0.7 is the lowest score that is common to all subjects analyzed here. Also, though two sets of goodness rating scores—corresponding to the 0.7 to 1.0 pert block and to the 1.0 to 1.3 pert block—were measured, the category width is calculated from the scores corresponding to the same perturbation direction used in the original SA protocol. (For example, the goodness rating scores for 0.7 pert SA subjects are calculated from the 0.7 to 1.0 pert block.)

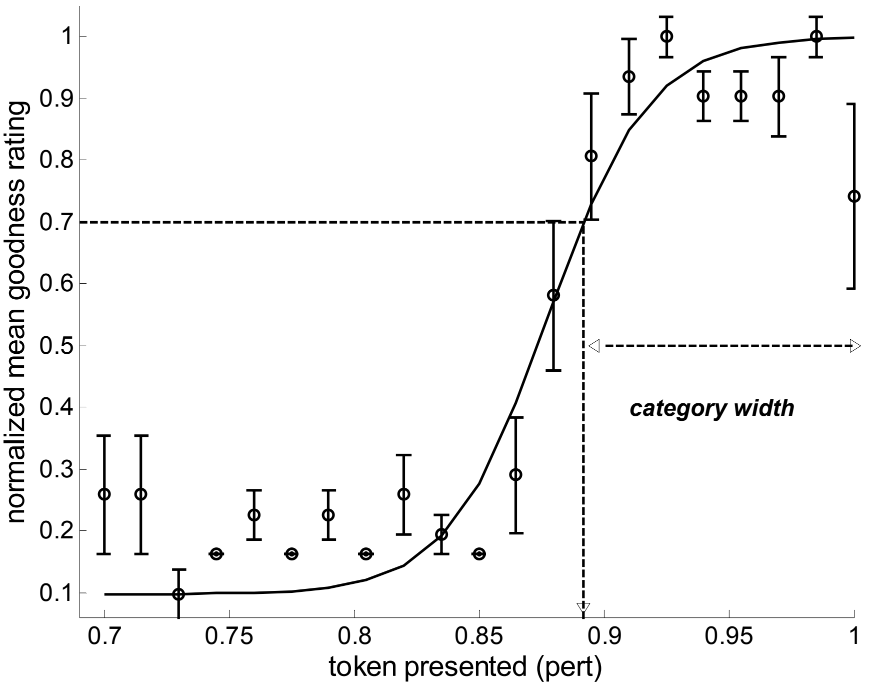

Figure F.1: Example of the calculation of category width from the goodness rating scores. The axes are the same as in **Figure 4.14**. The horizontal dashed line corresponds to the criterion normalized goodness rating score (here, 0.70). The vertical dashed line represents the pert level that intersects the criterion goodness rating score on the best fit curve. This category width is the difference between the intersecting pert level and 1.0.

Once the category width is computed, the cross-correlation between this perceptual property and adaptive response can be examined. Note that, because of the way the category width is calculated here, data from the two outlying subjects mentioned in section 4.3.5 were omitted. (These subjects had goodness rating curves have that increase in rating for tokens increasingly distant from the pert = 1.0 token.) Like the index of discrimination (*jnd*), the vowel category width is inversely related to perceptual acuity; thus, the vowel category width and adaptive response should be inversely related according to the relation between acuity and adaptation proposed in Section 4.1.1. However, Figure F.2 demonstrates that there is not a significant correlation between the vowel category width and the adaptive response index.

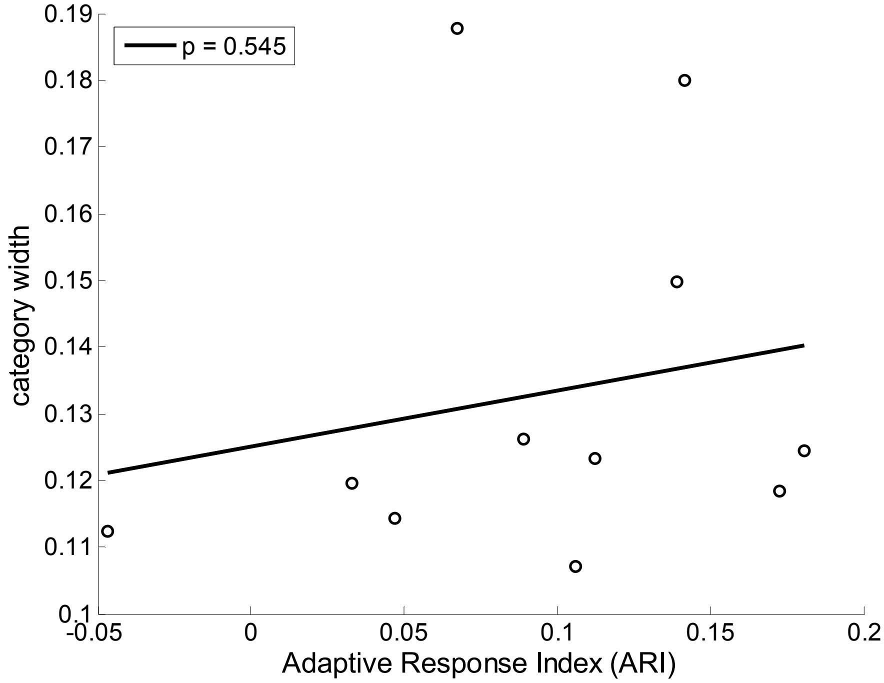

Figure F.2: Adaptive Response Index (ARI) is not correlated with the category width as determined from the normalized goodness rating scores. The abscissa is the adaptive response index. The ordinate is the category width determined from the subject's normalized goodness rating scores, measured on the block corresponding to the perturbation they were exposed to on the SA protocol. Subjects whose goodness rating scores were atypical (N=2) were not included here. The p-score for the regression line are shown in the legend.

The correlations between category width and adaptive response were determined for a range of criterion values, and were expanded to the category width corresponding to the goodness rating block that was *opposite* of the perturbation. Note that the opposite side goodness rating blocks did not contain goodness rating curves typical of the outliers described in Section 4.3.5; thus all 13 subjects were used in the calculation of $r_{cat.\ width,\ ARI}$. Also note that the goodness rating curves derived from the opposite side blocks had 0.6 pert (as compared to 0.7 pert for the same side block) as the lowest criterion goodness score that was common in all subjects.

The results of these studies are shown in Table F.1; none of the correlation coefficients in this table are significant ($p < 0.05$), though the correlation becomes nearly significant for at a couple criterion values. Moreover, most of the $r_{cat.width,ARI}$ calculated for the “same side” category widths are positive (left side of Table F.1), whereas the relation between category width and adaptive response is hypothesized to be negative.

same side of SA perturbation				**opposite side of SA perturbation**		
criterion	$r_{cat.\ width,\ ARI}$	*p-value*		criterion	$r_{cat.\ width,\ ARI}$	*p-value*
	*	*		0.60	-0.23	0.50
	*	*		0.65	-0.22	0.53
0.70	0.20	0.546		0.70	-0.21	0.54
0.75	0.32	0.331		0.75	-0.20	0.56
0.80	0.48	0.135		0.80	-0.19	0.57
0.85	0.59	0.057		0.85	-0.19	0.58
0.90	0.59	0.054		0.90	-0.18	0.59
0.95	0.55	0.083		0.95	-0.18	0.60

Table F.1: Correlation coefficients between category width and adaptive response index (ARI) with p-values for a range of criterion values. The criterion value is the goodness rating score on the subject’s goodness rating curve that is used to determine the category width. The left side of the table uses the category width derived from the goodness rating block on the same side as the perturbation the subject heard during the SA experiment; the right side uses the category width derived from the goodness rating block on the opposite side of the SA experiment perturbation. None of the correlation coefficients are significant.

Since analysis of the relation between *jnd* and ARI showed that the strength of the correlation between these scores increased when F1 separation was controlled for (Section 4.3.4), the partial correlation between *category width* and

ARI scores was also calculated with F1 separation controlled for. In this analysis, only the category widths from the "same-side" of the perturbation goodness rating scores are considered, since the "opposite-side" goodness rating scores all have large p-values. As shown in Table F.2, controlling for F1 separation does not alter the p-value greatly, and none of the correlations become significant (p< 0.05) when the partial correlation is calculated.

partial correlation coefficient		
criterion	*p-value,zero order*	*p-value, partial*
	*	*
	*	*
0.70	0.546	0.561
0.75	0.331	0.364
0.80	0.135	0.166
0.85	0.057	0.067
0.90	0.054	0.053
0.95	0.083	0.082

Table F.2: Comparison between p-values for correlation coefficients between *category width* and *ARI* scores, zero-order correlation compared to the partial correlation with F1 separation controlled for. Only the category widths from the goodness rating scores that were on the same side of the perturbation are considered here. The center column contains the same p-values shown in Table F.2; the right column contains the p-value from the partial correlation (with F1 separation controlled for).

Bibliography

Abbs JH, Gracco VL (1984) Control of complex motor gestures: Orofacial muscle responses to load perturbations of lip during speech. Journal of Neurophysiology 51(4):705-723.

Atkeson CG (1989) Learning Arm Kinematics and Dynamics. Ann Rev Neurosci 12:157-183.

Baum SR, McFarland DH (1997) The Development of Speech Adaptation to an Artificial Palate. Journal of the Acoustical Society of America 102:2353-2359.

Bedford F (1989) Constraints on learning new mappings between perceptual dimensions. Journal of Experimental Psychology: Human Perception and Performance 15:232-248.

Bhushan N, Shadmehr R (1999) Computational nature of human adaptive control during learning of reaching movements in force fields. Biological Cybernetics 81:39-60.

Blakemore SJ, Goodbody SJ, Wolpert DM (1998) Predicting the consequences of our own actions: the role of sensorimotor context estimation. Journal of Neuroscience 18:7511-7518.

Boyce S, Espy-Wilson CY (1997) Coarticulatory Stability in American English /r/. Journal of the Acoustical Society of America 101:3741-3753.

Buchsbaum BR, Hickok G, Humphries C (2001) Role of left posterior superior temporal gyrus in phonological processing for speech perception and production. Cognitive Science 25:663-678.

Bullock D, Grossberg S (1988) Neural dynamics of planned arm movements: emergent invariants and speed-accuracy properties during trajectory formation. Psychological Review 95:49-90.

Burnett TA, Freedland MB, Larson CR, Hain TC (1998) Voice F0 responses to manipulations in pitch feedback. Journal of the Acoustical Society of America 103:3153-3161.

Callan DE, Kent RD, Guenther FH, Vorperian HK (2000) An auditory-feedback-based neural network model of speech production that is robust to developmental changes in the size and shape of the articulatory system. Journal of Speech, Language, and Hearing Research 43:721-736.

Ghahramani Z, Wolpert DM, Jordan MI (1996) Generalization to Local Remappings of the Visuomotor Coordinate Transformation. Journal of Neuroscience 16:7095-7096.

Ghosh, S. S. (2004) Understanding cortical and cerebellar contributions to speech production through modeling and functional imaging. Unpublished doctoral thesis, Boston University

Guenther FH (1995) Speech sound acquisition, coarticulation, and rate effects in a neural network model of speech production. Psychological Review 102:594-621.

Guenther FH, Espy-Wilson CY, Boyce SE, Matthies ML, Zandipour M, Perkell JS (1999a) Articulatory tradeoffs reduce acoustic variability during American English /r/ production. Journal of the Acoustical Society of America 105:2854-2865.

Guenther, F. H. and Ghosh, S. S. (2003) A model of cortical and cerebellar function in speech. Paper presented at 15th ICPhS. Barcelona, 629-633.

Guenther FH, Ghosh SS, Tourville JA (2005) Neural Modeling and Imaging of the Cortical Interactions Underlying Syllable Production. Brain and Language in press.

Guenther FH, Hampson M, Johnson D (1998) A theoretical investigation of reference frames for the planning of speech movements. Psychological Review 105:611-633.

Guenther FH, Husain FT, Cohen MA, Shinn-Cunningham BG (1999b) Effects of categorization and discrimination training on auditory perceptual space. Journal of the Acoustical Society of America 106:2900-2912.

Guenther FH, Nieto-Castanon A, Ghosh SS, Tourville JA (2004) Representation of sound categories in auditory cortical maps. Journal of Speech, Language, and Hearing Research 47:46-57.

Hickok G, Poeppel D (2000) Toward a functional neuroanatomy of speech perception. Trends in Cognitive Sciences 4:131-138.

Honda M, Fujino A, Kaburagi T (2002) Compensatory responses of articulators of unexpected perturbations of the palate shape. Journal of Phonetics 30:281-302.

Houde, J. F. (1997) Sensorimotor Adaptation in Speech Production. Unpublished doctoral thesis, Massachusetts Institute of Technology

Houde JF, Jordan MI (2002) Sensorimotor adaptation of speech I: Compensation and adaptation. Journal of Speech, Language, and Hearing Research 45:295-310.

Houde JF, Jordan MI (1998) Sensorimotor Adaptation in Speech Production. Science 279:1213-1216.

Ito M (1974) The control of cerebellar motor systems. In: The Neurosciences: Third Study Program. (Schmitt FO, Worden FG, eds), pp 293-303. Cambridge: MIT Press.

Jones JA, Munhall KG (2000) Perceptual calibration of F0 production: Evidence from feedback perturbation. Journal of the Acoustical Society of America 108:1246-1251.

Kawahara H (1993) Transformed auditory feedback: Effects of fundamental frequency perturbation. ATR Human Information Processing Research Laboratories.

Kawato M (1999) Forward models for physiological motor control. Current Opinion in Neurobiology 9:718-727.

Kawato M, Gomi H (1992) The cerebellum and VOR/OKR learning models. Trends in Neurosciences 15:445-453.

Kelso JAS, Tuller B, Vatikiotis-Bateson E, Fowler CA (1984) Functionally specific articulatory cooperation following jaw perturbations during speech: Evidence for coordinative structures. Journal of Experimental Psychology 10(6):812-832.

Lane H, Tranel B (1971) The Lombard sign and the role of hearing in speech. Journal of Speech and Hearing Research 14(4):677-709.

Lindblom BEF, Lubker JF, Gay T (1979) Formant frequencies of some fixed-mandible vowels and a model of speech motor programming by predictive simiulation. Journal of Phonetics 7:147-161.

Macmillan NA, Creelman CD (2005) Detection Theory: A User's Guide. Mahwah: Lawrence Erlbaum Associates, Inc.

Maeda S (1990) Compensatory articulation during speech: evidence from the analysis and synthesis of vocal-tract shapes using an articulatory model. In: Speech Production and Speech Modelling. (Hardcastle WJ, Marchal A, eds), pp 131-149. Netherlands: Kluwer Academic Publishers.

Markel JD, Gray AH (1976) Linear prediction of speech. New York: Springer-Verlag.

Max, L., Wallace, M. E., and Vincent, I. (2003) Sensorimotor adaptation to auditory perturbations during speech: Acoustic and kinematic experiments. Paper presented at 15th ICPhS. Barcelona, 1053-1056.

Menard L, Perrier P, Savariaux C (2004) Exploring production-perception relationships for 4-year-old children: A study of compensation strategies to a lip-tube perturbation. Journal of the Acoustical Society of America 115:2629.

Menard L, Schwartz J-L, Boe L-J, Kandel S, Vallee N (2002) Auditory normalization of French vowels synthesized by an articulatory model simulating growth from birth to adulthood. Journal of the Acoustical Society of America 111:1892-1905.

Miall RC, Wolpert DM (1996) Forward models for physiological motor control. Neural Networks 9:1265-1279.

Miller JD (1989) Auditory-perceptual interpretation of the vowel. Journal of the Acoustical Society of America 85:2114-2134.

Newman RS (2003) Using links between speech perception and speech production to evaluate different acoustic metrics: A preliminary report. Journal of the Acoustical Society of America 113:2850-2860.

Nieto-Castanon A, Guenther FH, Perkell J, Curtin HD (2005) A modeling investigation of articulatory variability and acoustic stability during American English /r/ production. Journal of the Acoustical Society of America 117:3196-3212.

Oppenheim AV, Schafer RW (1999) Discrete-Time Signal Processing. Upper Saddle River: Prentice Hall, Inc.

Perkell JS (1997) Articulatory Processes. In: The Handbook of Phonetic Sciences (Hardcastle WJ, Laver J, eds), pp 333-370. Oxford, Eng.: Blackwell.

Perkell JS, Guenther FH, Lane H, Matthies M, Perrier P, Vick J, Wilhelms-Tricarico R, Zandipour M (2000) A theory of speech motor control and supporting data from speakers with normal hearing and with profound hearing loss. Journal of Phonetics 28:233-272.

Perkell JS, Guenther FH, Lane H, Matthies ML, Stockmann ES, Tiede M, Zandipour M (2004a) The distinctness of speakers' productions of vowel contrasts is related to their discrimination of the contrasts. Journal of the Acoustical Society of America 116:2338-2344.

Perkell JS, Matthies ML, Tiede M, Lane H, Zandipour M, Marrone N, Stockmann ES, Guenther FH (2004b) The distinctness of speakers' /s/-/sh/ contrast is related to their auditory discrimination and use of an articulatory saturation effect. Journal of Speech, Language, and Hearing Research 47:1259-1269.

Press WH, Teukolsky SA, Vetterling WT, Flannery BP (2002) Numerical recipes in C. Cambridge: Cambridge University Press.

Savariaux C, Perrier P, Orliaguet JP (1995) Compensation strategies for the perturbation of the rounded vowel [u] using a lip tube: A study of the control space in speech production. Journal of the Acoustical Society of America 98:2428-2842.

Savariaux C, Perrier P, Orliaguet J-P, Schwartz J-L (1999) Compensation strategies for the perturbation of French [u] using a lip tube. II. Perceptual analysis. Journal of the Acoustical Society of America 106:381-393.

Sinha NK (1994) Control Systems. New Delhi: Wiley Eastern Limited.

Stevens KN (1998) Acoustic Phonetics. Cambridge: MIT Press.

Tourville JA, Guenther FH, Ghosh SS, Bohland JW (2004) Effects of jaw perturbation on cortical activity during speech production. Journal of the Acoustical Society of America 116:2631.

Tourville, J. A., Guenther, F. H., Ghosh, S. S., Reilly, K. J., Bohland, J. W., and Nieto-Castanon, A. (2005) Effects of acoustic and articulatory perturbation on cortical activity during speech production. Paper presented at 11th Annual Meeting of the Organization for Human Brain Mapping. S49.

Vallabha GK, Tuller B (2002) Systematic errors in the formant analysis of steady-state vowels. Speech Communication 38:141-160.

von Helmholtz H (1962) Helmholtz's treatise on physiological optics. New York: Dover Press.

Wallace, M. E. and Max, L. (2004) Internal models of the vocal tract revealed by articulatory adaptation to formant-shifted auditory feedback. Paper presented at From Sound to Sense: 50 Years of Discovery in Speech Communication.

Welch RB (1978) Perceptual modification: Adapting to altered sensory environments. New York: Academic Press.

Xu Y, Larson CR, Bauer JJ, Hain TC (2004) Compensation for pitch-shifted auditory feedback during the production of Mandarin tone sequences. Journal of the Acoustical Society of America 116:1168-1178.

Yates AJ (1963) Delayed auditory feedback. Psychological Bulletin 60:213-232.

Biographical Note

Virgilio, son of Eugenio and Dulce Villacorta, was born in Berlin, Germany, and grew up for most of his youth in Anaheim, California. He has two younger sisters, Estella and Eugenie.

In 1995, the author received a Bachelors of Science in physics with specialization in biophysics from the University of California, San Diego. In 1999, he received a Masters in Medial Sciences from MCP*Hahnemann University. In 2005, he received a Doctor of Philosophy in Speech and Hearing Bioscience and Technology from the Harvard-MIT Division of Health Science and Technology.

While at M.I.T., he enlisted in the United States Army Reserves in 2001, and was later commissioned in 2004.

In his free time, the author enjoys running, cycling, baseball, and spending time with Jenny.